



Floral Meristem Termination in Aquilegia

Citation

Min, Ya. 2021. Floral Meristem Termination in Aquilegia. Doctoral dissertation, Harvard University Graduate School of Arts and Sciences.

Permanent link

<https://nrs.harvard.edu/URN-3:HUL.INSTREPOS:37370200>

Terms of Use

This article was downloaded from Harvard University's DASH repository, and is made available under the terms and conditions applicable to Other Posted Material, as set forth at <http://nrs.harvard.edu/urn-3:HUL.InstRepos:dash.current.terms-of-use#LAA>

Share Your Story

The Harvard community has made this article openly available.
Please share how this access benefits you. [Submit a story](#).

[Accessibility](#)

HARVARD UNIVERSITY
Graduate School of Arts and Sciences



DISSERTATION ACCEPTANCE CERTIFICATE

The undersigned, appointed by the
Department of Organismic and Evolutionary Biology
have examined a dissertation entitled
“Floral Meristem Termination in *Aquilegia*”
presented by
Ya Min
candidate for the degree of Doctor of Philosophy and hereby
certify that it is worthy of acceptance.

Signature *Elena Kramer*
Typed name: Professor Elena Kramer

Signature *Terrence D. Capellini*
Typed name: Professor Terrence Capellini

Signature *Cassandra Extavour*
Typed name: Professor Cassandra Extavour

Signature *William E. Friedman*
William E. Friedman (Aug 31, 2021 14:56 EDT)
Typed name: Professor William Friedman

Date: August 26, 2021

FLORAL MERISTEM TERMINATION
IN *AQUILEGIA*

A DISSERTATION PRESENTED
BY

YA MIN

TO
THE DEPARTMENT OF ORGANISMIC AND EVOLUTIONARY BIOLOGY

IN PARTIAL FULFILLMENT OF THE REQUIREMENTS FOR THE DEGREE OF

DOCTOR OF PHILOSOPHY

IN THE SUBJECT OF
BIOLOGY

HARVARD UNIVERSITY
CAMBRIDGE, MASSACHUSETTS
AUGUST 2021

©2021 – YA MIN

ALL RIGHTS RESERVED.

Floral Meristem Termination in *Aquilegia*

ABSTRACT

The persistent activity of stem cells in meristems is the foundation of continuous growth in plants. During the reproductive phase, vegetative meristems that produce leaves will be converted into floral meristems (FMs) to produce flowers. Unlike the vegetative meristems, which can generate new leaves continuously throughout the lifespan of a plant, the stem cell activity in a FM will always terminate at a specific time point, since each flower only has a finite number of organs. Floral meristem termination (FMT) is, therefore, one of the defining features of FM identity and variation in the timing of FMT is an essential source of generating floral morphological diversity. However, how this process is fine-tuned at a developmental and evolutionary level is still poorly understood. In this dissertation, I have sought to lay the groundwork for understanding how FMT is regulated in *Aquilegia* and thereby promote *Aquilegia* as a model system for studying FM regulation. In Chapter 1, I conducted in-depth transcriptome sequencing of finely dissected developmental stages of the FM of *A. coerulea*, covering the developmental window before and after FMT, and identified key genes that function as hub loci in major genetic modules or mark the transitions between key developmental stages. In Chapter 2, I analyzed how the dynamic between cell proliferation and cell expansion changes during primordia initiation and FMT using a newly developed quantitative live-confocal imaging method. This was the first live-imaging application for FMs that produce more than four whorls of floral organs with an apocarpous gynoecium and was the first investigation of

cell behavioral dynamics during the FMT developmental window in any plant. In Chapter 3, I used stamen whorl number as a quantitative trait to represent the timing of FMT and conducted QTL mapping in the F2 progeny of a cross between two sister species, *A. brevistyla* and *A. canadensis*. I discovered that the genetic architecture underlying variation in the timing of FMT consists of multiple QTL, each with moderate to small effect. By integrating the results of Chapter 1 and 3, I have also been able to generate the first list of candidate genes that may participate in the regulation of FMT timing.

TABLE OF CONTENT

ABSTRACT	iii
LIST OF FIGURES	vi
LIST OF TABLES	viii
ACKNOWLEDGEMENTS	x
INTRODUCTION	1
Floral meristem termination – What happens when stem cells are no longer needed?	
CHAPTER 1	18
Transcriptome profiling and weighted gene co-expression network analysis of early floral development in <i>Aquilegia coerulea</i>	
CHAPTER 2	56
Quantitative live-imaging of <i>Aquilegia</i> floral meristems reveals distinct patterns of floral organ initiation and cell-level dynamics of floral meristem termination	
CHAPTER 3	84
Genetic architecture underlying variation in floral meristem termination in <i>Aquilegia</i>	
CONCLUSION	118
APPENDIX A	124
Quantitative live confocal imaging of <i>Aquilegia</i> floral meristems	
APPENDIX B	153
Supplemental materials for Chapter 2	
APPENDIX C	156
Supplemental materials for Chapter 3	

LIST OF FIGURES

1	Models of how multiple whorls of organs can be theoretically generated based on our current understanding of the molecular basis underlying FMT.	11
2.1	<i>A. coerulea</i> and the floral developmental stages used for RNA-seq.	21
2.2	PCA of normalized reads of all samples and bar plot summary of DE genes between developmental stages.	27
2.3	GO term and KEGG pathway enrichment analysis of DE genes.	32
2.4	Expression profiles of type-II MADS-box genes, class-I KNOX genes, and genes involved in FM maintenance and termination pathways.	34
2.5	Associating gene co-expression modules with developmental stages.	36
2.6	Gene network of module green-s1.	39
2.7	Gene network of module brown-s4.	44
2.8	Gene network of module magenta-s4.	45
3.1	Floral morphology of <i>A. coerulea</i> flowers.	61
3.2	Developmental windows covered in the current study.	66
3.3	Overview of growth dynamics of each developmental window.	67
3.4	Initiation of st1 primordia.	69
3.5	Initiation of staminode and carpel primordia.	71
3.6	Early carpel primordia development.	74
4.1	FMT is an important and fine-tuned developmental process that occurs in all flowers.	87
4.2	Phenotyping SWN in the parental and F2s populations.	89
4.3	FM widths measurements of the parental species during the early developmental stages.	96
4.4	Genetic architecture and candidate genes.	98
4.5	<i>In situ</i> hybridization of <i>AqWUS</i> and candidate genes.	101

A1	Making plates for live-imaging.	130
A2	Developmental stages for dissecting FMs for imaging.	131
A3	Comparison of how a confocal stack look like in ImageJ and MGX before and after adjusting the brightness and contrast.	134
A4	Overall layout of MorphgraphX interface.	135
A5	Examples of over-segmented cells.	139
A6	Examples of under-segmented cells.	140
A7	Example of a cell with incorrect boundary.	141
A8	Removing cells on the boundary of the mesh.	142
A9	Examples of lineage tracing errors.	147
B1	Regions used for constructing growth alignment graphs.	154
C1	SWN and the position of flowers on inflorescences.	157
C2	F1-parent-of-origin has a significant impact on the distribution of SWN in the respective F2 progeny.	158
C3	Distribution of the SD of SWN among the parental and F2 populations.	159
C4	Diagram and summary statistics of the genetic map.	159
C5	Confirmation of QTL underlying SWN variation.	160
C6	Effect plots of the markers that have the highest LOD score under each QTL.	160
C7	Gene phylogeny for <i>AqROXYa</i>	161
C8	Gene phylogeny for <i>AqATH1</i>	162

LIST OF TABLES

4.1	Summary statistics for QTL.	99
B1	Pair-wise Tukey's HSD test for cell area expansion rates and average cell division numbers between different TP intervals for the growth alignment graphs.	154
C1	Pairwise comparison of FM widths through early.	163
C2	No significant evidence supporting the presence of a second QTL on any chromosome. developmental stages.	164
C3	Summary of number of genes under each potential QTL.	164
C4	Expressed genes under Q4.	165
C5	Information on candidate genes.	169
C6	Primers used for constructing <i>in situ</i> hybridization probes.	169

谨以此博士文献给我的父母，闵毅和兰学元。

ACKNOWLEDGEMENTS

First and foremost, this Ph.D. would not have been possible without my mentor, advisor, and role model, Prof. Elena Kramer. The amount of help and support I received from Elena over the past six years is infinite, and I had a hard time writing down anything because I did not know where to start. I started graduate school thinking Elena is the best advisor, and now I am finishing graduate school and still thinking the same. I used many “I” statements throughout this dissertation, but the truth is that Elena helped me develop, shape, and polish every idea presented here. Elena taught me how to science, how to teach, and how to mentor. During graduate school, discussing science with Elena is my favorite thing, and I am certain that it will continue to be my favorite thing.

I am incredibly grateful for my dissertation committee: Prof. Cassandra Extavour, Prof. William Ned Friedman, and Prof. Terrence Capellini. I thoroughly enjoyed my qualification exam, every DAC, and every private meeting with them. Their presence, guidance, and encouragement have been invaluable. Sometimes I cannot believe how fortunate I am to have a committee that understands my goals, helps me navigate through the unknowns, and celebrates my progress.

I would like to thank my undergraduate mentor, Prof. Fujita Tomomichi, at Hokkaido University, without whom I probably would not be a scientist. I joined the Fujita lab when I went to Japan in my junior year, and Fujita sensei taught me literally everything, from the most minor things like how to design primers, to how to be a scientist. Sensei was always extremely encouraging and patient with me, and he cultivated my curiosity in science.

The Kramer lab has treated very well over the past six years, and a special shout out to Claire, Steph, and Molly. Claire sensed my complete ignorance yet slight curiosity about American

culture when I first arrived, arranged weekly movie nights to go through all the 90s and 2000s high school movies – movies I would never have watched on my own, but it was a lot of fun when we were together as a group. To Steph, I always felt so fortunate to have her as a friend and a collaborator. And to Molly, my lab twin. We are so different from each other, but this difference became the strongest strength and support that we have for each other; it is magical.

I enjoyed my graduate school journey because of my friends and my cohort. Thank you to Chelsea Little, Andrés G. de la Filia, Daniel Souto, Reto Rufener, Pierre Baduel, Becky Povilus, Zhengyang Wang, Jess Gersony, Ben Goulet-Scott, Amaneet Lochab, Sofia Prado-Irwin, Dan Utter. To Brandon Enalls, who is a great friend and accompany, who shared my love for music, and who listened to all my complaints about all my failed experiments. To Kristel Schoonderwoerd, I cannot imagine an alternative timeline to go to graduate school without Kristel.

I am also grateful for the financial support and recognition from OEB, GSAS, and my professional societies. Over the past few years, I have been very vocal about my resentment that international students in the US do not get equal access to most awards and fellowships due to citizenship requirements. All these unequal opportunities unavoidably make our resumes thinner and much less competitive compared to our peers. However, I was fortunate and privileged enough to receive support from my department, school, and societies, making these dissertation projects possible. The Merit Fellowship reduce my teaching load, thanks to which I had enough time to finish some major experiments. Chapter 1 was entirely funded by the Graduate Student Research Funds from OEB. Chapter 2 was entirely funded by the Emerging Model Grant from the Society of Developmental Biology. The Professional Development Fund from the Graduate School of Arts and Sciences allowed me to attend and present in many conferences. Special thanks to the Botanical Society of America, which provided me with more than research and travel awards: skills and knowledge I would not have gained otherwise during graduate school, and a community.

To my husband, Weilin Meng, who provided me with infinite support in every possible way during this graduate school journey. He has been a source of joy, inspiration, and encouragement. To our cats, Penny and Nickel. I did not think I would like cats until I had them, and they became one of the most important parts of my life. The amount of comfort they gave me is, in fact, beyond words, especially during the entire Covid19 lockdown and during my dissertation writing.

Last but not the least, I am forever indebted to my parents. They endured tremendous loneliness and faced many doubts and pressure from others over the past years, but they chose to support me in pursuing my dreams without question. They give me the strongest love in the world.

INTRODUCTION

Floral meristem termination –

What happens when stem cells are no longer needed?

The aesthetic appeal of the seemingly infinite variety of floral form dates to the earliest days of human civilization. From a developmental perspective, flowers are produced by floral meristems (FMs), a specific category of plant meristem (Steeves & Sussex, 1989). Meristems are typically domes of stem cells that lay the foundation for the continuous developmental processes observed in plants. A vegetative shoot meristem, for instance, produces leaves, stems and branches continuously throughout the lifespan of a plant. By contrast, FMs produce the floral organs with little or no stem and no branching.

In the early 1800's, the foundation of understanding the developmental dynamics of plant meristems in general and FMs in particular was established using early microscopes to document the initiation and development of floral organs (e.g., Guillard, 1835; Duchartre, 1845; Payer, 1857). Today we are still seeking to characterize these same processes, but using far more advanced microscopes in combination with modern molecular genetics. Although we have gained an enormous amount of knowledge concerning the mechanisms regulating floral organ initiation, organ identity determination, and organ elaboration, an essential component is still lacking: the mechanisms controlling floral meristem termination (FMT), which is the regulated termination of stem cell activity in the FM. FMT represents one of the defining features of a FM relative to a vegetative meristem, which can produce an indeterminate number of leaves while the number of organs produced by a FM is always finite. In this Introduction, I will elaborate on why understanding FMT is fundamental to our knowledge of floral development and evolution, summarize our current progress in the molecular basis of FMT, and highlight some pressing and intriguing questions about the regulation of FMT. In addition, I will explain why *Aquilegia* is an ideal model system for addressing the gaps in our understanding of FMT, and how the studies from this dissertation will lay the groundwork for in-depth investigation of FMT in *Aquilegia*.

The nature of FMT and its contribution to floral diversity

Following the transition to reproductive growth, plants shift from producing vegetative shoot meristems to producing those with FM identity, which will give rise to the flowers themselves (Steeves & Sussex, 1989). This transition in meristem identity is marked by a number of changes in meristem behavior. Many aspects of this behavioral change, such as changes in phyllotaxy and the length of internodes, are developmental shifts that the shoot meristems exhibit in other phases of vegetative growth. However, some aspects are unique to the FM, particularly the production of lateral organs with different floral identities and the timed termination of meristem activity following production of a specific number of floral organs, which I have termed FMT.

Interestingly, the establishment of floral organ identity and the termination of the FM are tightly interconnected processes. A typical flower consists of four types of floral organs with defined positions relative to each other: sepals are in the outermost positions of a flower, followed by petals, then stamens, and finally carpels in the innermost position (Fig. 1). Therefore, unlike the vegetative meristems that always maintain a constant pool of stem cells and can theoretically produce organs continuously throughout the lifespan of a plant, the activity of a FM will always cease after a period of successive initiation of organs, and the remaining cells in the center of the floral apex will generally be incorporated into building carpels (the only exceptions being unisexual male flowers that never initiate carpels, a very rare phenomenon). The precise timing of FMT ensures that the correct number of organs are initiated, and the coordination between FMT and the floral organ identity programs ensures that all necessary floral parts are generated.

Variation in floral form can be generated through FMT in many ways. Floral organs are initiated in the peripheral zone of the FM in spirals or whorls (i.e., concentric rings), and thus variation in FMT directly gives rise to different numbers of whorls (or the total number of floral

organs in the case of spiral phyllotaxy). Consistent with this, an incredible range of floral organ numbers is observed in every major lineage of the flowering plants. Although the number of organs per whorl can vary, this value typically ranges only from two to five, meaning that significant increases in floral organ number are primarily associated with delays in FMT. Furthermore, delays in FMT most commonly give rise to an increase in stamen whorl numbers rather than carpels (Endress, 2011; Ronse De Craene, 2018). This reflects the fact that the number of carpels in a flower seems to be tightly correlated with whether the flower forms a syncarpous or an apocarpous gynoecium. A syncarpous gynoecium consists of a whorl of carpels that are fused into a single functional unit (Endress, 2014, 2019), while an apocarpous gynoecium is comprised of free carpels that remain distinct from each other at maturity. From a developmental perspective, these two morphologies have very different implications. In a flower with a syncarpous gynoecium, the floral apex is typically consumed by the production of a single, congenitally fused primordium that integrates all of the individual carpel primordia. In contrast, in flowers with apocarpous gynoecia, the floral apex will not be immediately consumed as the first carpels arise but, rather, will persist until the appropriate number have been produced. (Endress, 2014). It is observed that flowers with a large number of carpels almost always have apocarpous gynoecia (Endress, 2011). This is particularly evident in lineages that are nested within clades that otherwise have very stable carpel numbers and syncarpous gynoecia, such that the transition to apocarpous gynoecia is consistently accompanied with a dramatic increase in carpel numbers. For instance, many taxa in the Alismatales of the monocots, Rosaceae and Malvaceae of rosids, and Apocynaceae of the asterids have numerous unfused carpels, while their syncarpous relatives all have no more than five carpels (Igersheim *et al.*, 2001; Endress, 2011, 2014; Ronse De Craene, 2018).

The relationship between carpel numbers, gynoecium structure, and FMT is very interesting from a developmental perspective because carpels are always the last organs that are produced in a

flower, meaning that different gynoecia types might impose differing constraints on the nature of FMT. To construct a syncarpous gynoecium, a tight coordination in the timing of FMT and carpel primordia initiation is necessary, which in turn is predicted to impose strong constraints on the number of carpel primordia. Any degree of indeterminacy in such a flower has the potential to completely disrupt carpel and fruit development, significantly impacting fitness. On the other hand, since each carpel is an individual functional unit in an apocarpous gynoecium, the coordination between primordia initiation and FMT might be expected to be more flexible. Indeed, in addition to the above-mentioned correlation between apocarpy and an increase in carpel numbers, greater variation in carpel numbers is also observed in taxa with apocarpous gynoecia compared to those with syncarpous gynoecia (Endress, 2011, 2014).

Although every major lineage of the flowering plants exhibits a large range of floral organ whorl numbers, in some clades, the range is set by a few outlier taxa with extremely high whorl numbers while the majority of the members have only a few whorls with no variation. In fact, the transition from variable to stable whorl numbers in a flower is considered as a critical, consistent trend in the evolution of floral form (Endress, 1990). The majority of taxa in the asterids, rosids, and monocots have what are considered canalized floral structures, including a fixed number of floral whorl numbers (normally four or five whorls only), while the sister lineages of those groups display a much wider variation (Endress, 1990, 2011; Endress & Doyle, 2009; Ronse De Craene, 2018). In fact, such a variation is not only exhibited between species or genera, but also among plants of the same species, same population, and even the same individual (Diggle, 1995; Kitazawa & Fujimoto, 2014, 2016; Wang *et al.*, 2015), indicating a high degree of flexibility in the timing of FMT. Furthermore, lineages with stable whorl numbers tend to have lower whorl numbers compared to those with variable whorl numbers (Endress, 1990, 2011). The trend towards reduction in floral whorl numbers was also supported by the reconstruction of the ancestral angiosperm flower, which

was proposed to have at least nine whorls of organs, but the most probable ancestors of the Monocotyledoneae and the Eudicotyledoneae had five and seven whorls of organs, respectively (Sauquet *et al.*, 2017). Among the Eudicotyledoneae, ancestral reconstruction revealed additional reductions in the total whorl numbers, such that the ancestors of the Pentapetalae, representing 70% of all angiosperm species, had five floral whorls while several major lineages within the clade have only four (Sauquet *et al.*, 2017). Investigations in how regulations of FMT become canalized in different lineages will thus provide us valuable insight into major processes shaping angiosperm evolution.

Of course, stamen and carpel numbers are not merely a phylogenetic trait, they relate directly to aspects of plant fitness by determining how much pollen and ovules are produced and may reflect adaptation to different pollination strategies. It is observed that excessively high stamen numbers occur frequently in brush flowers that are pollinated by large animals, including beetles, bats, and birds (Endress, 2011). On the other hand, low and fixed stamen numbers are found in flowers with highly specialized structures, such as the gynostemium in Orchidaceae (Endress, 2011). An increase in the number of whorls also allows for the evolution of new organ types. For example, staminodes in many taxa are originated from modified stamens that have evolved highly elaborated morphologies and serve distinct functions such as pollinator attraction (Walker-Larsen & Harder, 2000). The evolution of such novel organs is not favored to occur when pollen production is limiting, meaning that higher stamen numbers are commonly correlated with the evolution of novel floral organ identities.

Molecular basis of FMT

In the FM, the stem cell population is maintained by a negative feedback loop between the critical loci *WUSCHEL* (*WUS*) and *CLAVATA3* (*CLV3*) (Schoof *et al.*, 2000; Lenhard, 2003;

Müller *et al.*, 2006). *WUS* specifies the stem cell identity and encodes a homeodomain protein, which functions non-cell autonomously to activate the expression of *CLV3*. Meanwhile, the small peptides encoded by *CLV3* diffuse into the *WUS* expression domain and activate a signal transduction cascade that limits *WUS* expression. This feedback loop both promotes stem cell identity and regulates the homeostasis of the stem cell population so that it is never too large or small. At the molecular level, FMT is marked by the cessation of stem cell activity in the FM, which corresponds to elimination of *WUS* expression. At the same time, the floral organ identities are established early in the FM by the so-called ABC program, in which three classes of genes function in different combinatorial codes to determine the four types of floral organs: A-class genes alone specify sepals, A and B together specify petals, B and C together control stamens, and C-class genes alone control the carpel identity (Coen & Meyerowitz, 1991). The C-class gene *AGAMOUS* (*AG*) and *WUS* also form a feedback loop, in which the expression of *AG* is activated by *WUS* in the center of the FM, while *AG* is ultimately responsible for FMT by negatively regulating the expression of *WUS* (Lenhard *et al.*, 2001). What is particularly interesting about this feedback loop is that the activation of *AG* by *WUS* and the termination of *WUS* by *AG* do not occur simultaneously, and thus the lag between these two regulatory interactions determines how long the stem cells in the FM can proliferate, i.e., the timing of FMT.

Over the past decades, the broad functional conservation of *WUS*, *AG*, and the *WUS-AG* feedback loop has been widely demonstrated in various angiosperm model systems (Nardmann & Werr, 2006; Litt & Kramer, 2010; Whitewoods *et al.*, 2020). We have also obtained a breadth of knowledge about how *AG* is regulated at all levels, from transcription to protein interactions. However, most of these regulatory steps function upstream of the *AG-WUS* feedback, and most studies have focused on loss-of-function mutations that lead to an uncontrolled proliferation of the

FM and, therefore, provide little information on how the time lag between the activation of *AG* and FMT is achieved.

To date, two pathways are known to act through *AG* to terminate the expression of *WUS*. On the one hand, in *A. thaliana*, *AG* has been shown to bind to the *WUS* locus *in vivo* and recruit Polycomb group (PcG) proteins to directly repress *WUS* expression (Liu *et al.*, 2011). On the other hand, in both *A. thaliana* and tomato (*Solanum lycopersicum*), *AG* also acts to indirectly terminate *WUS* via the C2H2 zinc-finger transcription factor *KNUCKLES* (*KNU*). How the activation of *KNU* is used as a “timer” was demonstrated through a series of elegant experiments (Sun *et al.*, 2009, 2014). *AG* activates *KNU* by occupying the PcG complex binding site on its promoter, which prevents the addition of epigenetic repressive markers onto *KNU*. It takes roughly two rounds of cell divisions (~2d) to sufficiently dilute the repressive markers and allow the expression of *KNU*, during which the stamen primordia initiate, and after which *KNU* immediately terminates *WUS* to achieve FMT. Either delay or acceleration in the cell cycle also delay or accelerate the induction of *KNU* and FMT, respectively (Sun *et al.*, 2014). In addition, the expression of *KNU* is necessary to maintain a stable epigenetic silencing of *WUS* at the chromatin level (Sun *et al.*, 2019).

A third known pathway for FMT in *A. thaliana* is through the gene *SUPERMAN* (*SUP*), which appears to function in an *AG*-independent manner (Xu *et al.*, 2018). *SUP* encodes a C2H2 zinc-finger transcriptional repressor and is expressed in a very tight boundary between the stamen and carpel whorls (i.e. the B/C boundary) during a limited developmental window early in the FM. This expression domain appears to be key to preventing expression of the B-class genes from entering the carpel whorl, as *sup* mutant flowers have extra stamens and defective carpels (Bowman *et al.*, 1992; Prunet *et al.*, 2017). At the organ boundary, *SUP* also directly represses auxin biosynthesis genes, an action which appears to have a non-cell-autonomous effect on the stem cell population in the FM such that in *sup* mutants (Xu *et al.*, 2018). Auxin levels are increased at the

boundary but decreased in the center of the FM, leading to a slightly enlarged stem cell population and slightly prolonged activity of the FM (Xu *et al.*, 2018).

How can variation in the timing of FMT be generated?

The above-mentioned studies have provided important insight into the molecular basis of FMT, but two key questions are still remaining: 1) Are these pathways conserved in other taxa? and 2) What is regulating the fine-tuning of FMT timing to generate flowers with different whorl numbers?

Although the *AG-KNU-WUS* pathway has been elegantly demonstrated in *A. thaliana* and tomato (Sun *et al.*, 2009, 2014; Bollier *et al.*, 2018), both systems make flowers with only four whorls. Particularly, since the duration of *KNU* activation only allows for the initiation of one whorl of stamens, it begs the question of how this pathway could function in taxa with more than one whorl of stamens. Moreover, whether *AG* directly binds to the *WUS* locus to recruit epigenetic repression markers in other taxa requires further investigation.

Regardless of whether the *AG-KNU-WUS* pathway is conserved, the “division-dependent epigenetic timer” model deserves attention when considering how FMT can be timed. Given two facts, 1) that the *ag* loss-of-function mutants are always associated with loss of determinacy (Litt & Kramer, 2010) and 2) that there always appears to be a lag between *AG* expression and FMT, it is reasonable to assume that, even if the function of *KNU* is lineage-specific, a functionally analogous factor is in place in other taxa, being activated by *AG* and responsible for repressing *WUS*. Under this circumstance, two components of this pathway can theoretically be modified to achieve flowers with additional whorls (Fig. 1a): either the activation of *KNU* (or other genes) by *AG* can be delayed, or the termination of *WUS* by *KNU* (or other genes) can be delayed. The delayed activation of *KNU* would be possible if there are, for instance, more epigenetic repressive markers covering the target locus, which would require more rounds of cell division to sufficiently dilute the marks and

allow for the expression of the negative regulator, allowing time for more whorls of organ initiation. Alternatively, it may be that KNU or its functional analog has lower affinity for the *WUS* promoter, requiring more time for protein to accumulate and achieve *WUS* repression.

Orthologs of *SUP* have been described in a small number of plant taxa, such as rice and *Petunia*, all of which display similar mutant phenotypes consistent with the function of *SUP* homologs as B/C organ boundary genes (Nandi *et al.*, 2000; Nakagawa *et al.*, 2004). A recent study also demonstrated at the molecular level that the *SUP* ortholog in *Medicago truncatula*, *MtSUP*, functions to control both the B/C boundary and FMT, as well as the number of flowers produced per node (Rodas *et al.*, 2021). These comparative studies suggest that it is likely that *SUP* homolog functions are conserved to a degree, but despite the studies in *A. thaliana* linking auxin concentration level to FMT via *SUP*, the molecular mechanism of how *SUP* regulates the timing of FMT is still lacking and no information is available on its conservation.

The very narrow expression domain of *SUP* in the FM, both spatially and temporally, is quite intriguing because it is only expressed at the boundary between the stamen whorl and the carpel whorl immediately before the initiation of carpels, which, as mentioned above, are the last whorl of organs to be produced in most flowers. Moreover, the subtle changes in auxin levels observed in *sup* mutants are suggestive that the inception of FMT requires a certain threshold level of auxin (Xu *et al.*, 2018). Floral organ initiation is an iterative process: the initiation of a new whorl of organs also means the establishment of a new boundary between the adaxial side of the primordia and the remaining FM, and this iteration ends with the establishment of a boundary between the last whorl of stamens and the carpels. Taking all this information together, one plausible model could be that during the early organ initiation process, auxin concentration must remain consistent across the most recently initiated whorl of primordia and the remaining FM. When the last whorl of stamen primordia is initiating, however, the expression of *SUP* leads to a decrease in auxin concentration at

the boundary and a slight increase in concentration in the FM itself, and this change disrupts the consistent iteration and acts as the signal that it is time to stop initiating organs (Fig. 1b). Thus, delaying expression of *SUP* could be critical to delay in FMT.

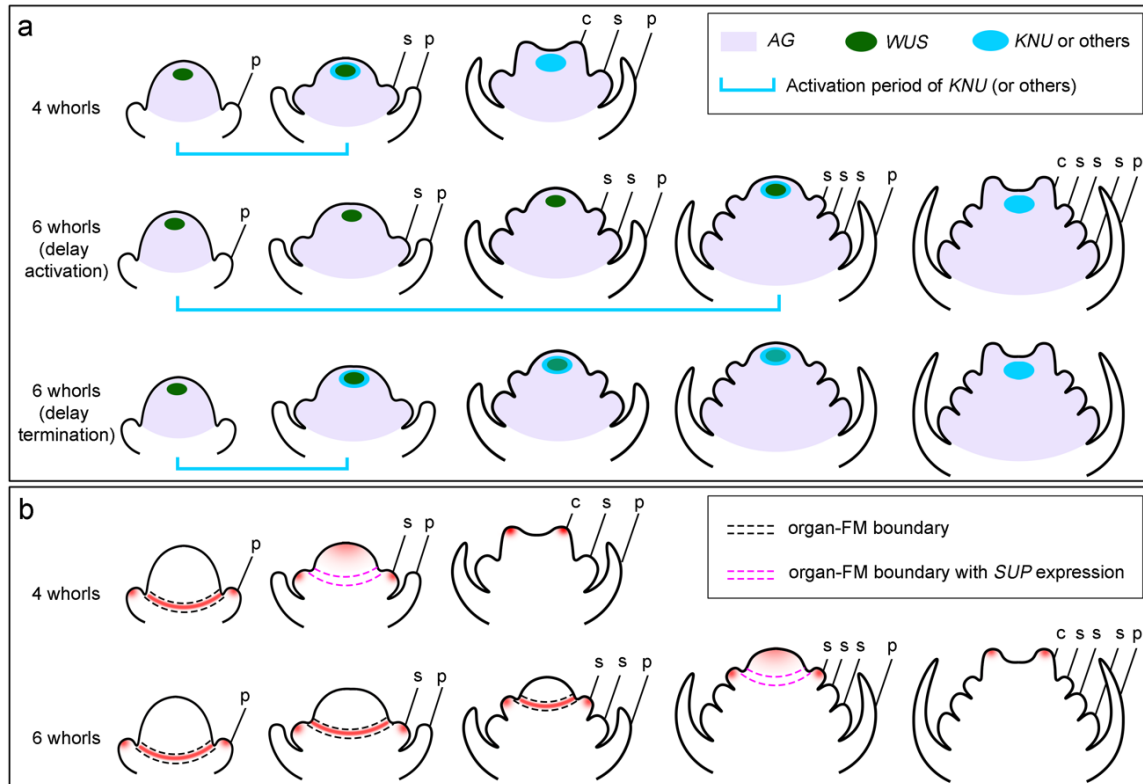


Figure 1. Models of how multiple whorls of organs can be theoretically generated based on our current understanding of the molecular basis underlying FMT. (a) Models of how modifications on the *AG-KNU* (or other genes)-*WUS* could generate more than four whorls of organs. The 4 whorls diagram is based on what is known in *A. thaliana*. Flowers with 6 whorls can be generated either by a delayed activation of *KNU* (or other genes) by *AG*, or by a delayed termination of *WUS* by *KNU* (or other genes). **(b)** Model of how *SUP* could act as the signal for the initiation of the last whorl organ in a flower by changing the auxin concentrations. The organ-FM boundary represents the boundary between the adaxial most edge of the newly initiated primordial whorl and the remaining FM. When the newly initiated whorl is *not* the last whorl of stamens, relatively high auxin concentration (indicated in red) can be found at the organ-FM boundary (black dotted lines) and in the newly initiated primordia. If the newly initiated whorl *is* the last whorl of stamens, due to the expression of *SUP* at the organ-FM boundary (pink dotted lines), the auxin concentration at the organ boundary decreases and while simultaneously increasing in the FM, which contributes to FMT. Under this scenario, increasing whorl number requires postponing *SUP* expression. Note, this diagram does not seek to indicate all potential locations of increased auxin concentration and the sepal whorls are not shown in any of the FM diagrams (i.e., a single whorl of sepals was assumed in all scenarios). p: petals; s: stamens; c: carpels.

Alternatively, there are several other molecular mechanisms that are used as “timers” in plants and animal development, which can be referred to as inspiration when considering how FMT

can be timed and how variation in the timing can be generated. For example, during somitogenesis in vertebrates, it has been found that the speed of initiation is partially dependent on the protein stability of the key genes and the speed of RNA splicing. By manipulating the number of introns in these key genes, the somitogenesis clock can be slowed down or accelerated (Hirata *et al.*, 2004; Takashima *et al.*, 2011). Similar complex patterns of transcription, RNA editing, and protein stability function in the regulation of the circadian clock in both plants and animals (Rosato *et al.*, 2006; Creux & Harmer, 2019), opening the possibility that they could likewise function in other developmental processes.

***Aquilegia* as a model system to investigate FMT**

The main reason for our lack of understanding of the regulation of FMT timing is that all currently established model systems belong to three main lineages of the flowering plants, and neither they nor their close relatives harbor any natural variation in floral organ whorl numbers. To this end, the genus *Aquilegia* is an ideal model system for providing crucial knowledge regarding FMT. *Aquilegia* belongs to the eudicot family Ranunculaceae, and contains approx. 70 species, which resulted from a recent adaptive radiation. Consistent with this, they share low interspecific sequence variation and a high degree of inter-fertility (Filiault *et al.*, 2018). An *Aquilegia* flower consists of one whorl of sepals, one whorl of petals, multiple whorls of stamens, two whorls of staminodes (except for *A. jonesii*), and one whorl of carpels that form an apocarpous gynoecium (Munz, 1946; Tucker & Hodges, 2005). All of the floral organs initiate in whorls of five organs and initiate successively in alternate positions such that a flower contains 10 orthostichies (vertical rows of organs) (Tucker & Hodges, 2005). All *Aquilegia* species share this floral structure, but the number of stamen whorls often varies between different species (Munz, 1946; Tucker & Hodges, 2005). This natural variation in stamen whorl number provides an outstanding opportunity for investigating natural variation in

the timing of FMT: a flower with earlier FMT will have fewer whorls of stamens compared to a flower that experiences later FMT. In addition, the model species *Aquilegia x coerulea* ‘Origami’ has a fully sequenced and well-annotated genome, with established molecular tools, such as *in situ* hybridization and virus-induced gene silencing, available for gene functional studies (Kramer, 2009).

During my Ph.D., I have sought to lay the groundwork for understanding how FMT is regulated in *Aquilegia* and thereby promote *Aquilegia* as a model system for studying FM regulation. In Chapter 1, I conducted in-depth transcriptome sequencing of finely dissected developmental stages of the FM of *A. coerulea*, covering the developmental window before and after FMT. In Chapter 2, we developed a quantitative live-imaging method and analyzed how the dynamic between cell proliferation and cell expansion changes during primordia initiation and FMT. In Chapter 3, utilizing the stable floral structure and the high inter-fertility of the *Aquilegia* species, I used stamen whorl number as a quantitative trait to represent the timing of FMT and conducted QTL mapping in the F2 progeny of a cross between two sister species, *A. brevistyla* and *A. canadensis*.

Results from Chapter 1 provided us with broad transcriptomic data on the earliest stages of floral development in *A. coerulea*, including identification of key genes that function as hub loci in major genetic modules or mark the transitions between different developmental stages. The live-imaging analysis in Chapter 2 represents the first live-imaging application for FMs that produce more than four whorls of floral organs and with an apocarpous gynoeceum and was the first investigation of cell behavioral dynamics during the FMT developmental window in any plant. In Chapter 3, we discovered that the genetic architecture underlying variation in the timing of FMT consists of multiple QTL, each with moderate to small effect. By integrating the results of Chapter 1 and 3, I have also been able to generate a promising list of candidate genes that may participate in the regulation of FMT timing.

REFERENCE

- Bollier N, Sicard A, Leblond J, Latrasse D, Gonzalez N, Gévaudant F, Benhamed M, Raynaud C, Lenhard M, Chevalier C, *et al.* 2018. At-MINI ZINC FINGER2 and SI-INHIBITOR OF MERISTEM ACTIVITY, a Conserved Missing Link in the Regulation of Floral Meristem Termination in Arabidopsis and Tomato. *The Plant Cell* 30: 83–100.
- Bowman JL, Sakai H, Jack T, Weigel D, Mayer U, Meyerowitz EM. 1992. *SUPERMAN*, a regulator of floral homeotic genes in Arabidopsis. *Development (Cambridge, England)* 114: 599–615.
- Coen ES, Meyerowitz EM. 1991. The war of the whorls: genetic interactions controlling flower development. *Nature* 353: 31–37.
- Creux N, Harmer S. 2019. Circadian Rhythms in Plants. *Cold Spring Harbor Perspectives in Biology* 11: a034611.
- Diggle PK. 1995. Architectural Effects and the Interpretation of Patterns of Fruit and Seed Development. *Annual Review of Ecology and Systematics* 26: 531–552.
- Duchartre PÉS. 1845. Observations sur l'organogénie de la fleur dans les plantes de la famille des Malvacées. 123–161.
- Endress PK. 1990. Patterns of floral construction in ontogeny and phylogeny. *Biological Journal of the Linnean Society* 39: 153–175.
- Endress PK. 2011. Evolutionary diversification of the flowers in angiosperms. *American Journal of Botany* 98: 370–396.
- Endress PK. 2014. Multicarpellate gynoecia in angiosperms: occurrence, development, organization and architectural constraints: Multicarpellate Gynoecia in Angiosperms. *Botanical Journal of the Linnean Society* 174: 1–43.
- Endress PK. 2019. The morphological relationship between carpels and ovules in angiosperms: pitfalls of morphological interpretation. *Botanical Journal of the Linnean Society* 189: 201–227.
- Endress PK, Doyle JA. 2009. Reconstructing the ancestral angiosperm flower and its initial specializations. *American Journal of Botany* 96: 22–66.
- Filiault DL, Ballerini ES, Mandáková T, Aköz G, Derieg NJ, Schmutz J, Jenkins J, Grimwood J, Shu S, Hayes RD, *et al.* 2018. The *Aquilegia* genome provides insight into adaptive radiation and reveals an extraordinarily polymorphic chromosome with a unique history. *eLife* 7: e36426.
- Guillard A. 1835. *Sur la Formation et le Développement des Organes Floraux.*
- Hirata H, Bessho Y, Kokubu H, Masamizu Y, Yamada S, Lewis J, Kageyama R. 2004. Instability of Hes7 protein is crucial for the somite segmentation clock. *Nature Genetics* 36: 750–754.

- Igersheim A, Buzgo M, Endress PK. 2001. Gynoecium diversity and systematics in basal monocots. *Botanical Journal of the Linnean Society* 136: 1–65.
- Kitazawa MS, Fujimoto K. 2014. A developmental basis for stochasticity in floral organ numbers. *Frontiers in Plant Science* 5.
- Kitazawa MS, Fujimoto K. 2016. Relationship between the species-representative phenotype and intraspecific variation in Ranunculaceae floral organ and Asteraceae flower numbers. *Annals of Botany* 117: 925–935.
- Kramer EM. 2009. *Aquilegia*: A New Model for Plant Development, Ecology, and Evolution. *Annual Review of Plant Biology* 60: 261–277.
- Lenhard M. 2003. Stem cell homeostasis in the *Arabidopsis* shoot meristem is regulated by intercellular movement of CLAVATA3 and its sequestration by CLAVATA1. *Development* 130: 3163–3173.
- Lenhard M, Bohnert A, Jürgens G, Laux T. 2001. Termination of Stem Cell Maintenance in *Arabidopsis* Floral Meristems by Interactions between *WUSCHEL* and *AGAMOUS*. *Cell* 105: 805–814.
- Litt A, Kramer EM. 2010. The ABC model and the diversification of floral organ identity. *Seminars in Cell & Developmental Biology* 21: 129–137.
- Liu X, Kim YJ, Müller R, Yumul RE, Liu C, Pan Y, Cao X, Goodrich J, Chen X. 2011. *AGAMOUS* Terminates Floral Stem Cell Maintenance in *Arabidopsis* by Directly Repressing *WUSCHEL* through Recruitment of Polycomb Group Proteins. *The Plant Cell* 23: 3654–3670.
- Müller R, Borghi L, Kwiatkowska D, Laufs P, Simon R. 2006. Dynamic and Compensatory Responses of *Arabidopsis* Shoot and Floral Meristems to *CLV3* Signaling. *The Plant Cell* 18: 1188–1198.
- Munz PA. 1946. *Aquilegia: the cultivated and wild columbines*. Ithaca. NY.
- Nakagawa H, Ferrario S, Angenent GC, Kobayashi A, Takatsuji H. 2004. The Petunia Ortholog of *Arabidopsis* *SUPERMAN* Plays a Distinct Role in Floral Organ Morphogenesis. *The Plant Cell* 16: 920–932.
- Nandi AK, Kushalappa K, Prasad K, Vijayraghavan U. 2000. A conserved function for *Arabidopsis* *SUPERMAN* in regulating floral-whorl cell proliferation in rice, a monocotyledonous plant. *Current Biology* 10: 215–218.
- Nardmann J, Werr W. 2006. The Shoot Stem Cell Niche in Angiosperms: Expression Patterns of *WUS* Orthologues in Rice and Maize Imply Major Modifications in the Course of Mono- and Dicot Evolution. *Molecular Biology and Evolution* 23: 2492–2504.
- Payer J-B. 1857. *Traité d'Organogénie Comparée de la Fleur*. Paris, V. Masson.

- Prunet N, Yang W, Das P, Meyerowitz EM, Jack TP. 2017. *SUPERMAN* prevents class B gene expression and promotes stem cell termination in the fourth whorl of *Arabidopsis thaliana* flowers. *Proceedings of the National Academy of Sciences* 114: 7166–7171.
- Rodas AL, Roque E, Hamza R, Gómez-Mena C, Minguet EG, Wen J, Mysore KS, Beltrán JP, Cañas LA. 2021. *MtSUPERMAN* plays a key role in compound inflorescence and flower development in *Medicago truncatula*. *The Plant Journal* 105: 816–830.
- Ronse De Craene L. 2018. Understanding the role of floral development in the evolution of angiosperm flowers: clarifications from a historical and physico-dynamic perspective. *Journal of Plant Research* 131: 367–393.
- Rosato E, Tauber E, Kyriacou CP. 2006. Molecular genetics of the fruit-fly circadian clock. *European Journal of Human Genetics* 14: 729–738.
- Sauquet H, von Balthazar M, Magallón S, Doyle JA, Endress PK, Bailes EJ, Barroso de Morais E, Bull-Hereñu K, Carrive L, Chartier M, *et al.* 2017. The ancestral flower of angiosperms and its early diversification. *Nature Communications* 8: 16047.
- Schoof H, Lenhard M, Haecker A, Mayer KFX, Jürgens G, Laux T. 2000. The Stem Cell Population of *Arabidopsis* Shoot Meristems Is Maintained by a Regulatory Loop between the *CLAVATA* and *WUSCHEL* Genes. *Cell* 100: 635–644.
- Steeves TA, Sussex IM. 1989. *Patterns in Plant Development*. Cambridge University Press.
- Sun B, Looi L-S, Guo S, He Z, Gan E-S, Huang J, Xu Y, Wee W-Y, Ito T. 2014. Timing Mechanism Dependent on Cell Division Is Invoked by Polycomb Eviction in Plant Stem Cells. *Science* 343: 1248559–1248559.
- Sun B, Xu Y, Ng K-H, Ito T. 2009. A timing mechanism for stem cell maintenance and differentiation in the *Arabidopsis* floral meristem. *Genes & Development* 23: 1791–1804.
- Sun B, Zhou Y, Cai J, Shang E, Yamaguchi N, Xiao J, Looi L-S, Wee W-Y, Gao X, Wagner D, *et al.* 2019. Integration of Transcriptional Repression and Polycomb-Mediated Silencing of *WUSCHEL* in Floral Meristems. *The Plant Cell* 31: 1488–1505.
- Takashima Y, Ohtsuka T, González A, Miyachi H, Kageyama R. 2011. Intronic delay is essential for oscillatory expression in the segmentation clock. *Proceedings of the National Academy of Sciences* 108: 3300–3305.
- Tucker SC, Hodges SA. 2005. Floral Ontogeny of *Aquilegia*, *Semiaquilegia*, and *Enemion* (Ranunculaceae). *International Journal of Plant Sciences* 166: 557–574.

- Walker-Larsen J, Harder LD. 2000. The evolution of staminodes in angiosperms: patterns of stamen reduction, loss, and functional re-invention. *American Journal of Botany* 87: 1367–1384.
- Wang P, Liao H, Zhang W, Yu X, Zhang R, Shan H, Duan X, Yao X, Kong H. 2015. Flexibility in the structure of spiral flowers and its underlying mechanisms. *Nature Plants* 2: 1–10.
- Whitewoods CD, Cammarata J, Venza ZN, Sang S, Crook AD, Aoyama T, Wang XY, Waller M, Kamisugi Y, Cuming AC, *et al.* 2020. *CLAVATA* Was a Genetic Novelty for the Morphological Innovation of 3D Growth in Land Plants. *Current Biology* 30: 2645–2648.
- Xu Y, Prunet N, Gan E-S, Wang Y, Stewart D, Wellmer F, Huang J, Yamaguchi N, Tatsumi Y, Kojima M, *et al.* 2018. *SUPERMAN* regulates floral whorl boundaries through control of auxin biosynthesis. *The EMBO Journal*: 14.

CHAPTER 1.

Transcriptome profiling and weighted gene co-expression network analysis of early floral development in *Aquilegia coerulea*

Reformatted from the original publication: Min, Y., & Kramer, E. M. (2020). Transcriptome profiling and weighted gene co-expression network analysis of early floral development in *Aquilegia coerulea*. *Scientific reports*, 10(1), 1-15.

Article and supplement available at: <https://doi.org/10.1038/s41598-020-76750-7>

ABSTRACT

The earliest phases of floral development include a number of crucial processes that lay the foundation for the subsequent morphogenesis of floral organs and success in reproduction. Currently, key transcriptional changes during this developmental window have been characterized in the model species *Arabidopsis thaliana*, but little is known about how transcriptional dynamics change over the course of these developmental processes in other plant systems. Here, we have conducted the first in-depth transcriptome profiling of early floral development in *Aquilegia* at four finely dissected developmental stages, with eight biological replicates per stage. Using differential gene expression analysis and weighted gene co-expression network analysis, we identified both crucial genes whose expression changes mark the transitions between developmental stages and hub genes in co-expression modules. Our results support the potential functional conservation of key genes in early floral development that have been identified in other systems, but also reveal a number of previously unknown or overlooked loci that are worthy of further investigation. In addition, our results highlight not only the dynamics of transcriptional regulation during early floral development, but also the potential involvement of the complex, essential networks of small RNA and post-translational regulation to these developmental stages.

INTRODUCTION

The earliest phase of floral meristem (FM) development requires exquisite coordination among many different developmental processes. These include the proper initiation and patterning of the floral organs, maintenance of the size of the FM during organ initiation, the eventual termination of the FM activity to ensure the correct number of whorls, and the overlay of the floral organ identity programs onto the primordia so that the boundaries of gene expression domains synchronize precisely with the physical boundaries between the primordia. Coordination of these processes is achieved through crosstalk between numerous regulatory frameworks at multiple levels, ranging from transcriptional regulation, to RNA stability, to epigenetic modification, and protein stability.

During the past 30 years, key regulatory mechanisms involved in early floral development have been characterized thanks to in-depth studies of model species such as *Arabidopsis thaliana*.

These include the ABCE model of organ identity (Coen & Meyerowitz, 1991; Ditta *et al.*, 2004), the *WUSCHEL* (*WUS*)-*CLAVATA* (*CLV*) feedback loop for meristem maintenance (Schoof *et al.*, 2000), the *AGAMOUS* (*AG*)-*KNUCKLES* (*KNU*)-*WUS* pathway for FM termination (Sun *et al.*, 2009, 2014), the auxin signaling pathway for primordia initiation (Cheng & Zhao, 2007), as well as genes specifying the boundaries between organs or gene expression domains (Yu & Huang, 2016). However, novel genes and pathways contributing to these processes are constantly being discovered, and it is not yet clear how cross-regulation between different pathways and between different levels of the regulatory framework is controlled. Furthermore, although the orthologs of many genes have been studied in multiple plant model systems, relatively little is known about the degree of conservation of these programs across major lineages of flowering plants. To obtain a comprehensive view of the molecular basis of the early floral development, the conventional forward and reverse genetics approaches need to be coupled with global analysis at the transcriptional and genomic levels.

In this study, we have conducted the first in-depth transcriptional profiling of early floral development in *Aquilegia coerulea* at four finely-dissected stages (Fig. 2.1). The genus *Aquilegia* belongs to the basal eudicot buttercup family Ranunculaceae and is a model system for floral evolutionary developmental studies (Kramer, 2009). Analysis of floral ontogeny (Tucker & Hodges, 2005) has shown that *Aquilegia* floral organ primordia initiate in whorls of five organs each, which are arranged in 10 orthostichies (vertical rows of organs), with alternate orthostichies either above the sepals or the petals (Fig. 2.1c). *Aquilegia* flowers all have multiple whorls of stamens, which is one of the major differences relative to other established model systems (e.g. *A. thaliana*, petunia, snapdragon) that all have only one whorl of stamens. The flowers of *A. coerulea*, as well as those of almost all other *Aquilegia* species, possess a fifth type of floral organ, the staminodes, which initiate in two whorls positioned between the stamens and carpels (Fig. 2.1). Unlike the syncarpous gynoecium of other

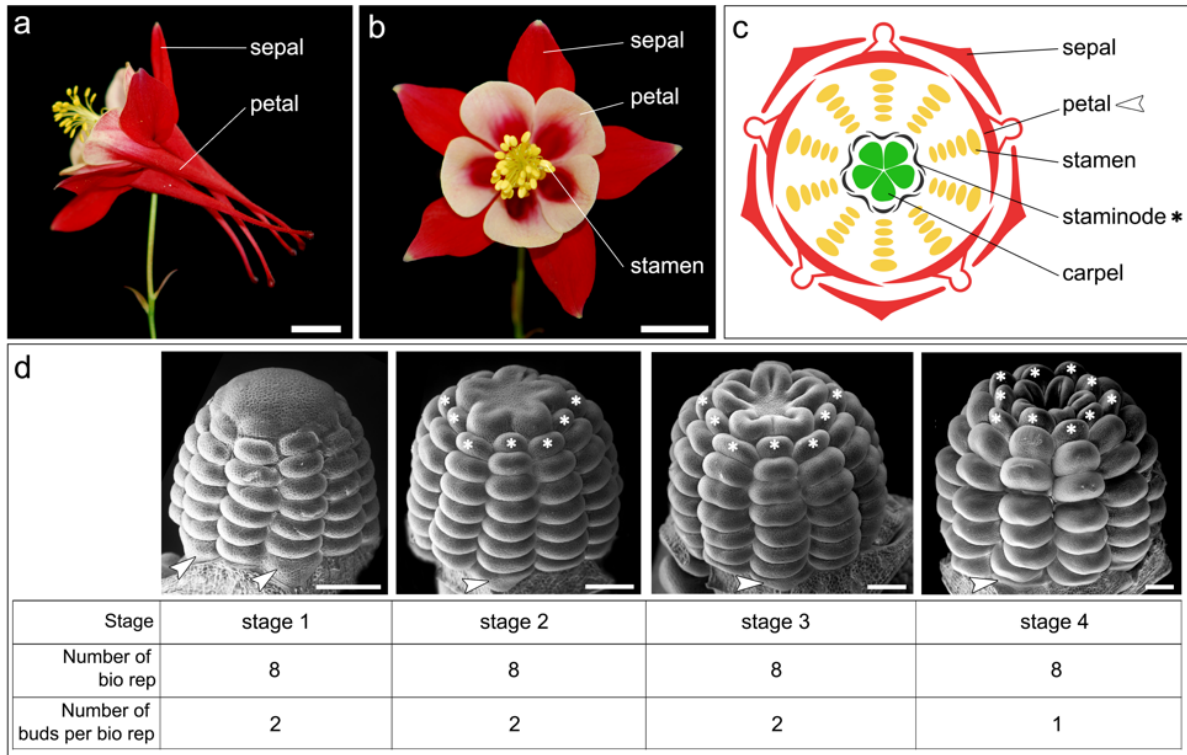


Figure 2.1. *A. coerulea* and the floral developmental stages used for RNA-seq. **(a)** Side view of a mature *A. coerulea* flower. **(b)** Front view of a mature *A. coerulea* flower. **(c)** Floral diagram of a typical *A. coerulea* flower. **(d)** Developmental stages, the number of biological replicates per stage, and the number of floral buds used for each biological replicate that were used for RNA-seq. Asterisks indicate staminodes and arrowheads indicate petals. Scale bar: a,b = 1 cm; d = 100 μ m.

model systems, *Aquilegia* is apocarpous with five distinct carpel primordia (Fig. 2.1). Using a candidate gene approach, previous studies have revealed the sub-functionalization of the B-class organ identity genes (Kramer *et al.*, 2007; Sharma & Kramer, 2013; Sharma *et al.*, 2019b) and that the *JAGGED* homolog is crucial for initiation of the floral organ primordia (Min & Kramer, 2017), but genome scale studies to date have focused on late stage floral organ development (Yant *et al.*, 2015; Ballerini *et al.*, 2019; Meaders *et al.*, 2020).

The current experiment was designed to obtain a broad characterization of the genetic pathways acting in early *Aquilegia* FM development. In order to ensure the power and accuracy of our sequencing results, we used eight biological replicates per developmental stage and obtained an

average of 18x sequencing depth per sample. The developmental window we sequenced sampled stages that started with a late phase of stamen initiation, covered the period of FM termination, and ended with the initial stage of morphogenesis of the floral organs. Using differential expression (DE) analysis and weighted gene co-expression network analysis (WGCNA), we identified crucial genes marking the transitions between developmental stages, and hub genes in co-expression modules that are strongly associated with these developmental stages. Our results support the potential functional conservation of key genes in early floral development that have been identified in other systems, but also revealed a number of previously unknown or overlooked loci that are worthy of further investigation. In addition, our results highlight not only the dynamics of transcriptional regulation during early floral development, but also the potential involvement of the complex, essential networks of small RNA and post-translational regulation in this process.

MATERIALS AND METHODS

Plant materials: growing conditions and dissection

Seeds of *Aquilegia x coerulea* 'Kiragami' were purchased from Swallowtail Garden Seeds (Santa Rosa, CA, USA). Seeds were germinated in wet soil and seedlings were grown under conditions of 16h daylight at 18°C and 8 h dark at 13°C. Once the plants developed approx. six true leaves, they were transferred into vernalization conditions (16h daylight at 6°C and 8h dark at 6°C) for three to four weeks, and subsequently moved back to the regular growth condition. Once the inflorescences started to develop, axillary FMs were quickly dissected on ice using surgical needles and flash frozen in liquid nitrogen. Three sepals were removed from every floral bud collected.

Scanning electron microscopy

Floral buds were dissected using the same method as above, fixed in FAA (10% formaldehyde, 50% ethanol, 5% acetic acid), and stored at 4°C. Prior to imaging, samples were dehydrated through a graded ethanol series to 100% and then critical point dried with CO₂ (Autosamdri-815, Tousimis, MD, USA). Images were taken with the JSM-6010 LC Scanning Electron Microscope (JEOL, MA, USA) at the Arnold Arboretum of Harvard University.

RNA extraction, library construction, and sequencing

The total RNA of all samples was extracted using the RNeasy Micro Kit (Qiagen, Netherlands). The integrity of extracted RNA was measured by using a 2200 TapeStation (Aligent Technologies, CA, USA). Subsequently, each RNA sample was diluted to a concentration of 1.25 ng/μl, measured by using Qubit RNA HS Assay Kit (Thermo Fisher Scientific, MA, USA). Sequencing libraries were prepared by the Bauer Core facility of Harvard University using the SMART-Seq v4 Ultra Low Input RNA Kit (Takara Bio USA, Inc., CA, USA) for cDNA synthesis and Illumina Nextera XT (Illumina) for library preparation. Libraries were fragmented to an average size of 350 bp. Library concentrations were examined using a Qubit 2.0 (Thermo Fisher Scientific, MA, USA) and qRT-PCR, and the insert sizes measured using a Bioanalyzer 2100 (Aligent Technologies, CA, USA). Libraries were then pooled and diluted to a final concentration of 3 nmol. Sequencing was conducted at Novogene (Beijing, China) using the 150 bp paired-end Illumina HiSeq4000 sequencing platform.

Mapping reads to the reference transcriptome

The raw sequencing reads were filtered by removing adapters and low-quality reads using Trim Galore v0.6.5 (Krueger, 2020) (quality Phred score cutoff = 20) and mapped to the *Aquilegia x coerulea* ‘Goldsmith’ v3.1 reference transcriptome (<https://phytozome.jgi.doe.gov/>) using Kallisto

v0.46.1(Bray *et al.*, 2016). Raw and processed reads are deposited under the GEO accession number GSE158507.

Differential expression (DE) analysis

Read counts and transcript per million reads (TPMs) were generated using the R package tximport v1.0.3 and the lengthScaledTPM method (Soneson *et al.*, 2015). Lowly expressed transcripts were filtered based on analyzing the mean-variance trend, and transcripts with more than 1 counts per million reads in at least one of the 32 samples were retained. Reads were normalized using the variance stabilizing transformation (VST) method to perform principal component analysis (PCA). Differential gene expression analysis was conducted following the DESeq2 R package v1.28.1(Love *et al.*, 2014). For DE genes, the log₂ fold change of gene abundance was calculated between pairwise groups, and the significance of expression changes was determined using the Student's *t*-test. P-values were adjusted with the Benjamini-Hochberg Procedure to correct for the false discovery rate (Benjamini & Yekutieli, 2001). A gene was considered to be significant if it had adjusted p-value < 0.05 and log₂ fold change ≥ 1 . A heatmap of all DE genes was produced using the R package ComplexHeatmap v2.2.0. Hierarchical clustering was used to partition the DE genes into two clusters with Euclidean distance and ward.D2 clustering algorithm.

Gene ontology (GO) enrichment and Kyoto Encyclopedia of Genes and Genomes (KEGG) pathway analysis

Gene Ontology (GO) analysis for DE groups and WGCNA modules of interest was calculated using agriGO v2 (<http://systemsbiology.cau.edu.cn/agriGOv2/>) (Du *et al.*, 2010; Tian *et al.*, 2017) and the KEGG pathway analysis(Kanehisa & Goto, 2000; Kanehisa *et al.*, 2016) was performed using the DAVID Bioinformatics Resources 6.8 (<https://david.ncifcrf.gov/>) (Huang *et*

al., 2009a,b). For both analyses, the identifiers of the top-hit *A. thaliana* loci were obtained from the *A. coerulea* “Goldsmith” v3.1 reference genome annotation (<https://phytozome.jgi.doe.gov/>), all of the expressed genes in the *Aquilegia* RNA-seq data were used as the background reference.

Enrichment in GO terms or pathways was calculated with Fisher’s exact test, and p-values were adjusted for the false discovery rate using the Benjamini-Hochberg procedure. The minimum number of mapping entries for a GO category was set to be 5, and the count threshold for KEGG pathway analysis was set to be 2. Enrichment figures were produced using the R package ggplot2.

WGCNA

Weighted gene correlation network analysis (WGCNA) (Langfelder & Horvath, 2008) was constructed using the R package WGCNA v1.68 following the package tutorials; the illustrated workflow is shown in Fig. S1. To avoid noise from lowly expressed genes, all genes that had read counts less than 10 in more than 90% of the samples (i.e. 29 samples) were removed. The expression of the resultant 18303 genes was then normalized using the varianceStabilizingTransformation function from the R package DESeq2 (Love *et al.*, 2014). The adjacency matrix was calculated using a soft thresholding power of 5. Compared to a hard threshold, of which the correlation values above or below are considered to be connected or not, respectively; the soft threshold is used to raise the correlation to a power so that the difference between strong and weak correlations are exaggerated rather than defined into binary terms. The topological overlap matrix was calculated using a deepSplit value of 4, minModuleSize was set to 20, and mergeCutHeight was set to 0.2. Node and edge information of modules of interest were exported using the exportNetworkToCytoscape function of the WGCNA package. The node and edge files were then transformed into .json format using the R package jsonlite v1.6.1, and visualized using customized scripts modified based on the D3 JavaScript library.

Gene phylogenies

Neighbor-joining phylogenetic trees for genes that are discussed in the main text were constructed if the homologs in *A. coerulea* and *A. thaliana* were not each other's reciprocal top BLAST hits. Potential homologs of the genes of interest were identified from the genomes of diverse species on Phytozome, all amino acid sequences were aligned using ClustalW (Larkin *et al.*, 2007) and the neighbor-joining trees were constructed using MacVector v17.5.5 (Gary, NC, USA).

RESULTS AND DISCUSSION

Developmental stages and sequencing information for transcriptome profiling

In order to finely dissect and capture the transcriptional dynamics during early phases of *Aquilegia* floral development, we defined four developmental stages for RNA sequencing (Fig. 2.1d). At stage 1 (s1), the dome of the FM is round and visible, and stamen primordia are in the progress of initiating. At stage 2 (s2), all the stamen and staminode primordia have completed initiation, the five carpel primordia are about to initiate, and the apex of the floral bud is star-shaped and flattened. At stage 3 (s3), the outer rim of each carpel primordium is elevated but the development of carpel primordia has not consumed all the cells of the apex, and the stamen and staminode primordia are still morphologically indistinguishable. At stage 4 (s4), the carpel primordia continue to develop and elongate, all the cells in the apex have been consumed by carpel development, and the staminode primordia have started to expand laterally, making them morphologically distinct from the stamen primordia.

A total of 72 floral buds were dissected from 30 individual plants for RNA extraction. For s1, s2, and s3, each biological replicate contained two floral buds from two individuals, while s4 contained one floral bud per biological replicate (Fig. 2.1d). The amount of total RNA per extraction

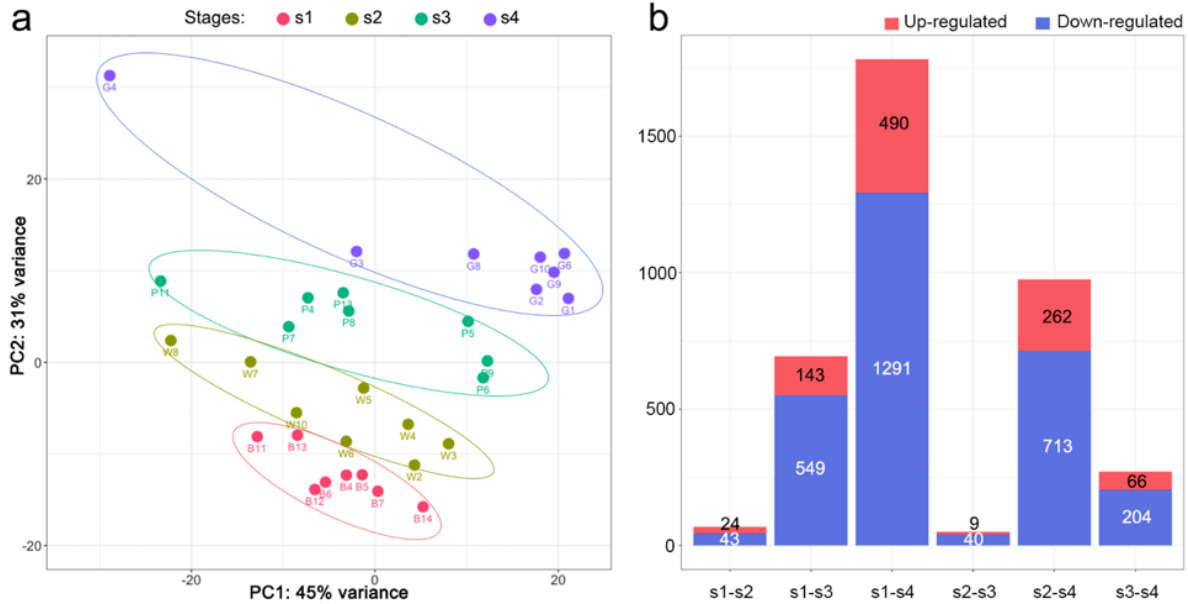


Figure 2.2. PCA of normalized reads of all samples (a) and bar plot summary of DE genes between developmental stages (b).

varied from 20.2 ng to 138 ng. After quality assessment, eight samples at each stage with the best RNA qualities were used for subsequent library construction. All 32 selected samples had RNA integrity numbers higher than 8.9.

A total of 993.64 million raw reads (323.1G raw data) were generated from the 150 bp paired-end Illumina HiSeq4000 sequencing platform. The number of reads generated per sample ranged between 25 million to 36 million (Fig. S2), and the average reads per developmental stage ranged from 29.3 million to 32.9 million (Fig. S2). After filtering reads by quality (Phred score cutoff = 20), the fraction of reads retained ranged from 80.2% to 88.4% (Fig. S2). Retained reads were then mapped to the *Aquilegia x coerulea* ‘Goldsmith’ v3.1 reference transcriptome, generating on average 17.6x to 19.8x sequencing coverage per developmental stage (Fig. S2), and a total of 30023 raw transcripts were mapped. Subsequently, lowly expressed transcripts were filtered if a transcript had less than 1 million read count in more than 31 samples, which resulted in 20473 expressed genes in all samples. To conduct a preliminary exploration of the 32 samples, normalized reads of all samples

were used to perform a principal component analysis (PCA; Fig. 2.2a). The two primary PCs explained 76% of the total variance among all samples and a clear clustering by developmental stages was observed (Fig. 2.2a).

Differential expression analysis between developmental stages

To identify genes that were significantly differentially expressed (DE) between developmental stages, the log₂ fold change of the gene abundance was calculated between different stages. A gene was considered DE if it had an adjusted p-value of <0.05 and an absolute value of log₂ ratio ≥1. A total of 1944 DE genes were identified, with more genes upregulated at s4 compared to any other developmental stage (Fig. S3; Supp. Data 1). For each pairwise comparison, there were consistently more genes down-regulated at the earlier stage relative to the later stage (Fig. 2.2b; Supp. Data 1).

A small number of DE genes, 67 and 49, were identified when comparing s1 to s2, and s2 to s3, respectively. Among these 67 and 49 DE genes, only five loci (Table S1) appeared in both comparisons, suggesting that although s2 appeared to be transcriptionally similar to both s1 and s3, the similarities lay in different aspects in each comparison. One of the five genes in common, *Aqcoe7G234000*, is the homolog to the *ARABIDOPSIS HISTIDINE PHOSPHOTRANSFER PROTEIN 6* (*AHP6*). It is also the top DE gene that is significantly up-regulated in s1 compared to s2, and among the top DE genes that are up-regulated at s2 compared to s3 (Table S1). In *A. thaliana*, *AHP6* is one of the key genes mediating crosstalk between the auxin and cytokinin signaling pathways, and participates in a number of crucial developmental processes, including specifying the founder cells for lateral roots, protoxylem, and procambium (Chandler & Werr, 2015). In shoot apical meristems (SAMs), inflorescence meristems (IMs), and FMs, *AHP6* is involved in the patterning of phyllotaxy and organ initiation (Besnard *et al.*, 2014a, b, p. 6; Chandler & Werr, 2015).

In particular, the AHP6 protein functions non-cell-autonomously to create a cytokinin-signaling inhibition field that contributes to the robustness of the auxin-signaling inhibition field for phyllotaxy and organ patterning (Besnard *et al.*, 2014a). We hypothesize that the *AHP6* homolog in *Aquilegia* is functionally conserved since the expression level of *AqAHP6* sharply declines as organ initiation ceases during the progression of s1 to s4 (Fig. S4)

Among the 24 genes that were found to be significantly up-regulated at s1 relative to s2, *Aqcoe3G399500* is the top DE gene after *AqAHP6* (Table S1). The *A. thaliana* homolog of this locus is *PERLANTHIA* (*PAN*), which has been shown to regulate floral architecture and directly activate the expression of the C-class gene *AGAMOUS* (*AG*) (Maier *et al.*, 2009). Homologs of other genes that specify meristem and organ primordia boundaries during early floral development also appeared to be significantly up-regulated at s1, including *CUP SHAPED COTYLEDON3* (Hibara *et al.*, 2006) (*AqCUC3*; *Aqcoe6G165500*) and *HANABA TARANU* (Ding *et al.*, 2015) (*AqHAN*; *Aqcoe5G190300*), as well as loci that are known to regulate floral organ size and growth, such as *STERILE APETALA* (Li *et al.*, 2018) (*AqSAP*; *Aqcoe1G384300*) and *AINTEGUMENTA-like 6* (Krizek, 2009) (*ATL6/PLT3*; *Aqcoe6G092100*).

Interestingly, two key genes controlling stomata development in various plant lineages, *AqMUTE* and *AqEPF1* (Torii, 2015; Hepworth *et al.*, 2018), were both expressed at very low levels at s1, but significantly up-regulated in s2 followed by consistent high expression at later stages (Fig. S4). This may suggest that although s1 sepals have already achieved reasonable sizes, stomatal development does not initiate until s2. Other genes that were shown to be up-regulated in s2 compared to s1 include the adaxial identity gene *AqCRC*, which is consistent with previous studies showing that strong *AqCRC* expression coincident with the initiation of the carpel primordia (Meaders *et al.*, 2020).

The top DE gene that is up-regulated in s2 relative to s3, *Aqcoe7G055500*, encodes a non-specific serine-threonine kinase with a predicted RNA-binding domain, which does not appear to be a member of any of the better-known serine-threonine classes (Hardie, 1999). Its homolog in *A. thaliana*, *AT5G51800*, has not been studied functionally but is highly expressed in the shoot apex, inflorescence meristem, developing carpels, and stigma (Arabidopsis eFP Browser 2.0). However, this gene is highly expressed at s2 in the current study, in which the FM has just completed organ primordia initiation, and it will, therefore, be interesting to examine its function in early *Aquilegia* floral development.

Gene ontology (GO) analysis of DE genes revealed a wide range of enrichment terms for every DE comparison except for [s1 vs. s2] and [s2 vs. s3], likely due to the small numbers of DE genes in these two comparisons, as mentioned above (Supp. Data 2). In general, there seems to be a large portion of overlap in GO terms in DE genes that were up- or down-regulated during early stages compared to later stages (Fig. 2.3a). For instance, GO terms that are related to organ formation, patterning, and development are enriched for DE genes that are up-regulated at s1 and s2. On the other hand, genes that are up-regulated at s3 and s4 are heavily enriched in metabolic and enzymatic activities, including active transmembrane transportation, carboxylesterase activity, oxidoreductase activity, and glucosyltransferase activity, all of which are involved in broader metabolic processes during plant development.

Subsequently, we conducted KEGG pathway enrichment analysis with the DE genes, and we observed a similar pattern for genes that are up-regulated in s4, in that they participate in various metabolic pathways (Fig. 2.3b). For instance, genes involved in nitrogen metabolic pathways are up-regulated and enriched in s4, indicating active amino acid biosynthesis and protein synthesis at s4 compared to earlier developmental stages. On the other hand, all the genes that are up-regulated at

the earlier stages in each DE comparison are almost exclusively enriched in plant hormone signal transduction pathways (Fig. 2.3b).

We then examined the hormonal signaling pathways that were enriched for each DE list, which revealed several interesting points (Fig. 2.3c). Firstly, all DE lists contained genes in the auxin signaling pathways. The DE genes up-regulated in s1 compared to s4 included genes in all major components in auxin signaling, while all other DE lists only showed enrichment in a few components in the pathway. This indicates a gradual decrease in the number of highly expressed auxin signaling genes from s1 to s4. Secondly, as mentioned previously, *AqAHP6* appeared to be differentially expressed at the earlier stages in all DE comparisons, which was also captured by the KEGG pathway analysis as enriched in AHP family members. Besides *AqAHP6*, homologs of the Arabidopsis Response Regulator (ARRs) proteins were shown to be up-regulated in s1 compared to s4, and ARRAs are downstream of AHPs in the cytokinin signaling pathway, which emphasizes the decrease in cytokinin signaling from s1 to s4. Thirdly, genes that are up-regulated at s1 compared to s4 are detected from the abscisic acid, brassinosteroid, and salicylic acid signaling pathways, suggesting a complex interplay between multiple plant hormone pathways during the early stages of floral development.

We profiled the expression of type-II MADS-box genes (Pabón-Mora *et al.*, 2013; Sharma & Kramer, 2014) and class-I KNOTTED-like homeodomain (KNOX) genes (Yant *et al.*, 2015), because many members of these families are known to play important roles during early floral development, along with additional homologs of genes involved in FM identity and maintenance (Fig. 2.4). Among the type-II MADS-box genes, the C-class gene *AqAG2* and *AGAMOUS-LIKE 12* (*AqAGL12*) showed a significant increase in the expression levels from s1 to s4. This might be expected for *AqAG2*, which is known to be strongly expressed in carpels (Kramer *et al.*, 2007), but

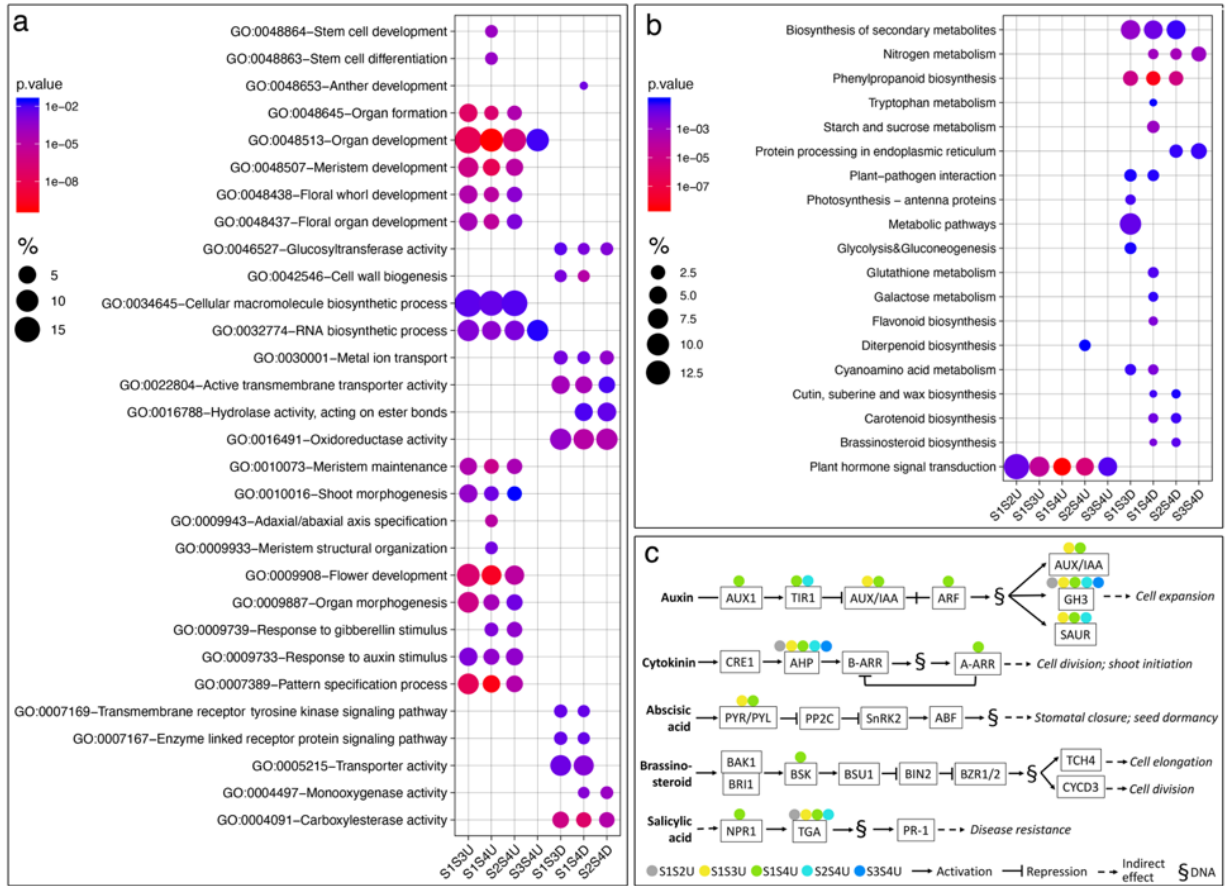


Figure 2.3. GO term and KEGG pathway enrichment analysis of DE genes. (a) Selected enriched GO terms from different DE comparisons. (b) Selected enriched KEGG pathways from different DE comparisons. (c) Enriched plant hormone signal transduction pathways from different DE comparisons. % in a and b were calculated as: number of genes that hit the specific GO term or KEGG pathway/total number of genes in the input DE list*100. Each DE comparison is noted as: earlier stage vs. later stage, up- (U) or down (D)-regulated at the earlier stage.; for instance: S1S2U means genes that are DE between s1 and s2 and are up-regulated at s1.

expression of *AqAGL12* has not previously been investigated in *Aquilegia*. While the majority of the MADS-box genes showed a decrease in their expression levels from s1 to s4, this trend was only significant for *SUPPRESSOR OF OVEREXPRESSION OF CONSTANS 1* (*AqSOC1.1*), *FRUITFULL-LIKE 2* (*AqFL2*), *SEPALLATA1* (*AqSEP1*) and *APETALA3-3* (*AqAP3-3*) (Fig. 2.4). Similarly, most of the class-I KNOX genes and FM-related genes showed the highest expression levels at s1 with a decrease at subsequent stages, but *AqKXL3* appeared to be expressed at the highest levels at s2 (Fig. 2.4).

Since the meristem stages we sampled captured the transition from organ primordia initiation to FM termination (i.e. the end of organogenesis), we also examined the expression of the homologs of genes in the known FM termination pathways (Sun *et al.*, 2009, 2014, 2019; Yamaguchi *et al.*, 2017, 2018; Bollier *et al.*, 2018) (Fig. 2.4). Interestingly, several lines of evidence suggest limited conservation of these pathways, particularly the *KNU-WUS* pathway, between *A. thaliana* and *A. coerulea*. In *A. thaliana*, *KNU* has been shown to be essential in terminating the expression of *WUS* in the FM, and continuous expression of *KNU* appeared to be necessary to maintain the suppression of *WUS* via both transcriptional suppression and heterochromatinization (Sun *et al.*, 2019), but the expression of *AqKNU* (Fig. S4, S6) decreased after s2. Furthermore, *KNU* and *SPLAYED* (*SYD*) function antagonistically by competing for a binding site in *WUS* promoter, but *AqKNU* and *AqSYD* showed similar, rather than the opposite, patterns of expression over s1 to s4 (Fig. S4). Additionally, FERTILIZATION-INDEPENDENT ENDOSPERM (*FIE*) is a key polycomb repressive complex2 component, which has been shown to physically interact with *KNU* to deposit repressive H3K27me3 marks and maintain the stable silencing of *WUS* in later developmental stages (Sun *et al.*, 2019). Unlike what was observed in silencing *FIE* expression in *A. thaliana*, however, a previous study has shown that the silencing of *AqFIE* did not lead to indeterminacy in the flowers (Gleason & Kramer, 2013). MINI ZINC FINGER2 (*MIF2*) was shown to be a component of a protein complex together with *KNUCKLES* (*KNU*), *TOPLESS* (*TPL*) and *HISTONE DEACETYLASE-like 19* (*HDA19*) to suppress the expression of *WUS* in the FM (Bollier *et al.*, 2018), but the read counts of the *MINI ZINC FINGER2* (*MIF2*) homolog were extremely low in all sample of all stages and this gene is considered as not expressed in our dataset. Besides the *KNU-WUS* pathway, *TORNADO2* (*TRN2*) functions downstream of *CRC* in coordinating FM termination and carpel primordia formation in *A. thaliana* (Yamaguchi *et al.*, 2017), but phylogenetic

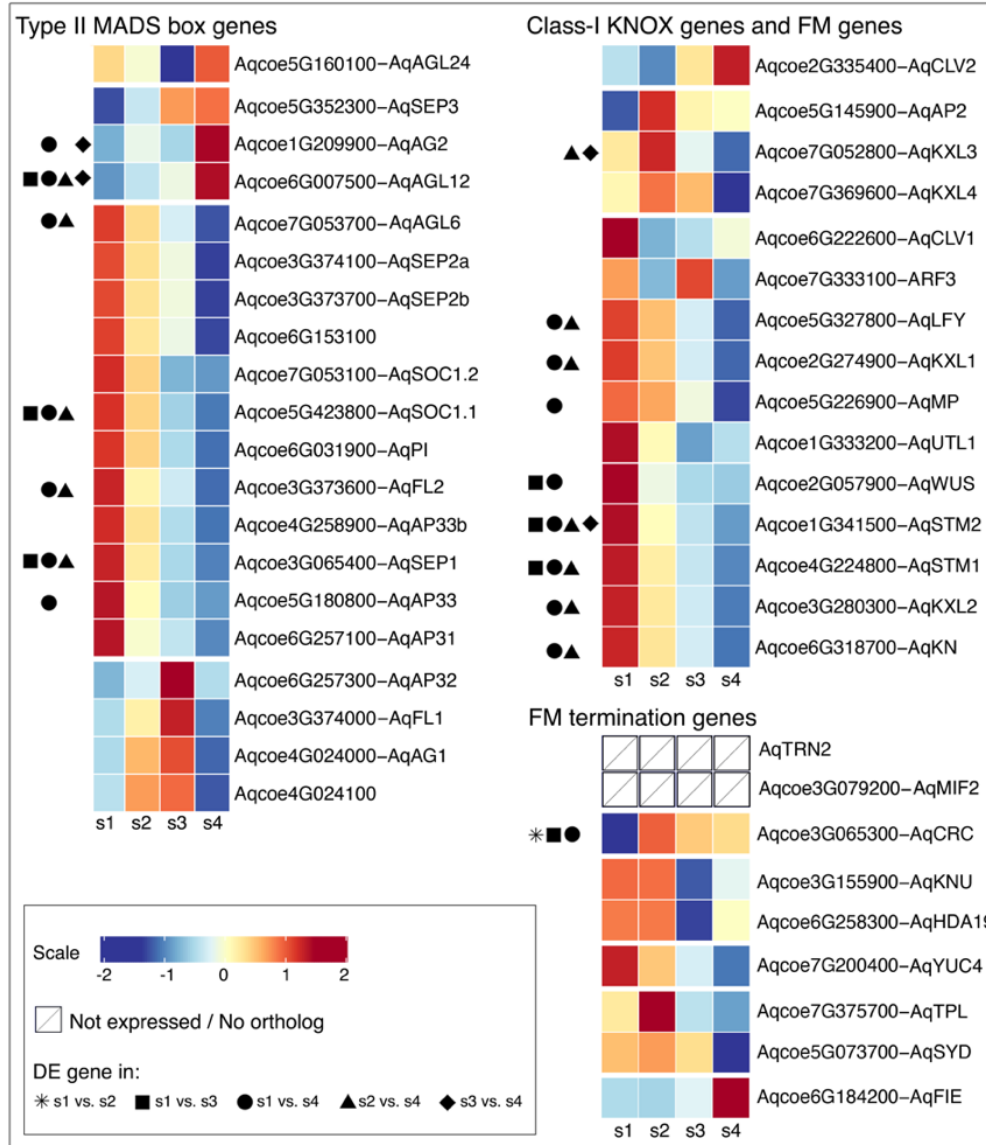


Figure 2.4. Expression profiles of type-II MADS-box genes, class-I KNOX genes, and genes involved in FM maintenance and termination pathways. Expression levels of each gene over the developmental stages were scaled as the average expression of all biological replicates per stage subtracted by the average expression of all replicates of all stages, then divided by the standard deviation of the expression of all replicates of all stages. DE genes were indicated with symbols of each DE comparison.

analysis did not recover any ortholog of *TRN2* the *Aquilegia* genome (Fig. S5). These findings suggest that the *A. thaliana* mechanisms controlling FM termination are not well conserved in *Aquilegia*.

Gene co-expression analysis, identification of module hub genes, and network construction of modules of interest

The DE analysis provided us with a good starting point of what genes might be functionally relevant to a certain developmental stage based on the changes in their expression levels, but a strong limitation for DE analysis is that each gene is considered in isolation while in reality, genes and gene products function in networks. In order to discover co-expressed genetic modules that are significantly associated with different stages during early floral development in *Aquilegia*, we conducted weight gene co-expression network analysis (WGCNA) using the RNA-seq data (refer to Fig. S1 for an illustrated workflow). Using a soft threshold power = 5 (Fig. S7), a total of 24 co-expression modules were constructed from 18303 genes, with the smallest module (darkgrey) containing 21 genes and the largest module (turquoise) containing 6206 genes (Fig. 2.5a). Subsequently, we looked at the association between the modules and the four developmental stages by correlating the eigengene value (i.e. a value equivalent to the first component of the module; a singular value decomposition to summarize the expression levels of all genes in that module) of the modules with the stages. Among the 24 modules, we determined three modules to be of particular interest based on their correlation (Fig. 2.5a) and close distance in the hierarchical dendrogram clustering (Fig. 2.5b): the green module for its strong association with s1, and the brown and magenta modules for their strong association with s4. We will refer to the modules as green-s1, brown-s4, and magenta-s4 hereafter for clarity.

To obtain a broad overview of genes in the three modules of interest, we performed GO and KEGG pathway analysis on these modules (Fig. 2.5c; Supp. Data 2). GO analysis revealed that although the green-s1 module has a moderate size (781 genes) compared to other modules, it has the largest number of enriched GO terms, most of which are specific to early floral developmental stages, such as stem cell/meristem maintenance and development, axis specification, and organ

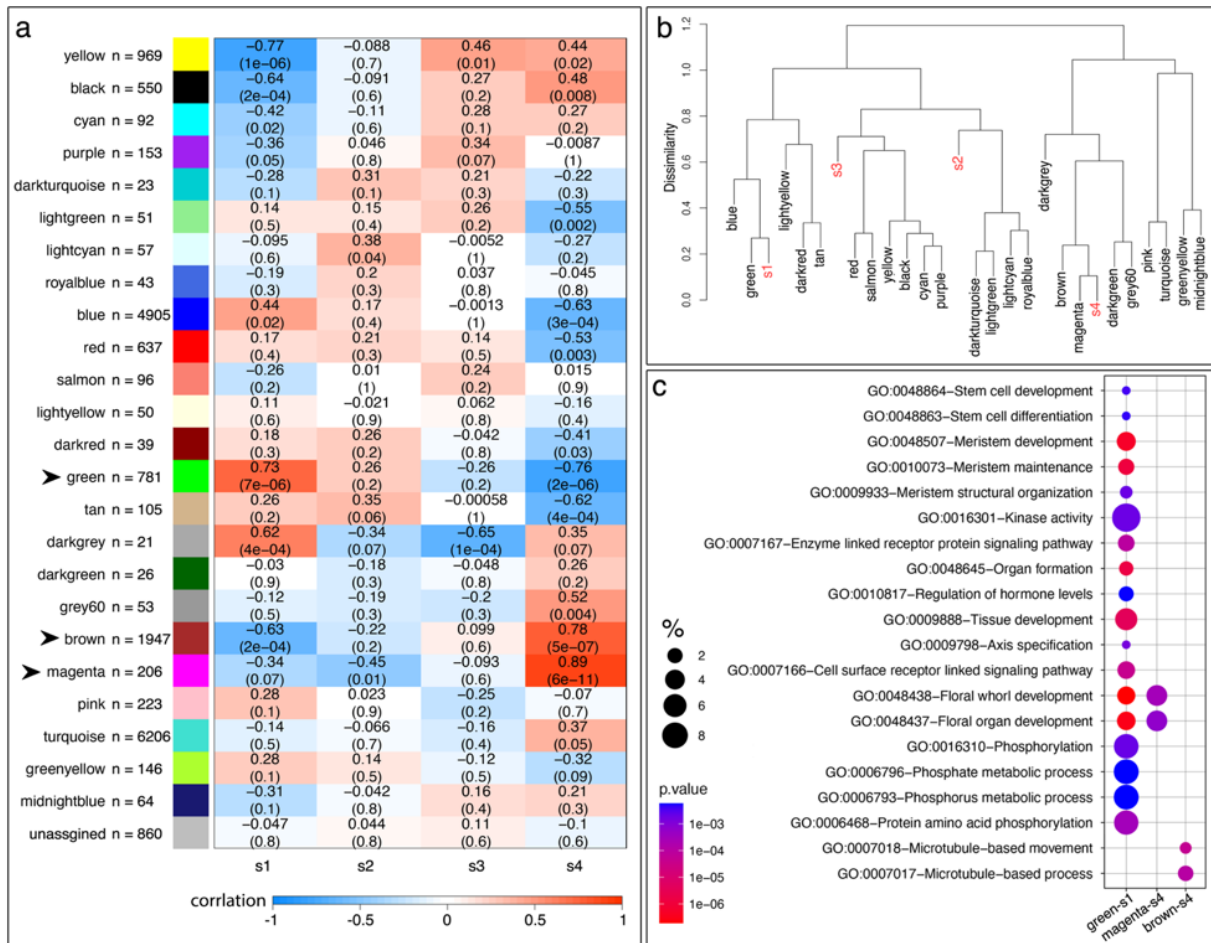


Figure 2.5. Associating gene co-expression modules with developmental stages. (a) Correlation between module eigengene values and the developmental stages. The first number in each cell represents the correlation value, and the second number in the parenthesis represents the p-value of the correlation. Arrowheads pointed to modules of interest. (b) Hierarchical clustering dendrogram of the eigengenes of modules and the developmental stages. (c) Selected GO term enriched from modules of interest. % was calculated as: number of genes hit the specific GO term/total number of genes in the input list*100.

formation (Fig. 2.5c; Supp. Data 2). On the other hand, the brown-s4 module has a relatively large number of genes (1947 genes) but only two highly related cellular process GO terms are found to be significant, microtubule-based processes and movement (Fig. 2.5c; Supp. Data 2). The magenta-s4 module also shows strong and significant association with s4, but genes in this module are enriched in “floral whorl” and “floral organ development”, particularly in androecium, perianth, and gynoecium development (Fig. 2.5c; Supp. Data 2). This suggests that the WGCNA has identified

modules that are significantly associated with different aspects of floral development at s4: genes in the brown-s4 module appear to be focused on the rapid growth of all floral organs in s4, in which active mobilization of the microtubules is necessary for rapid cell expansion; while genes in the magenta-s4 module are specific to the elaboration and maturation of each floral organ identity.

KEGG analysis revealed that the green-s1 and brown-s4 modules both contain genes that are involved in the starch and sucrose metabolism pathways (Supp. Data 2). In addition, genes in the green-s1 module are significantly enriched in the plant hormone signal transduction pathways, and genes in the brown-s4 module are significantly enriched in several sugar metabolic pathways, including fructose and mannose metabolism, and amino sugar and nucleotide sugar metabolism (Supp. Data 2). Sugar metabolism has been implicated in various aspects of plant development, especially the amino sugar and nucleotide sugar interconversion pathways that are required for cell wall biosynthesis (Seifert, 2004). Together with the GO enrichment in microtubule-based movement and processes for module brown-s4, this again emphasizes the initiation of rapid organ growth during s4 of floral development in *Aquilegia*. No pathway enrichment was found for genes in the magenta-s4 module, possibly due to the small module size.

Subsequently, we identified the potential hub genes of each module of interest based on the value of signed module membership (MM) and trait significance (TS). The former describes the correlation between a gene and the eigengene value of a module, while the latter describes the correlation between a gene and the trait of interest; the potential hub genes of a module should have significant and strong correlations with both MM and TS (Fig. S1; S8). We, therefore, defined the hub genes as having their absolute values of MM and TS above the 90th percentile of the distribution of MM and TS of all the genes of the module. This approach identified 33, 56, and 14 hub genes for the green-s1, brown-s4, and magenta-s4 modules, respectively (Fig 2.6; Table S2). Moreover, although every gene is connected to all other genes in a module, the strengths of the connection

between gene pairs vary and the hub genes, by definition, should have the strongest values of connectivity. To better visualize the gene co-expression networks of each module, we only retained the edges that have the highest weight values (i.e. having the strongest connectivity) with the hub genes in the network for visualization (Fig. S8; Fig. 2.6-2.8). To facilitate navigation among a group of highly interconnected genes (particularly in the case of the green-s1 and brown-s4 modules), we moved all the genes with the largest numbers of connections to the periphery of the visualized network and thus genes left in the center of the network had fewer connections compared to those of at the periphery.

Hub genes of the green module revealed new candidate genes associated with s1 floral development

The green-s1 module contains 33 potential hub genes and 17 of these encode transcription factors (TFs). The homologs of many of these TF-coding genes are involved in early FM and floral development, such as class-I KNOX genes (*AqSTM1*, *AqSTM2*, *AqKXL2*), *AqAS1*, *AqSEP1*, *AqPAN*, and the homologs of *CUP SHAPED COTYLEDON3* (*Aqcoe6G165500*; *AqCUC3*), *HOMEODOMAIN-BOX-3* (*Aqcoe1G245800*; *AqHB3*), *PHABULOSA* (*Aqcoe1G178700*; *AqPHB*), *LATERAL SUPPRESSOR* (*Aqcoe1G411100*; *AqLAS*), *BLADE ON PETIOLE2* (*Aqcoe2G033300*; *AqBOP*), and *STERILE APETALA* (*Aqcoe1G384300*; *AqSAP*). Of these, *AqPAN* also showed the strongest association with s1 (Table S2).

Interestingly, although all the potential hub genes have similarly high MM and TS values (Table S2), the number of edges connected to the hub genes in the network appeared to be highly variable (Fig. 2.6), indicating a hierarchy of connectedness even among the hub genes. For instance, we have identified nine hub genes that have a strong negative association with the module and the s1 developmental stage (Table S2), but all of them except one (*Aqcoe4G281800*) have only a few

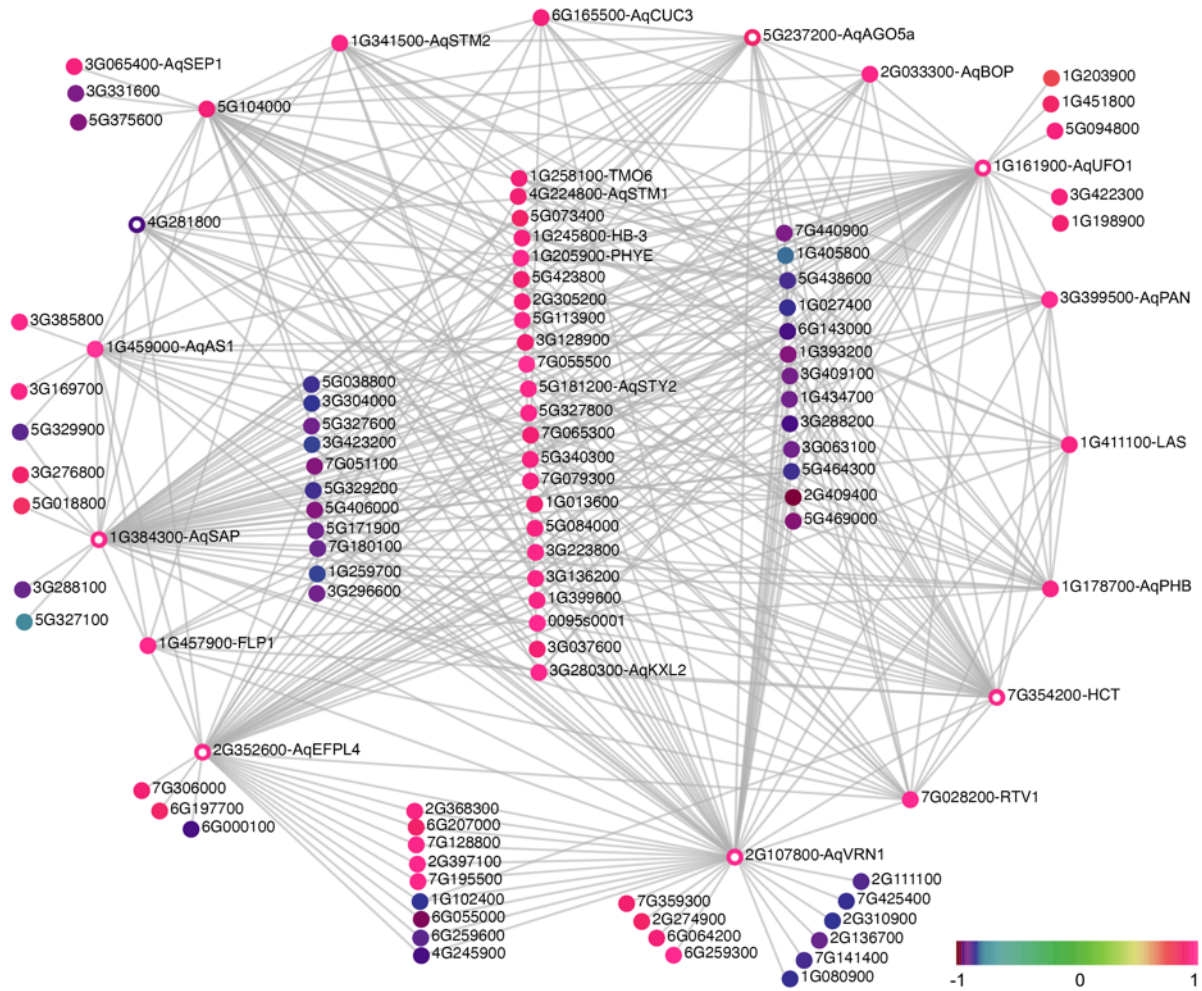


Figure 2.6. Gene network of module green-s1. Color scale represents the value of MM for each gene. The “Aqcoe” prefix of a gene identifier was removed to facilitate the visualization. All the genes with the largest number of connections are at the periphery of the network (i.e., genes in the center have fewer connections compared to genes at the periphery). Genes that are presented as colored circles (instead of a solid dot) are genes that were discussed in the main text.

edges connecting them with other genes in the network (and thus were not placed in the periphery of the network). *Aqcoe4G281800* encodes a wax synthase that is involved in constructing cell walls, and also only has a moderate number of edges compared to the those associated with other periphery hub genes. By contrast, the five periphery hub genes with the largest number of edges are (Fig. 2.6): *AqVRN1* (*Aqcoe2G107800*, homologous to *VERNALIZATION1*, *VRN1*, in *A. thaliana*); *AqHCT* (*Aqcoe7G354200*, codes for a hydroxycinnamoyl-Coenzyme A shikimate/quinic

hydroxycinnamoyltransferase, HCT); *AqUFO1* (*Aqcoe1G161900*; UNUSUAL FLORAL ORGANS1; Sharma *et al.*, 2019b), *AqSAP*; and *AqEPFL4* (*Aqcoe2G352600*, homologous to EPIDERMAL PATTERNING FACTOR-LIKE4, *EPFL4*, in *A. thaliana*). The functional implications of some of these loci are unclear. For instance, *A. thaliana* *VRN1* belongs to the AP2/B3-like transcriptional factor family, and its function is primarily understood to be the regulation of the vernalization locus *FLOWERING LOCUS C* (*FLC*; Bastow *et al.*, 2004). However, although *Aquilegia* does require vernalization to flower (Ballerini & Kramer, 2011), it lacks an *FLC* homolog (Sharma *et al.*, 2019a), and *AqVRN1* is expressed in the early FM (Fig. S4), which differs considerably from the broad expression of *AtVRN1* in various organs and developmental stages of *A. thaliana* (Levy, 2002; Bastow *et al.*, 2004). The potential role for *AqHCT* is equally enigmatic, as the enzyme appears to function in phenylpropanoid biosynthesis, a pathway that supports highly diverse cellular functions (Hoffmann *et al.*, 2004).

Luckily, the remaining hub genes are better understood. Homologs of *UFO* encode F-box proteins that generally function with *LEAFY* (*LFY*) homologs to promote FM identity and activate B-class gene expression across diverse dicot model systems (Lee *et al.*, 1997; Samach *et al.*, 1999; Durfee *et al.*, 2003; Levin & Meyerowitz, 1995; Wilkinson & Haughn, 1995). In *Aquilegia*, the closely related paralogs *AqUFO1* and *AqUFO2* promote the transition from inflorescence to FM identity in conjunction with *AqLFY*, although there is no clear role in B gene activation (Sharma *et al.*, 2019b). In addition to the expected contribution to FM identity, the *AqUFO1/2* paralogs also appear to promote the initiation of the stamen whorls, as whorl number dramatically decreases in silenced flowers from the usual 7-8 whorls to only 4-5. This function is intriguing for several reasons. First, the phenotype is only observed in *AqUFO1/2*-silenced flowers and not with *AqLFY*-silencing, suggesting that this function is specific to the F-box proteins and not a joint function with *AqLFY*. Second, it underscores a critical difference in *Aquilegia* floral development relative to other model

systems in that, like many angiosperm flowers, *Aquilegia* has multiple whorls of stamens. The identification of *AqUFO1* as a critical hub gene in early floral development is consistent with this novel role in promoting stamen initiation and/or continued FM proliferation and points to other loci that may function as novel co-factors for this role.

In *A. thaliana*, *SAP* plays a number of roles, including acting as a cadastral gene that prevents *AG* from entering the perianth whorls, and controlling both inflorescence architecture and ovule development (Byzova *et al.*, 1999). Interestingly, similar to UFO, *SAP* also contains an F-box motif and was recently shown to be a component of an Skp1-cullin 1-F-box (SCF) E3 ubiquitin-protein ligase complex that controls lateral organ size by promoting cell proliferation, a function that has been demonstrated both in *A. thaliana* (Wang *et al.*, 2016) and cucumber (Yang *et al.*, 2018). To date, the only genes that have been identified as the direct targets of the *SAP*-mediated E3 ligase complex are *PEAPOD1/2* (*PPD1/2*), which control organ growth (Wang *et al.*, 2016; Li *et al.*, 2018). The homolog of *PPD1* and *PPD2* in *Aquilegia*, *Aqcoe5G048100*, showed relatively stable expression from s1 to s4 (Fig. S4) and was assigned to the turquoise module (Fig. 2.5). It will be worth investigating whether this interaction is conserved in *Aquilegia* and what may be the other targets of the ligase complex during early floral development.

AqEPFLA belongs to the EPFL gene family that encodes small, secreted cysteine-rich ligands. The best-studied members of the family are the *EPIDERMAL PATTERNING FACTORS1/2*, which are key regulators in stomata development (Torii, 2015). As mentioned above, *AqEPF1* was identified as one of the DE genes that is up-regulated at s2 compared to s1 (Table S1). In contrast, in *A. thaliana* the close homologs *EPFLA* and *EPFL6* have been shown to have distinct functions in inflorescence growth (Abrash *et al.*, 2011; Uchida *et al.*, 2012). However, two very recent studies revealed that *EPFLA* and *EPFL6* are also expressed in the periphery of the shoot apical meristem (SAM) and function redundantly with *EPFL1* and *EPFL2* to regulate the meristem size

and leaf initiation (Kosentka *et al.*, 2019; Zhang *et al.*, 2020). In particular, signaling downstream of EPFL ligands and their receptors confines the WUS-CLV3 pathway to the center of the SAM by inhibiting its expression in the meristem periphery (Zhang *et al.*, 2020). In this regard, it is especially interesting that *AqEPFL4* came out as one of the most connected hub genes in a module that is strongly associated with s1, suggesting that our results provide further evidence for the role of the EPFLs in the meristem homeostasis.

Perhaps the most surprising observation regarding the green-s1 module network is that one gene, *AqAGO5a* (*Aqcoe5G237200*, homologous to *ARGONAUTE5*, *AtAGO5*, in *A. thaliana*; Fig. S9), was not initially identified as a hub gene since neither its MM nor TS values were above the 90th percentile of distributions (Table S2), but it did come up as a potential hub gene in the network visualization due to its strong connections with all the other hub genes. *AGO* genes encode RNA slicers that are involved in post-transcriptional gene silencing by selectively recruiting microRNAs and siRNAs. In *A. thaliana*, *AtAGO5* physically interacts with *miRNA156* and regulates the phase transition from the vegetative to reproductive state of the meristem (Roussin-Léveillé *et al.*, 2019). Other *AtAGO* genes, such as *AtAGO1* and *AtAGO10*, have also been shown to function in establishing polarity in floral organs and regulating meristematic activities in the FM by interacting with *miRNA165/166* (Kidner & Martienssen, 2005; Tucker *et al.*, 2008; Ji *et al.*, 2011; Zhu *et al.*, 2011; Roodbarkelari *et al.*, 2015). Moreover, based on our gene phylogeny (Fig. S9a), the *Aquilegia* genome contains a close paralog of *AqAGO5a*, *Aqcoe2G159700* (*AqAGO5b*), which shares 81.4% of similarity with *AqAGO5a* (Fig. S9b). The expression level of *AqAGO5a* was the highest at s1 and then gradually decreases from s2 to s4, while its paralog *AqAGO5b*, showed very stable expression from s1 to s4 (Fig. S9c). It will thus be intriguing to determine what are the targets of these two close paralogs and the potential functional divergence between them.

The brown and magenta modules captured different aspects of s4 floral development

Interestingly, among the 56 potential hub genes for the brown-s4 module, only three genes code for transcription factors (TFs), and there seemed to be an over-representation of genes coding for key components of the ubiquitination pathways (Table S2). Six out of the 22 hub genes that exhibit a negative association with s4 encode key components in the SCF E3 ligase complexes, including F-box family proteins (*Aqcoe2G310400*, *Aqcoe7G317700*, *Aqcoe7G317600*), RING/U-box family proteins (*Aqcoe7G340300*, *Aqcoe3G311800*), and HCP-like superfamily protein (*Aqcoe5G357900*). In addition, two hub genes that have positive associations with s4 code for a ubiquitin-related protein (*Aqcoe3G298400*) and a subunit of the COP9 complex (*Aqcoe7G310200*), respectively.

The gene network of the brown-s4 module revealed that most of the identified hub genes are highly interconnected to each other and thus are mostly placed at the periphery of the network (Fig. 2.7). One hub gene, *Aqcoe7G340300*, however, appeared to have strong connections not only to most of the other hub genes but also to a large number of additional module members. *Aqcoe7G340300* codes for a RING/U-box type protein and its homologs, *DA2* and *GRAIN WIDTH AND WEIGHT2* (*GW2*) have been functionally studied in *A. thaliana* (Xia *et al.*, 2013) and rice (Song *et al.*, 2007), respectively. Both *DA2* and *GW2* have E3 ubiquitin ligase activity and exhibit conserved functions in regulating organ size by restricting cell divisions in both systems (Dong *et al.*, 2017). The expression level of *Aqcoe7G340300* steadily declined from s1 to s4 (Fig. S4), and if its function in suppressing cell division in lateral organs is conserved, the low expression level at s4 may indicate the onset of cell proliferation in the floral organs.

In contrast to what was observed for the brown-s4 module, in which most of the hub genes were directly connected to each other, the 14 hub genes for the magenta-s4 module were connected to each other via a number of common non-hub genes in the network (Fig. 2.8).

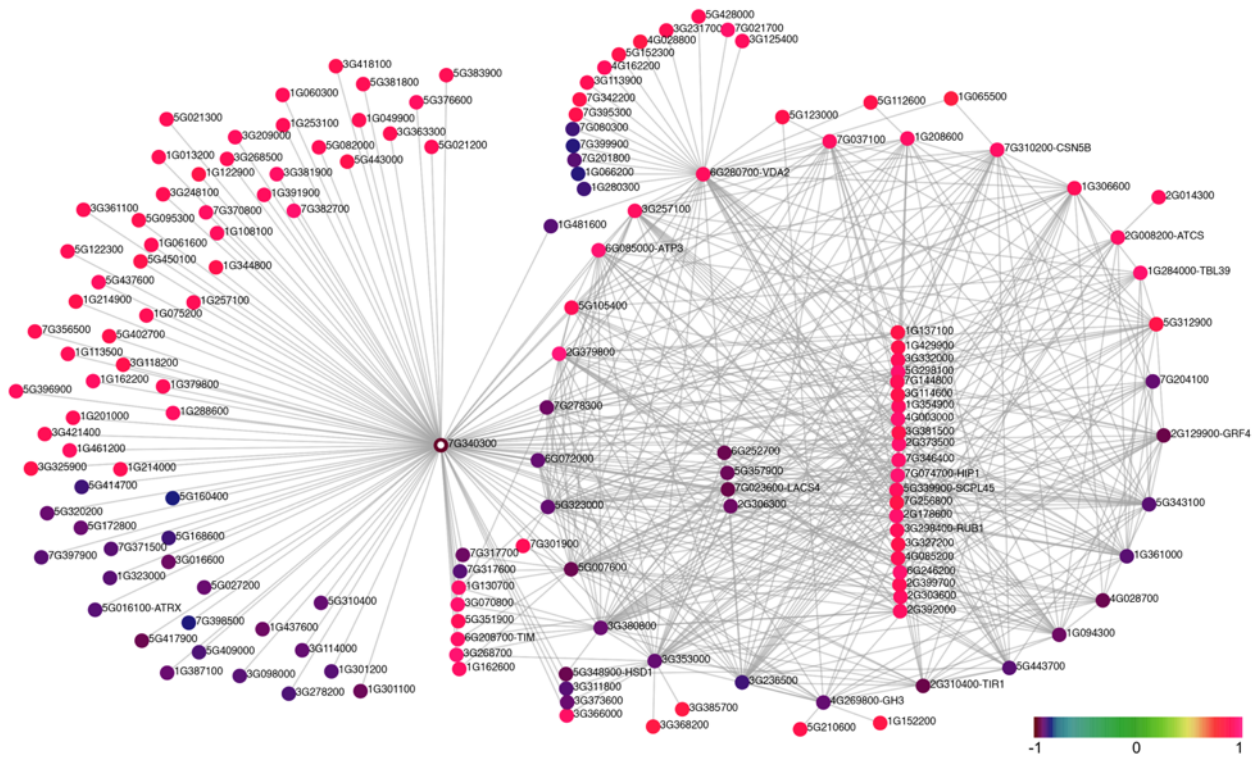


Figure 2.7. Gene network of module brown-s4. Color scale represents the value of MM for each gene. The “Aqcoe” prefix of a gene identifier was removed to facilitate the visualization. All the genes with the largest number of connections are at the periphery of the network (i.e. genes in the center have fewer connections compared to genes at the periphery). Genes that are presented as colored circles (instead of a solid dot) are genes that were discussed in the main text.

Among the magenta-s4 hub genes that have negative MMs, *Aqcoe2G063200* encodes a small ubiquitin-like modifier (SUMO) and is homologous to *SUM2* in *A. thaliana*. Sumoylation mediated by SUMOs is an important post-translational protein modification mechanism in plants and is involved in regulating diverse plant physiological and developmental processes, including flowering time (Park *et al.*, 2011). Interestingly, another hub gene with negative MM, *Aqcoe2G315500*, codes for a copper/zinc superoxide dismutase (CSD) and the protein stability of its *A. thaliana* homolog CSD1 has been shown to be maintained via sumoylation (Chen *et al.*, 2011). This relationship was captured in our network analysis, making their function in early floral development an interesting target for further study. In addition, *Aqcoe5G226900*, the *Aquilegia* homolog of *MONOPTEROS* (*AqMP*) is another magenta-s4 hub gene with expression level that was highest at s1 and then

steadily declining from s2 to s4. In *A. thaliana*, *MP* is critical to maintaining stem cell homeostasis in the SAM (Luo *et al.*, 2018) so this decline is consistent with the cessation of FM proliferation (Fig. 2.4). On the other hand, the homolog of *Aqcoe2G426800*, *EXCESS MICROSPOROCTES1* (*EXS*), is expressed during the differentiation of microsporocytes and tapetal cells and controls the somatic and reproductive cell fates in *A. thaliana* anthers (Canales *et al.*, 2002). If functional conservation is assumed, the sharp increase in the expression of *Aqcoe2G426800* at s4 (Fig. S4) likely marks the beginning of microsporogenesis in *Aquilegia*.

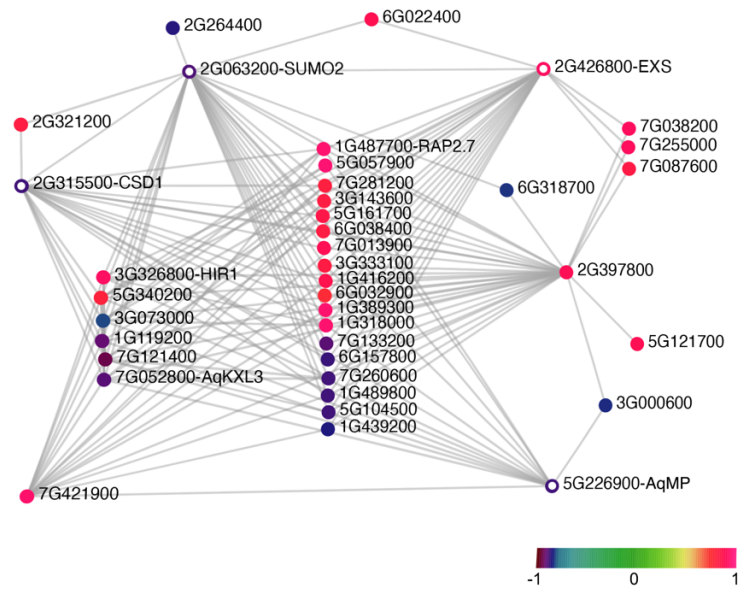


Figure 2.8. Gene network of module magenta-s4. Color scale represents the value of MM for each gene. The “Aqcoe” prefix of a gene identifier was removed to facilitate the visualization. Genes that are presented as colored circles (instead of a solid dot) are genes that were discussed in the main text.

CONCLUSIONS

The current study is the first in-depth transcriptome profiling of early *Aquilegia* floral development. Similar studies at finely dissected stages of early floral development have only been done in the model species *A. thaliana* (Wellmer *et al.*, 2006; Ryan *et al.*, 2015; Klepikova *et al.*, 2016), although analyses have also been performed in tomato SAMs, and early inflorescences of model

monocot species (Lemmon *et al.*, 2016; Feng *et al.*, 2017). In contrast to the previous *A. thaliana* work, the relatively large size of *Aquilegia* FMs allowed us to visually confirm the developmental stage of dissected meristems and perform a large number of biological replicates. Overall, our results reveal similar themes to the *A. thaliana* analyses, with down-regulation of meristem maintenance corresponding to a shift towards primordium proliferation and differentiation. For the developmental window on which we chose to focus, the morphological changes between successive floral developmental stages are subtle, which helped us to tease apart the dynamic transcriptional changes between the stages. In particular, we have uncovered small numbers of DE genes when comparing s1 to s2 (67), and s2 to s3 (49), with only five genes appearing in common between both DE lists (Table S1). These two groups of DE genes mark two important processes during early floral development: the DE genes between s1/s2 appear to correspond to the termination of the FM and the end of organogenesis, while the DE genes between s2/s3 as associated with the onset of floral organ morphogenesis. Analyzing the homologs of known genes in the FM termination pathway (Fig. 2.4) provided evidence that the *A. thaliana* mechanisms are likely not conserved in *Aquilegia*. We have also identified a number of key genes that are likely of importance for different stages of early floral development in *A. coerulea*, including *AqPAN*, *AqSAP*, *AqEFLP4*, and *AqAGO5*, as well as many top DE genes and hub genes for which the homologs have not been studied in *A. thaliana*. Thus, our study is the third study to date to indicate that the EPFLs play a previously overlooked role in the meristem homeostasis (Fig. 2.6), as supported by its identification as one of the core hub genes for the green-s1 module.

In addition, understanding the mechanisms leading to functional divergence of close paralogs is an important component of understanding gene evolution in general. Utilizing DE analysis and WGCNA, we have uncovered evidence of potential functional divergence between the close paralogs of several key genes expressed during early floral development in *Aquilegia*.

These include the close paralogs of *AqSTM1* and *AqSTM2*, *AqUFO1* and *AqUFO2*, and *AqAGO5a* and *AqAGO5b*, of which only *AqSTM2*, *AqUFO1*, and *AqAGO5a* were recovered as core hub genes of the green-s1 module (Fig. 2.6; Table, S2). These observations help to direct future investigations on the mechanisms and consequences of the functional divergence between close paralogs; for instance, whether or not *AqAGO5a* and *AqAGO5b* function in different tissues or have the same miRNA targets.

Finally, our results highlight the dynamics and potential role of several post-transcriptional and post-translational regulatory mechanisms during early floral development in *A. coerulea*. In terms of post-transcriptional regulation, in our network analysis for the green-s1 module, *AqAGO5a* appeared as a hub gene due to its strong connections to all the other hub genes in the network, suggesting an important role in small RNA regulation in s1 (Fig. 2.6). The Argonaute protein family is a critical player in the RNA silencing process as an essential component of the RNA-induced silencing complex (Fang & Qi, 2016). Homologs of the *AGO1/5/10* clade have been studied in *A. thaliana*, rice, tomato, and tobacco, all of which participate in various important aspects in plant development, including regulation of SAM, FM, germ cell development, and stress responses (Jones *et al.*, 2006; Hendelman *et al.*, 2013; Zhang *et al.*, 2015; Fang & Qi, 2016). Nonetheless, small RNA regulation has not yet been explored in *Aquilegia*, making *AqAGO5a* a good starting point for further exploration. It is also clear that post-translational regulation via protein stability plays a major role in the transition from primordium initiation to floral organ morphogenesis in the *Aquilegia* FM. This is supported by the ubiquitination-related hub genes of the brown-s4 module coding for RING/U-box proteins, as well as an abundance of hub genes for both the green-s1 and the brown-s4 modules coding for F-box proteins, which are the components of the SCF E3 ligase complex (Table S2). Some of these genes, such as *UFO* and *SAP*, are long known to participate in floral development in *A. thaliana* (Samach *et al.*, 1999; Durfee *et al.*, 2003; Wang *et al.*, 2016; Li *et al.*, 2018),

but the connection between other F-box coding genes and floral development still needs further investigation. For instance, only recently *BOP2* was discovered to serve as the substrate adaptor in an SCF E3 ligase complex to regulate LFY post-transcriptionally (Chahtane *et al.*, 2018).

Sumoylation is another important post-translational regulation mechanism that stabilizes proteins rather than promoting their turnover, and one of the hub genes for the magenta-s4 module codes for a SUMO (Fig. 2.8; Table, S2). SUMOs have been studied in the context of environmental stress, nitrogen assimilation, and flowering time, but little is known about their role in floral development (Park *et al.*, 2011). GO term enrichment analysis showed that genes in the magenta-s4 module are significantly involved in floral organ development (Fig. 2.5c; Supp. Data 2), including the SUMO hub gene, making it interesting to explore their connections.

ACKNOWLEDGMENT

The authors would like to thank Pierre Baduel, the sequencing team at the Bauer Core Facility at the Harvard University and the Harvard FAS Informatics team for discussing analysis strategies, Dan Utter and Brian Arnold for help troubleshooting the Linux scripts, Weilin Meng for help troubleshooting and optimizing the network visualization, and the R package developers and bioinformaticians Michael Love, Kevin Blighe, and Peter Langfelder for actively responding to questions on online forums. We thank the Department of Organismic and Evolutionary Biology Ph.D. program at Harvard University for providing funding to support this project.

AUTHOR CONTRIBUTIONS

The study was conceived of and designed by Y.M. and E.M.K. All experiments and data analysis were conducted by Y.M. with oversight provided by E.M.K. Manuscript was written by Y.M. with revisions by E.M.K.

REFERENCE

- Abrash EB, Davies KA, Bergmann DC. 2011. Generation of Signaling Specificity in *Arabidopsis* by Spatially Restricted Buffering of Ligand–Receptor Interactions. *The Plant Cell* 23: 2864–2879.
- Ballerini ES, Kramer EM. 2011. Environmental and molecular analysis of the floral transition in the lower eudicot *Aquilegia formosa*. *EvoDevo* 2: 4.
- Ballerini ES, Kramer EM, Hodges SA. 2019. Comparative transcriptomics of early petal development across four diverse species of *Aquilegia* reveal few genes consistently associated with nectar spur development. *BMC Genomics* 20: 668.
- Bastow R, Mylne JS, Lister C, Lippman Z, Martienssen RA, Dean C. 2004. Vernalization requires epigenetic silencing of FLC by histone methylation. *Nature* 427: 164–167.
- Benjamini Y, Yekutieli D. 2001. The Control of the False Discovery Rate in Multiple Testing under Dependency. *The Annals of Statistics* 29: 1165–1188.
- Besnard F, Refahi Y, Morin V, Marteaux B, Brunoud G, Chambrier P, Rozier F, Mirabet V, Legrand J, Lainé S, *et al.* 2014a. Cytokinin signalling inhibitory fields provide robustness to phyllotaxis. *Nature* 505: 417–421.
- Besnard F, Rozier F, Vernoux T. 2014b. The *AHP6* cytokinin signaling inhibitor mediates an auxin-cytokinin crosstalk that regulates the timing of organ initiation at the shoot apical meristem. *Plant Signaling & Behavior* 9: e28788.
- Bollier N, Sicard A, Leblond J, Latrasse D, Gonzalez N, Gévaudant F, Benhamed M, Raynaud C, Lenhard M, Chevalier C, *et al.* 2018. At-MINI ZINC FINGER2 and SI-INHIBITOR OF MERISTEM ACTIVITY, a Conserved Missing Link in the Regulation of Floral Meristem Termination in *Arabidopsis* and Tomato. *The Plant Cell* 30: 83–100.
- Bray NL, Pimentel H, Melsted P, Pachter L. 2016. Near-optimal probabilistic RNA-seq quantification. *Nature Biotechnology* 34: 525–527.
- Byzova MV, Franken J, Aarts MGM, de Almeida-Engler J, Engler G, Mariani C, Van Lookeren Campagne MM, Angenent GC. 1999. *Arabidopsis* *STERILE APETALA*, a multifunctional gene regulating inflorescence, flower, and ovule development. *Genes & Development* 13: 1002–1014.
- Canales C, Bhatt AM, Scott R, Dickinson H. 2002. EXS, a Putative LRR Receptor Kinase, Regulates Male Germline Cell Number and Tapetal Identity and Promotes Seed Development in *Arabidopsis*. *Current Biology* 12: 1718–1727.
- Chahtane H, Zhang B, Norberg M, LeMasson M, Thévenon E, Bakó L, Benlloch R, Holmlund M, Parcy F, Nilsson O, *et al.* 2018. *LEAFY* activity is post-transcriptionally regulated by *BLADE ON PETIOLE2* and *CULLIN3* in *Arabidopsis*. *New Phytologist* 220: 579–592.
- Chandler JW, Werr W. 2015. Cytokinin–auxin crosstalk in cell type specification. *Trends in Plant Science* 20: 291–300.

- Chen C-C, Chen Y-Y, Yeh K-C. 2011. Effect of Cu content on the activity of Cu/ZnSOD1 in the Arabidopsis SUMO E3 ligase *siz1* mutant. *Plant Signaling & Behavior* 6: 1428–1430.
- Cheng Y, Zhao Y. 2007. A Role for Auxin in Flower Development. *Journal of Integrative Plant Biology* 49: 99–104.
- Coen ES, Meyerowitz EM. 1991. The war of the whorls: genetic interactions controlling flower development. *Nature* 353: 31–37.
- Ding L, Yan S, Jiang L, Zhao W, Ning K, Zhao J, Liu X, Zhang J, Wang Q, Zhang X. 2015. *HANABA TARANU* (*HAN*) Bridges Meristem and Organ Primordia Boundaries through *PINHEAD*, *JAGGED*, *BLADE-ON-PETIOLE2* and *CYTOKININ OXIDASE 3* during Flower Development in Arabidopsis (XW Deng, Ed.). *PLoS Genetics* 11: e1005479.
- Ditta G, Pinyopich A, Robles P, Pelaz S, Yanofsky MF. 2004. The *SEP4* Gene of *Arabidopsis thaliana* Functions in Floral Organ and Meristem Identity. *Current Biology* 14: 1935–1940.
- Dong H, Dumenil J, Lu F-H, Na L, Vanhaeren H, Naumann C, Klecker M, Prior R, Smith C, McKenzie N, *et al.* 2017. Ubiquitylation activates a peptidase that promotes cleavage and destabilization of its activating E3 ligases and diverse growth regulatory proteins to limit cell proliferation in *Arabidopsis*. *Genes & Development* 31: 197–208.
- Du Z, Zhou X, Ling Y, Zhang Z, Su Z. 2010. agriGO: a GO analysis toolkit for the agricultural community. *Nucleic Acids Research* 38: W64–W70.
- Durfee T, Roe JL, Sessions RA, Inouye C, Serikawa K, Feldmann KA, Weigel D, Zambryski PC. 2003. The F-box-containing protein *UFO* and *AGAMOUS* participate in antagonistic pathways governing early petal development in *Arabidopsis*. *Proceedings of the National Academy of Sciences* 100: 8571–8576.
- Fang X, Qi Y. 2016. RNAi in Plants: An Argonaute-Centered View. *The Plant Cell* 28: 272–285.
- Feng N, Song G, Guan J, Chen K, Jia M, Huang D, Wu J, Zhang L, Kong X, Geng S, *et al.* 2017. Transcriptome Profiling of Wheat Inflorescence Development from Spikelet Initiation to Floral Patterning Identified Stage-Specific Regulatory Genes. *Plant Physiology* 174: 1779–1794.
- Gleason EJ, Kramer EM. 2013. Conserved roles for *Polycomb Repressive Complex 2* in the regulation of lateral organ development in *Aquilegia x coerulea* ‘Origami’. *BMC Plant Biology* 13: 185.
- Hardie DG. 1999. PLANT PROTEIN SERINE/THREONINE KINASES: Classification and Functions. *Annual Review of Plant Physiology and Plant Molecular Biology* 50: 97–131.
- Hendelman A, Kravchik M, Stav R, Zik M, Lugassi N, Arazi T. 2013. The developmental outcomes of P0-mediated ARGONAUTE destabilization in tomato. *Planta* 237: 363–377.

- Hepworth C, Caine RS, Harrison EL, Sloan J, Gray JE. 2018. Stomatal development: focusing on the grasses. *Current Opinion in Plant Biology* 41: 1–7.
- Hibara K, Karim MR, Takada S, Taoka K, Furutani M, Aida M, Tasaka M. 2006. *Arabidopsis* CUP-SHAPED COTYLEDON3 Regulates Postembryonic Shoot Meristem and Organ Boundary Formation. *The Plant Cell* 18: 2946–2957.
- Hoffmann L, Besseau S, Geoffroy P, Ritzenthaler C, Meyer D, Lapierre C, Pollet B, Legrand M. 2004. Silencing of Hydroxycinnamoyl-Coenzyme A Shikimate/Quinate Hydroxycinnamoyltransferase Affects Phenylpropanoid Biosynthesis. *The Plant Cell* 16: 1446–1465.
- Huang DW, Sherman BT, Lempicki RA. 2009a. Systematic and integrative analysis of large gene lists using DAVID bioinformatics resources. *Nature Protocols* 4: 44–57.
- Huang DW, Sherman BT, Lempicki RA. 2009b. Bioinformatics enrichment tools: paths toward the comprehensive functional analysis of large gene lists. *Nucleic Acids Research* 37: 1–13.
- Ji L, Liu X, Yan J, Wang W, Yumul RE, Kim YJ, Dinh TT, Liu J, Cui X, Zheng B, *et al.* 2011. ARGONAUTE10 and ARGONAUTE1 Regulate the Termination of Floral Stem Cells through Two MicroRNAs in Arabidopsis (L-J Qu, Ed.). *PLoS Genetics* 7: e1001358.
- Jones L, Keining T, Eamens A, Vaistij FE. 2006. Virus-Induced Gene Silencing of *Argonaute* Genes in *Nicotiana benthamiana* Demonstrates That Extensive Systemic Silencing Requires *Argonaute1*-Like and *Argonaute4*-Like Genes. *Plant Physiology* 141: 598–606.
- Kanehisa M, Goto S. 2000. KEGG: Kyoto Encyclopedia of Genes and Genomes. *Nucleic Acids Research* 28: 27–30.
- Kanehisa M, Sato Y, Kawashima M, Furumichi M, Tanabe M. 2016. KEGG as a reference resource for gene and protein annotation. *Nucleic Acids Research* 44: D457–462.
- Kidner CA, Martienssen RA. 2005. The role of ARGONAUTE1 (*AGO1*) in meristem formation and identity. *Developmental Biology* 280: 504–517.
- Klepikova AV, Kasianov AS, Gerasimov ES, Logacheva MD, Penin AA. 2016. A high resolution map of the *Arabidopsis thaliana* developmental transcriptome based on RNA-seq profiling. *The Plant Journal* 88: 1058–1070.
- Kosentka PZ, Overholt A, Maradiaga R, Mitoubi O, Shpak ED. 2019. EPFL Signals in the Boundary Region of the SAM Restrict Its Size and Promote Leaf Initiation. *Plant Physiology* 179: 265–279.
- Kramer EM. 2009. *Aquilegia*: A New Model for Plant Development, Ecology, and Evolution. *Annual Review of Plant Biology* 60: 261–277.

- Kramer EM, Holappa L, Gould B, Jaramillo MA, Setnikov D, Santiago PM. 2007. Elaboration of B Gene Function to Include the Identity of Novel Floral Organs in the Lower Eudicot *Aquilegia*. *The Plant Cell* 19: 750–766.
- Krizek B. 2009. *AINTEGUMENTA* and *AINTEGUMENTA-LIKE6* Act Redundantly to Regulate Arabidopsis Floral Growth and Patterning. *Plant Physiology* 150: 1916–1929.
- Krueger F. 2020. *FelixKrueger/TrimGalore*.
- Langfelder P, Horvath S. 2008. WGCNA: an R package for weighted correlation network analysis. *BMC Bioinformatics* 9: 559.
- Larkin MA, Blackshields G, Brown NP, Chenna R, McGettigan PA, McWilliam H, Valentin F, Wallace IM, Wilm A, Lopez R, *et al.* 2007. Clustal W and Clustal X version 2.0. *Bioinformatics (Oxford, England)* 23: 2947–2948.
- Lee I, Wolfe DS, Nilsson O, Weigel D. 1997. A *LEAFY* co-regulator encoded by *UNUSUAL FLORAL ORGANS*. *Current Biology* 7: 95–104.
- Lemmon ZH, Park SJ, Jiang K, Van Eck J, Schatz MC, Lippman ZB. 2016. The evolution of inflorescence diversity in the nightshades and heterochrony during meristem maturation. *Genome Research* 26: 1676–1686.
- Levin JZ, Meyerowitz EM. 1995. UFO: An Arabidopsis Gene Involved in Both Floral Meristem and Floral Organ Development. *The Plant Cell* 7(5): 529-548.
- Levy YY. 2002. Multiple Roles of *Arabidopsis* *VRN1* in Vernalization and Flowering Time Control. *Science* 297: 243–246.
- Li N, Liu Z, Wang Z, Ru L, Gonzalez N, Baekelandt A, Pauwels L, Goossens A, Xu R, Zhu Z, *et al.* 2018. *STERILE APETALA* modulates the stability of a repressor protein complex to control organ size in *Arabidopsis thaliana*. *PLOS Genetics* 14: e1007218.
- Love MI, Huber W, Anders S. 2014. Moderated estimation of fold change and dispersion for RNA-seq data with DESeq2. *Genome Biology* 15: 550.
- Luo L, Zeng J, Wu H, Tian Z, Zhao Z. 2018. A Molecular Framework for Auxin-Controlled Homeostasis of Shoot Stem Cells in *Arabidopsis*. *Molecular Plant* 11: 899–913.
- Maier AT, Stehling-Sun S, Wollmann H, Demar M, Hong RL, Haubeiss S, Weigel D, Lohmann JU. 2009. Dual roles of the bZIP transcription factor *PERLANTHIA* in the control of floral architecture and homeotic gene expression. *Development* 136: 1613–1620.
- Meaders C, Min Y, Freedberg KJ, Kramer E. 2020. Developmental and molecular characterization of novel staminodes in *Aquilegia*. *Annals of Botany* 126: 231–243.

- Min Y, Kramer EM. 2017. The *Aquilegia* JAGGED homolog promotes proliferation of adaxial cell types in both leaves and stems. *New Phytologist* 216: 536–548.
- Pabón-Mora N, Sharma B, Holappa LD, Kramer EM, Litt A. 2013. The *Aquilegia* FRUITFULL-like genes play key roles in leaf morphogenesis and inflorescence development. *The Plant Journal* 74: 197–212.
- Park HJ, Kim W-Y, Park HC, Lee SY, Bohnert HJ, Yun D-J. 2011. SUMO and SUMOylation in plants. *Molecules and Cells* 32: 305–316.
- Roodbarkelari F, Du F, Truernit E, Laux T. 2015. ZLL/AGO10 maintains shoot meristem stem cells during Arabidopsis embryogenesis by down-regulating ARF2-mediated auxin response. *BMC Biology* 13: 74.
- Roussin-Léveillé C, Silva-Martins G, Moffett P. 2019. ARGONAUTE5 Mediates Fine-Tuning of Vegetative-to-Reproductive Phase Transition Through Its Interaction with miR156 in Arabidopsis. *bioRxiv*: 640680.
- Ryan PT, Ó'Maoiléidigh DS, Drost H-G, Kwaśniewska K, Gabel A, Grosse I, Graciet E, Quint M, Wellmer F. 2015. Patterns of gene expression during *Arabidopsis* flower development from the time of initiation to maturation. *BMC Genomics* 16: 488.
- Samach A, Klenz JE, Kohalmi SE, Risseuw E, Haughn GW, Crosby WL. 1999. The UNUSUAL FLORAL ORGANS gene of *Arabidopsis thaliana* is an F-box protein required for normal patterning and growth in the floral meristem. *The Plant Journal*: 13.
- Schoof H, Lenhard M, Haecker A, Mayer KFX, Jürgens G, Laux T. 2000. The Stem Cell Population of *Arabidopsis* Shoot Meristems Is Maintained by a Regulatory Loop between the CLAVATA and WUSCHEL Genes. *Cell* 100: 635–644.
- Seifert GJ. 2004. Nucleotide sugar interconversions and cell wall biosynthesis: how to bring the inside to the outside. *Current Opinion in Plant Biology* 7: 277–284.
- Sharma B, Batz TA, Kaundal R, Kramer EM, Sanders UR, Mellano VJ, Duhan N, Larson RB. 2019a. Developmental and Molecular Changes Underlying the Vernalization-Induced Transition to Flowering in *Aquilegia coerulea* (James). *Genes* 10: 734.
- Sharma B, Kramer E. 2013. Sub- and neo-functionalization of APETALA3 paralogs have contributed to the evolution of novel floral organ identity in *Aquilegia* (columbine, Ranunculaceae). *New Phytologist* 197: 949–957.
- Sharma B, Kramer EM. 2014. The MADS-Box Gene Family of the Basal Eudicot and Hybrid *Aquilegia coerulea* 'Origami' (Ranunculaceae). *Annals of the Missouri Botanical Garden* 99: 313–322.

- Sharma B, Meaders C, Wolfe D, Holappa L, Walcher-Chevillet C, Kramer EM. 2019b. Homologs of *LEAFY* and *UNUSUAL FLORAL ORGANS* Promote the Transition From Inflorescence to Floral Meristem Identity in the Cymose *Aquilegia coerulea*. *Frontiers in Plant Science* 10: 1218.
- Soneson C, Love MI, Robinson MD. 2015. Differential analyses for RNA-seq: transcript-level estimates improve gene-level inferences. *F1000Research* 4: 1521.
- Song X-J, Huang W, Shi M, Zhu M-Z, Lin H-X. 2007. A QTL for rice grain width and weight encodes a previously unknown RING-type E3 ubiquitin ligase. *Nature Genetics* 39: 623–630.
- Sun B, Looi L-S, Guo S, He Z, Gan E-S, Huang J, Xu Y, Wee W-Y, Ito T. 2014. Timing Mechanism Dependent on Cell Division Is Invoked by Polycomb Eviction in Plant Stem Cells. *Science* 343: 1248559–1248559.
- Sun B, Xu Y, Ng K-H, Ito T. 2009. A timing mechanism for stem cell maintenance and differentiation in the *Arabidopsis* floral meristem. *Genes & Development* 23: 1791–1804.
- Sun B, Zhou Y, Cai J, Shang E, Yamaguchi N, Xiao J, Looi L-S, Wee W-Y, Gao X, Wagner D, *et al.* 2019. Integration of Transcriptional Repression and Polycomb-Mediated Silencing of *WUSCHEL* in Floral Meristems. *The Plant Cell* 31: 1488–1505.
- Tian T, Liu Y, Yan H, You Q, Yi X, Du Z, Xu W, Su Z. 2017. agriGO v2.0: a GO analysis toolkit for the agricultural community, 2017 update. *Nucleic Acids Research* 45: W122–W129.
- Torii KU. 2015. Stomatal differentiation: the beginning and the end. *Current Opinion in Plant Biology* 28: 16–22.
- Tucker MR, Hinze A, Tucker EJ, Takada S, Jurgens G, Laux T. 2008. Vascular signalling mediated by *ZWILLE* potentiates *WUSCHEL* function during shoot meristem stem cell development in the *Arabidopsis* embryo. *Development* 135: 2839–2843.
- Tucker SC, Hodges SA. 2005. Floral Ontogeny of *Aquilegia*, *Semiaquilegia*, and *Enemion* (Ranunculaceae). *International Journal of Plant Sciences* 166: 557–574.
- Uchida N, Lee JS, Horst RJ, Lai H-H, Kajita R, Kakimoto T, Tasaka M, Torii KU. 2012. Regulation of inflorescence architecture by intertissue layer ligand-receptor communication between endodermis and phloem. *Proceedings of the National Academy of Sciences* 109: 6337–6342.
- Wang Z, Li N, Jiang S, Gonzalez N, Huang X, Wang Y, Inzé D, Li Y. 2016. SCFSAP controls organ size by targeting PPD proteins for degradation in *Arabidopsis thaliana*. *Nature Communications* 7: 11192.
- Wellmer F, Alves-Ferreira M, Dubois A, Riechmann JL, Meyerowitz EM. 2006. Genome-Wide Analysis of Gene Expression during Early *Arabidopsis* Flower Development. *PLOS Genetics* 2: e117.

- Wilkinson MD, Haughn GW. 1995. UNUSUAL FLORAL ORGANS Controls Meristem Identity and Organ Primordia Fate in Arabidopsis. *The Plant Cell* 7(9): 1485-1499.
- Xia T, Li N, Dumenil J, Li J, Kamenski A, Bevan MW, Gao F, Li Y. 2013. The Ubiquitin Receptor DA1 Interacts with the E3 Ubiquitin Ligase DA2 to Regulate Seed and Organ Size in *Arabidopsis*. *The Plant Cell* 25: 3347–3359.
- Yamaguchi N, Huang J, Tatsumi Y, Abe M, Sugano SS, Kojima M, Takebayashi Y, Kiba T, Yokoyama R, Nishitani K, *et al.* 2018. Chromatin-mediated feed-forward auxin biosynthesis in floral meristem determinacy. *Nature Communications* 9: 5290.
- Yamaguchi N, Huang J, Xu Y, Tanoi K, Ito T. 2017. Fine-tuning of auxin homeostasis governs the transition from floral stem cell maintenance to gynoecium formation. *Nature Communications* 8: 1125.
- Yang L, Liu H, Zhao J, Pan Y, Cheng S, Lietzow CD, Wen C, Zhang X, Weng Y. 2018. LITTLELEAF (LL) encodes a WD40 repeat domain-containing protein associated with organ size variation in cucumber. *The Plant Journal* 95: 834–847.
- Yant L, Collani S, Puzey J, Levy C, Kramer EM. 2015. Molecular basis for three-dimensional elaboration of the *Aquilegia* petal spur. *Proceedings of the Royal Society B: Biological Sciences* 282: 20142778.
- Yu H, Huang T. 2016. Molecular Mechanisms of Floral Boundary Formation in Arabidopsis. *International Journal of Molecular Sciences* 17.
- Zhang L, DeGennaro D, Lin G, Chai J, Shpak ED. 2020. ERECTA family signaling constrains *CLAVATA3* and *WUSCHEL* to the center of the shoot apical meristem. *Developmental Biology*.
- Zhang H, Xia R, Meyers BC, Walbot V. 2015. Evolution, functions, and mysteries of plant ARGONAUTE proteins. *Current Opinion in Plant Biology* 27: 84–90.
- Zhu H, Hu F, Wang R, Zhou X, Sze S-H, Liou LW, Barefoot A, Dickman M, Zhang X. 2011. *Arabidopsis Argonaute10* Specifically Sequesters miR166/165 to Regulate Shoot Apical Meristem Development. *Cell* 145: 242–256.

CHAPTER 2.

Quantitative live-imaging of *Aquilegia* floral meristems
reveals distinct patterns of floral organ initiation
and cell-level dynamics of floral meristem termination

The following authors contributed to this chapter:

Min, Y.*, Conway, S. J.*, & Kramer, E. M. (* co-first authors)

ABSTRACT

In-depth investigation of meristem behavior requires not only knowledge of different molecular regulatory networks, but also how such networks directly control precise patterns of cell division and expansion over time. Floral meristem development is crucial to the reproductive success of a plant and is distinct from shoot meristem development for many reasons, including the fact that these meristems are determinate and undergo floral meristem termination (FMT). Using a recently developed live-imaging approach in the eudicot species *Aquilegia coerulea* (Ranunculaceae), we have characterized developmental dynamics during the initiation of stamen, staminode and carpel primordia, as well as FMT. Our results reveal how the dynamics between cell proliferation and expansion change as the FM transitions from production of stamens to staminodes to carpels, and uncover distinct patterns of primordium initiation between stamens and staminodes compared to carpels as well as subtle distinctions between the two whorls of staminodes. This study has also provided insight into the process of FMT, which is discernible based on cell division dynamics preceding carpel initiation. To our knowledge, this study is both the first cellular characterization of FMT in any flowering plant and the first quantitative live imaging of meristem development in a non-conventional model system. Our results will lay the foundation for investigating gene expression in *A. coerulea* FMs in real time, providing crucial information for our understanding of how the spatial-temporal regulation of floral meristem behavior is achieved in both an evolutionary and developmental context.

INTRODUCTION

The spatial-temporal regulation of cell proliferation and expansion is a fundamental aspect of development in all multicellular organisms. It is particularly crucial in plants because programmed cell death and cell migration play no role in most developmental processes, while morphogenesis and organogenesis occur throughout the entire lifespan of a plant (Steeves & Sussex, 1989). The foundation of continuous growth in a plant is the presence of meristems, which are groups of cells that possess stem cell properties and are typically located at the tips of all growing axes. Meristem activities must be well regulated to maintain a pool of pluripotent cells and give rise to differentiating cells. Based on the types of tissues and organs produced, meristems can be categorized into several types. For instance, vegetative meristems produce vegetative organs such as leaves; root apical meristems are responsible for the growth of roots; and in flowering plants, there are inflorescence

meristems, which give rise to reproductive branches, and floral meristems (FMs), which produce floral organs. Meristems that produce leaves and roots are indeterminate by nature and can make new organs and tissues continuously. The properties of the inflorescence meristems are more variable, and whether they grow indeterminately or determinately differs across plant lineages (Kirchoff & Claßen-Bockhoff, 2013; Bartlett & Thompson, 2014). FMs, however, are always determinant because every FM is responsible for the production of one flower, and every flower terminates after the production of a relatively finite number of organs, typically culminating in carpels. These consistently determinate meristems are particularly interesting to study in terms of the spatial-temporal regulation of cell behaviors in plants. On the one hand, just like other meristems, FMs need to maintain homeostasis of their stem cell pools to ensure the successive production of organs. On the other hand, this proliferation must be terminated at a specific time point during floral organ initiation, a process called floral meristem termination (FMT). FMT results in the loss of pluripotency of all the cells that remain in the FM, which will then be incorporated into production of the innermost organs of the flower.

Over the past few decades, studies using mitotic index and clonal sectors have revealed that most meristems are highly organized structures, composed of a central zone (CZ) and a peripheral zone (PZ), which harbor the stem cells and organogenic cells, respectively (Stewart & Dermen, 1970; Marc & Palmer, 1982; Steeves & Sussex, 1989). Thus, the maintenance of stem cell identity in the CZ is key to meristem indeterminacy, and many key genes controlling meristem homeostasis have been identified. Perhaps the most critical is the stem cell identity gene *WUSCHEL* (*WUS*), which is exclusively expressed at the base of the central zone (also called the organizing center (Laux *et al.*, 1996; Mayer *et al.*, 1998). The WUS protein functions non-cell autonomously to induce the expression of the gene *CLVATA3* (*CLV3*), which codes for a small peptide that in turn diffuses back to repress *WUS* expression (Schoof *et al.*, 2000; Yadav *et al.*, 2011). This WUS-*CLV3* feedback

loop is critical for maintaining the homeostasis of stem cells in the meristems and was found to be widely conserved among land plants (Schoof *et al.*, 2000; Lenhard, 2003; Yadav *et al.*, 2011; Whitewoods *et al.*, 2020). Therefore, when we consider the FMT process, we are explicitly asking when and how *WUS* expression is permanently down-regulated, a process that is best understood in the model systems *Arabidopsis thaliana* and tomato (Sun *et al.*, 2009, 2014; Bollier *et al.*, 2018). However, it remains to be seen whether these genetic pathways are more broadly conserved and, perhaps most importantly, both of these models have rather simple flowers with only four whorls of organs, representing only a small fraction of the diversity seen in angiosperms (Endress, 1990).

Another key component of investigating FMT from a developmental perspective is achieving a detailed understanding of cell division and expansion dynamics. Most previous work has relied on histology, scanning electron microscopy, *in situ* hybridization, or immunolocalization, all of which require fixation and, in most cases, sectioning of the tissues, rendering the dynamics static (Sappl & Heisler, 2013; Prunet & Duncan, 2020). Recent advancements in live imaging techniques have allowed researchers to analyze how gene activities regulate the spatial-temporal dynamic of cellular behaviors quantitatively, at unprecedented resolutions and in real time (Sappl & Heisler, 2013; Prunet & Duncan, 2020). Implementation of quantitative live imaging has provided answers to many long-standing questions in plant development, such as the timing of the establishment of adaxial/abaxial polarities during primordium initiation (Zhao & Traas, 2021), functions of the gene *SUPERMAN* in regulating organ boundaries and FMT (Prunet *et al.*, 2017), and mechanisms generating the giant cells in the *A. thaliana* sepals (Roeder *et al.*, 2010). Therefore, to gain an in-depth understanding of the dynamics of meristem function, we need both knowledge of different molecular regulatory networks and an understanding of how such networks directly control the precise actions of cell division and expansion over time, ideally in as many plant taxa as possible. So far, quantitative live imaging of meristems has only been developed for and applied to a small

number of model species: the vegetative meristems of tomato, moss, and *A. thaliana* (Reddy & Roy-Chowdhury, 2009; Harrison *et al.*, 2009; Hamant *et al.*, 2019); the inflorescence meristems of *Gerbera hybrida*, *Brachypodium distachyon*, and *A. thaliana* (Heisler & Ohno, 2014; O'Connor, 2018; Zhang *et al.*, 2021); the root meristems of *A. thaliana* (Rahni & Birnbaum, 2019); and the early FMs of *Cardamine hirsuta* and *A. thaliana* (Prunet *et al.*, 2016; Monniaux *et al.*, 2018).

In this study, we have applied a recently developed live confocal microscope imaging technique ([Appendix A](#)) to produce the first quantitative characterization of the cellular dynamics in the FMs of *Aquilegia coerulea*, with a particular focus on FMT. *Aquilegia coerulea* is a member of the buttercup family (Ranunculaceae) and is a model system for evolutionary developmental studies with a well-annotated genome and a number of functional tools (Kramer, 2009; Filiault *et al.*, 2018). We chose to focus on the developmental window of FMT because of its crucial role in flower development, but also because the cell dynamic changes during FMT have not yet been described quantitatively in any model systems. In addition, the FMs of *A. coerulea* have several significant differences compared to the FMs of *A. thaliana*, one being that they are maintained for a longer period before FMT to allow for the production of 15 to 17 whorls of floral organs compared to the four whorls of organs in *A. thaliana*. Moreover, FMT is very different between these two systems from a morphological perspective. After FMT, the carpel primordia of *A. thaliana* arise as a single syncarpous gynoecium (Hill & Lord, 1989), incorporating all of the cells that remained in the apex of the FM. By contrast, carpels of *A. coerulea* are formed from five distinct primordia (i.e., an apocarpous gynoecium) such that the apex of the FM is not spontaneously consumed by their emergence (Tucker & Hodges, 2005). Currently, we have no information regarding how different patterns of carpel primordia initiation influence FMT in flowering plants.

By imaging the same *A. coerulea* FMs in tissue culture at repeated time intervals and using the software MorphoGraphX (Barbier de Reuille *et al.*, 2015), we conducted lineage tracing of cells and

quantified the rate and distribution of cell division, as well as the degree and direction of cell expansion, over multiple developmental stages. Our results have revealed how the dynamics between cell proliferation and expansion change as the FM transitions from production of stamens to staminodes to carpels, allowing a detailed description of the initial developmental stages of floral organ primordia. To our knowledge, this study is both the first cellular characterization of FMT and the first quantitative live imaging development in a non-conventional model system. Our results will lay the foundation for investigating gene expressions in the *A. coerulea* FMs in real time, providing crucial information for our understanding of how the spatial-temporal regulation of meristem behavior is achieved in both an evolutionary and developmental context.

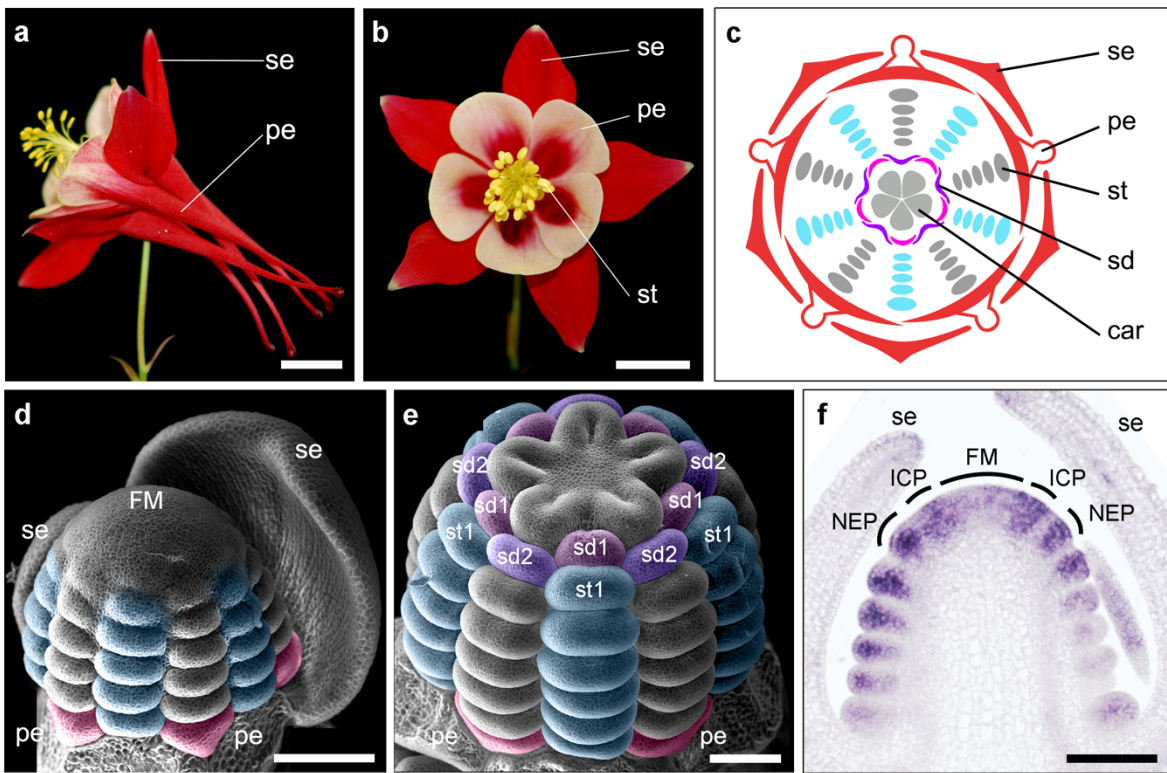


Figure 3.1. Floral morphology of *A. coerulea* flowers. (a) Side view of a mature flower. (b) Front view of a mature flower. (c) Floral diagram of a typical *A. coerulea* flower. (d) A young FM in the process of producing stamens. (e) A young floral bud in the initial stage of carpel development. (f) *In situ* hybridization of abaxial gene *AqFIL* in a young *A. coerulea* FM. Expression pattern was obtained by C. Meaders. se: sepals, pe: petals, st: stamens, sd: staminodes, car: carpels; FM: floral meristem; ICP: incipient primordia; NEP: newly initiated primordia. Scale bars: a, b = 1 cm; d-f = 100 μ m.

MATERIALS AND METHODS

Plant materials, growth conditions, and dissection

Seeds of *Aquilegia x coerulea* 'Kiragami' were purchased from Swallowtail Garden Seeds (Santa Rosa, CA, USA) and germinated in damp soil. The regular growth condition for seedlings and young plants is 16 h daylight at 18 °C and 8 h dark at 13 °C, with humidity under 40%. Once the plants developed approx. six true leaves, they were transferred into vernalization conditions (16 h daylight at 6 °C and 8 h dark at 6 °C) for three to four weeks, and then moved back to the regular growth conditions. When the primary inflorescences started to develop, young side branches with axillary meristems were cut off from the plant, washed in 10% bleach for 20 min, and then thoroughly rinsed with double-distilled water three times. Axillary meristems on the branches were then dissected using a surgical needle under a dissecting microscope. After all the sepals were removed, the floral meristems placed on a petri dish with tissue culture medium composed of 0.5X Linsmaier & Skoog medium (Caisson Labs, Smithfield, UT), with 3% sucrose, 0.8% UltraPure Agarose (Invitrogen), 10^{-6} M kinetin (MilliporeSigma, Burlington, MA), and 10^{-7} M gibberellic acid (GA3, MilliporeSigma, Burlington, MA). The Petri dishes were placed in a tissue culture growth chamber with 16 h light at 20 °C and 8 h dark at 13 °C.

Imaging

FMs were stained with 0.5mg/mL propidium iodide solution in double-distilled water (Sigma-Aldrich, Inc, St. Louis, MO) by immersing the tissue in stain solution for 2.5 minutes for the initial timepoint and then 2 minutes for subsequent timepoints. The stain was removed, and the tissue washed in double distilled water three times. Meristems were imaged immediately after

staining using a LSM 980 NLO Multi-photon confocal laser scanning microscope (Zeiss, Germany) equipped with a water immersion objective (W Plan-Apochromat 20x/1.0 DIC UV-IR M27 75mm, Zeiss). A DPSS 514nm laser was used for excitation and emission was collected between 580-670nm. Scans were frame averaged 2x and z-sections taken at 2 μ m intervals. After imaging, the remaining water in the petri dishes was carefully removed using a pipette and the petri dishes were returned to the tissue culture growth chamber. All samples were imaged every 48 hours, and most of the samples were imaged up to three to four times (i.e., 3 to 4 TPs). Since in the current study we have covered a developmental window covered 6 TPs in total, we have stacked multiple independent time-lapse imaging series to cover the 6 TPs. For instance, there are four independent time-lapse imaging from spanning stages that were equivalent from TP1 to TP4, and four independent time-lapse imaging spanning stages that were equivalent from TP3 to TP6. Every successive TP interval had at least three biological replicates (i.e., independent time-lapse imaging), which were also used as biological replicates to construct the growth alignment graphs (Fig. 3F). Stacking several time-lapse experiments (with replicates) to achieve a larger developmental window is common in long-time live imaging studies (e.g. Kuchen *et al.*, 2012; Kierzkowski *et al.*, 2019).

Imaging processing and data analysis

The confocal image files were transformed into .tif files in ImageJ (<https://imagej.nih.gov/ij/>) and processed in MorphoGraphX (<https://morphographx.org/>) following the steps listed in (Appendix A). Briefly, all image stacks were Gaussian Blurred twice with a radius of 1 on all X/Y/Z sigma, and all meshes were subdivided and smoothed (with 10 passes for each smooth) three times. Cells on the surfaces were segmented by using auto-segmentation, and all the segmentation errors were corrected manually. Heatmap graphs and values were generated by MorphoGraphX, and statistical analysis (ANOVA, Tukey's HSD) was done in R (version 1.1.456).

For the growth alignment graphs, we had four biological replicates for every developmental interval except TP5-TP6, which had three biological replicates. The distance between the center of each floral apex to the edge of the newly emerged primordia (NEP; defined in Results below) was normalized and divided into six equal bins. For each bin, the biological replicates were pooled and means for cell area expansion and cell division were calculated.

RESULTS

The developmental window covered in the study

The *A. coerulea* flower is composed of five organ types, which, arranged from outermost to innermost, are the sepals, petals, stamens, staminodes, and carpels (Fig. 3.1). The five sepals are initiated in spiral phyllotaxy while all other organs are produced synchronously in whorls of five (Fig. 3.1d). Each adjacent whorl initiates in alternating positions, either directly above the sepals or the petals, resulting in 10 orthostichies (i.e., vertical rows of organs) (Fig. 3.1c-e). Each flower consists of one whorl of sepals, one whorl of petals, an average of 10 to 12 whorls of stamens, two whorls of staminodes, and one whorl of carpels. Since we have focused on the later stages of FM development in the current study, the FMs we dissected for live imaging had typically initiated 8 to 10 whorls of stamens. For each stage, we designate the youngest primordial whorl as 1 and the subsequent whorl as 1+n; therefore, sd1 represents the inner whorl of staminodes that are produced after sd2, and st1 represents the last whorl of stamens initiated in the flower (Fig. 3.1e). In addition, we define "newly emerging primordia (NEP)" as the youngest organ primordia of the floral bud, which just bulges out at the periphery of the meristem and can be distinguished morphologically; while the "incipient primordia (ICP)" are the primordia that are initiating after the NEP but cannot be distinguished morphologically yet. Both NEP and ICP can be visualized by examining expression of the

previously studied abaxial polarity gene *FILAMENTOUS FLOWER* (*AqFIL*) in *Aquilegia* (Fig. 3.1f; Meaders *et al.*, 2020).

We used a 48-hour imaging interval because we have observed that a new whorl of stamen or staminode primordia became visible roughly every 48 hours in our experimental conditions, and almost all cells that underwent a cell division during this imaging interval only divided once. Based on this imaging interval, we defined six time points (TP) in our study, resulting in five comparative developmental windows (Fig. 3.2). The first four TPs are distinguished by the successive initiation of floral organ whorls: st1 during TP1; sd2 during TP2; sd1 during TP3; and carpels during TP4. At TP5, the five carpel primordia formed a completely flat, star-shaped apex. At TP6, the carpel primordia each form an elevated ridge at their distal periphery. The meristematic dome was maintained until TP4, at which point the initiation of the carpel primordia resulted in flattening of the apex (Fig. 3.2). The overall distribution of observed cell sizes was consistent with previous observations (Steeves & Sussex, 1989) that cells in the center of the apex are generally larger than the cells in the periphery regions (Fig. 3.2).

Overall growth dynamics over the developmental windows

We used the imaging data to conduct lineage tracing of the epidermal cells of the floral apices to quantify their growth dynamics (Fig. 3.3). To determine whether there were any quantifiable differences in the patterns of growth between the TPs, we constructed growth alignment graphs by plotting the cell area expansion rates and the average number of cell divisions based on the locations of cells along the radial axis of each apex (Fig. 3.3, B1). For each apex, these radial transects were calculated from the center of the floral apex to the inner edges of the NEP whorl based on the curvature heatmap, dividing the transects into six equal bins (Fig. B1).

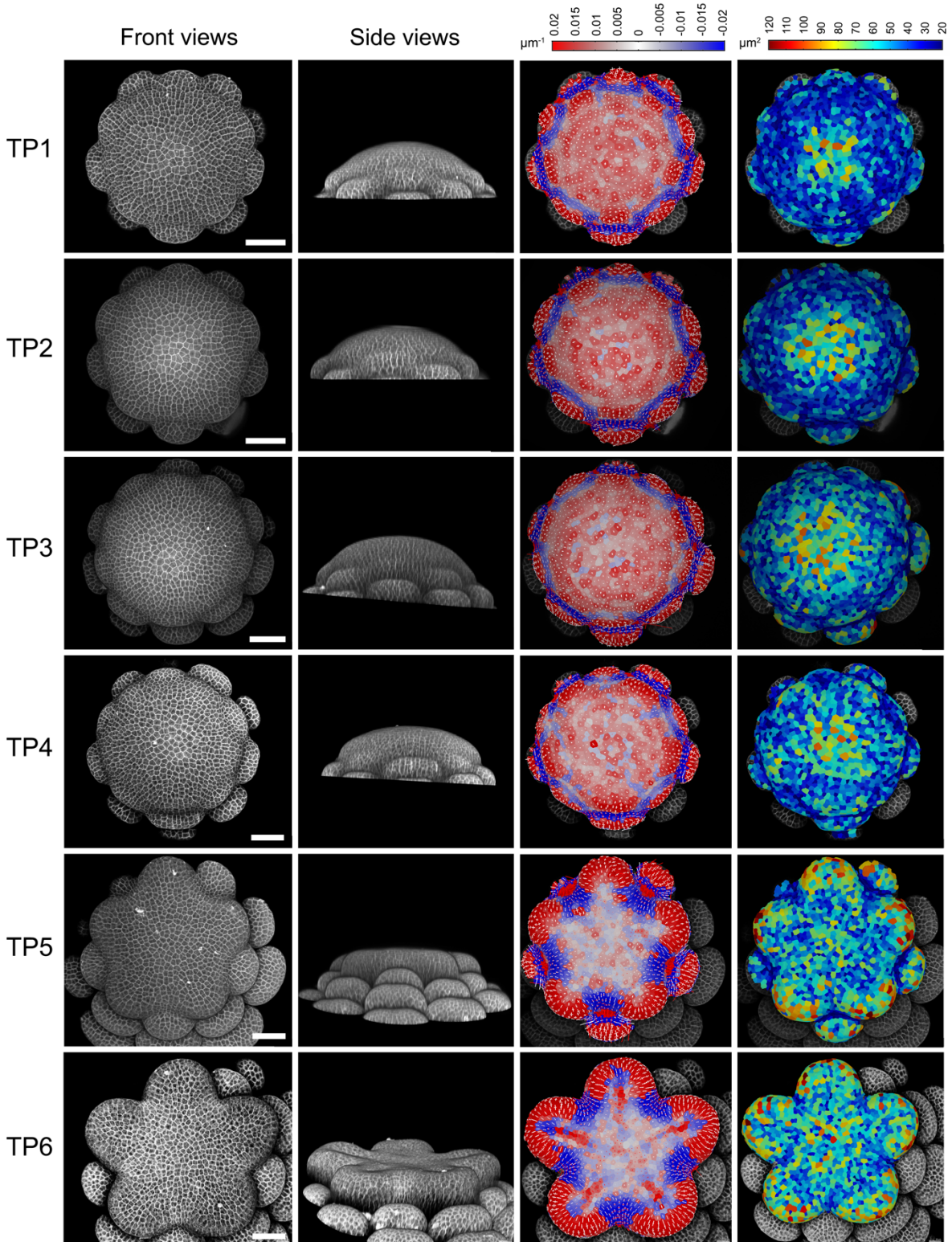
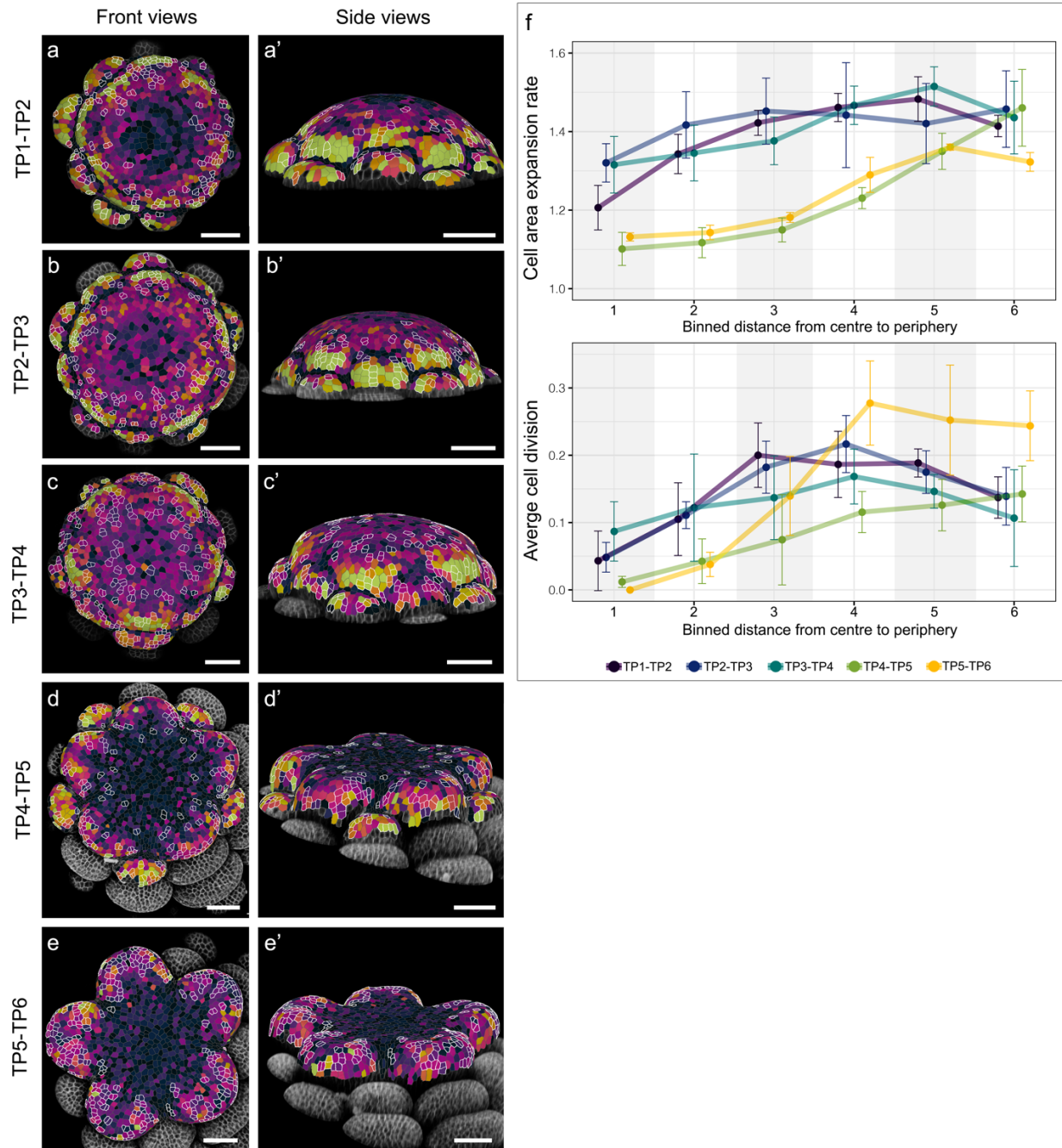


Figure 3.2. Developmental windows covered in the current study. Columns from the left to the right are the front view, side view, front view with curvature heatmap, and cell area heatmap of each time point (TP), respectively. Scale bars = 50 μm .



All developmental windows showed a general pattern that cell area expansion rates were lower at the center and higher at the periphery close to the NEP, but the overall expansion rates after TP4 (i.e., carpel primordia initiation; Fig. 3.3d-e', f) were significantly lower than the earlier developmental windows (Table B1). The area expansion rates were relatively consistent across the entire meristem between TP2 to TP3 (Fig. 3.3b, b', f), during which the *sd1* primordia initiate. The cell area expansion rate displayed the largest difference between cells at the center and the periphery during the transition from TP4 to TP5 (Fig. 3.3d, d', f), when the newly initiated carpel primordia were forming the flat star apex. Interestingly, the TP5 to TP6 (Fig. 3.3e, e') window showed very similar cell area expansion patterns compared to TP4 to TP5 (Fig. 3.3d, d'), only differing in cells close to the periphery, in which the cell area expansion rates are significantly higher in TP4 to TP5 (Fig. 3.3f; Table B1).

Overall, rates of cell division were uniformly low in the center of the meristems across all time points (Fig. 3.3d-e', f), although there was a significant uptick between TP3-TP4 preceding initiation of the carpel primordia (Fig. 3.3c, c'; Table B1). Moving outward in the meristems, rates of cell division generally increased progressively, regardless of the stage (Fig. 3.3). The one distinct exception was in TP5-TP6, during which rates were dramatically low in the center but sharply increased in the third bin domain, a pattern that was statistically different from the other stages (Fig. 3.3f; Table B1).

Floral organ primordia initiation

Subsequently, we analyzed how the initial outgrowth of organ primordia was achieved. Using *st1* primordium initiation as an example, at TP1 the physical bulging of the primordia became visible (Fig. 3.4a, d, g). To precisely describe the growth each primordium, we defined the lateral axis as the axis that is parallel to the circumference of the dome of the FM, and the radial axis as the axis that

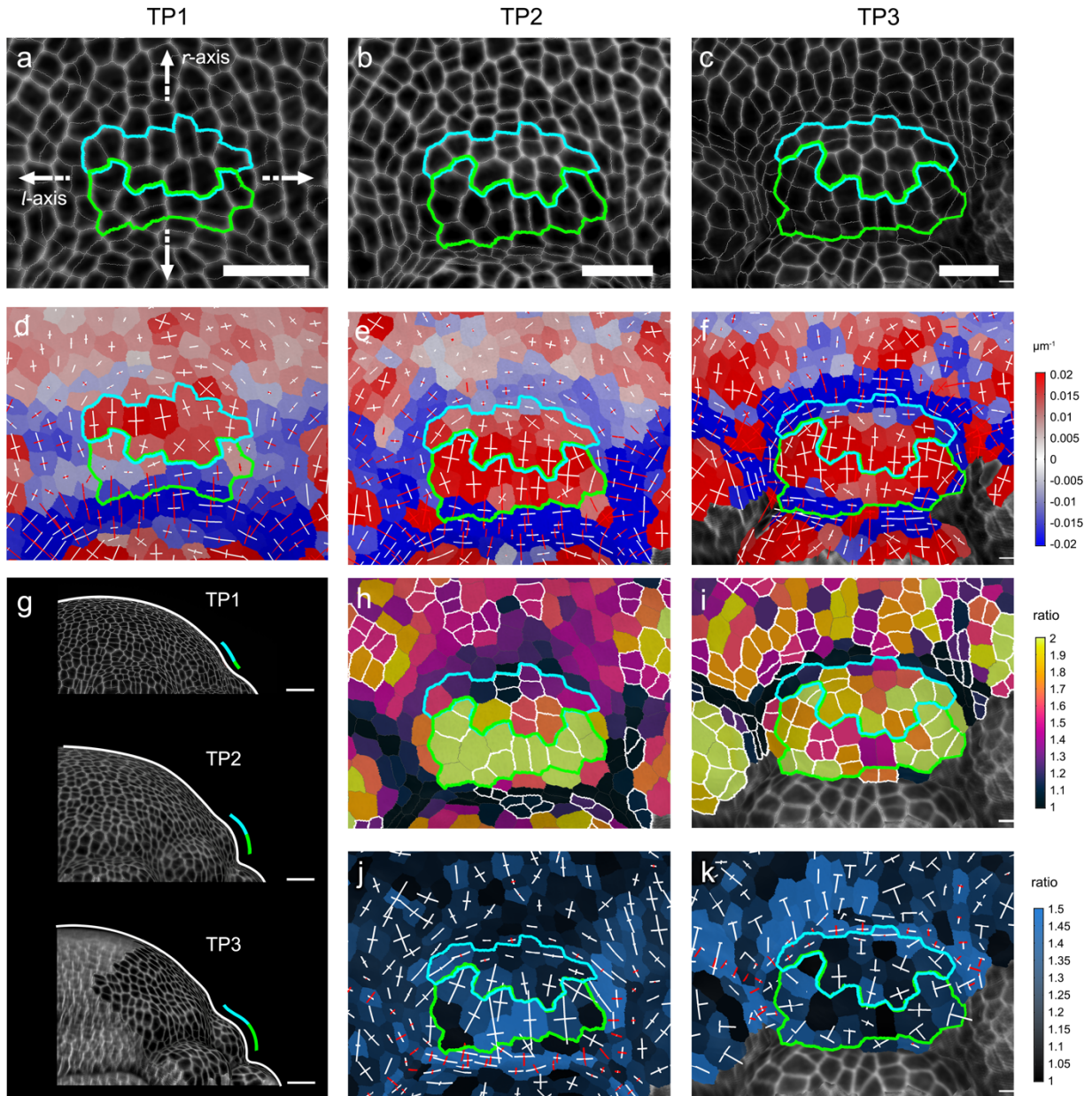


Figure 3.4. Initiation of *st1* primordia. (a-c) Front view of a *st1* primordium at TP1, TP2, and TP3, respectively. Cells outlined in green show the highest growth rates at TP1-TP2 (h) while cells outlined in blue show the highest curvature at TP1 (d). (d-f) Surface curvature heatmaps of A, B, and C, respectively. (g) Side views of the FM at the equivalent TPs. The white line outlines the overall shape of the FMs while the blue/green lines indicate the side view of the *st1* primordium. (h, i) The cell area expansion heatmaps between TP1 to TP2, and TP2 to TP3, overlaid on B and C, respectively. Cells outlined in white are cells that experienced cell division during the interval. (j, k) Cell expansion anisotropy heatmaps between TP1 to TP2, and TP2 to TP3, overlaid on b and c, respectively. The color of a cell represents the value of the ratio between the changes in the longest axis and the shortest axis during the interval, and lines inside of the cell represent the degree and direction of cell expansion. White and red lines show the expansion, or compression, of the cell shape along the indicated axis, respectively. *r*-axis: radial axis; *l*-axis: lateral axis. Scale bars: a, b, c = 20 μm ; g = 50 μm .

runs from the center of the meristem to the center of the primordium (Fig. 3.4a). At TP1, Fig. 3.4A shows 10 cells of this NEP that are outlined in blue, representing the majority of the cells that exhibited positive surface curvature (i.e., are physically bulging out) compared to their surrounding cells, while the 10 cells outlined in green mainly had negative surface curvature (Fig. 3.4d). This includes part of the boundary region that separates this NEP from the primordium in the whorl positioned below (Fig. 3.4d). At TP2, the cells of the green domain, which have become the abaxial surface of the primordium (Fig. 3.4e), were the only cells that exhibited high growth rates during this developmental window (Fig. 3.4h). Cell division occurred on both the abaxial and adaxial sides (Fig. 3.4h), suggesting that this higher growth rate was mainly driven by cell expansion, which was supported by the cell anisotropy map (Fig. 3.4j). Cells on the abaxial side exhibited strong anisotropy along the radial axis, while cells on the adaxial side almost exclusively showed cell expansion along the lateral axis (Fig. 3.4j). At TP3, cell division occurred on both adaxial and abaxial sides of the primordium, and almost all cells in the primordium were exhibiting relatively high growth rates (Fig. 3.4i). The direction of cell expansion for the abaxial cells were more isotropic at this point (Fig. 3.4k). Interestingly, the adaxial-most layer of the cells at TP3 experienced significant compression along the radial axis while continuing to expand along the lateral axis (Fig. 3.4k), indicating these cells were incorporated into the formation of the organ boundary.

This phenomenon, that the initial outgrowth of the primordium was mainly achieved by high growth rates of the abaxial cells, was also observed for the initiation of staminode and carpel primordia (Fig. 3.5). Before entering the rapid growth phase, the abaxial cells were initially comprised of only one or two layers and were less than 10 cells wide (e.g., sd1 in Fig. 3.5a and car in Fig. 3.5b). These cells were located at the abaxial-most position of the ICP, and many (if not most) of them had negative surface curvatures (e.g., sd1 in Fig. 3.5d and car in Fig. 3.5e). They then exhibited substantial, directional cell expansion along the radial axis, coupled with cell divisions so

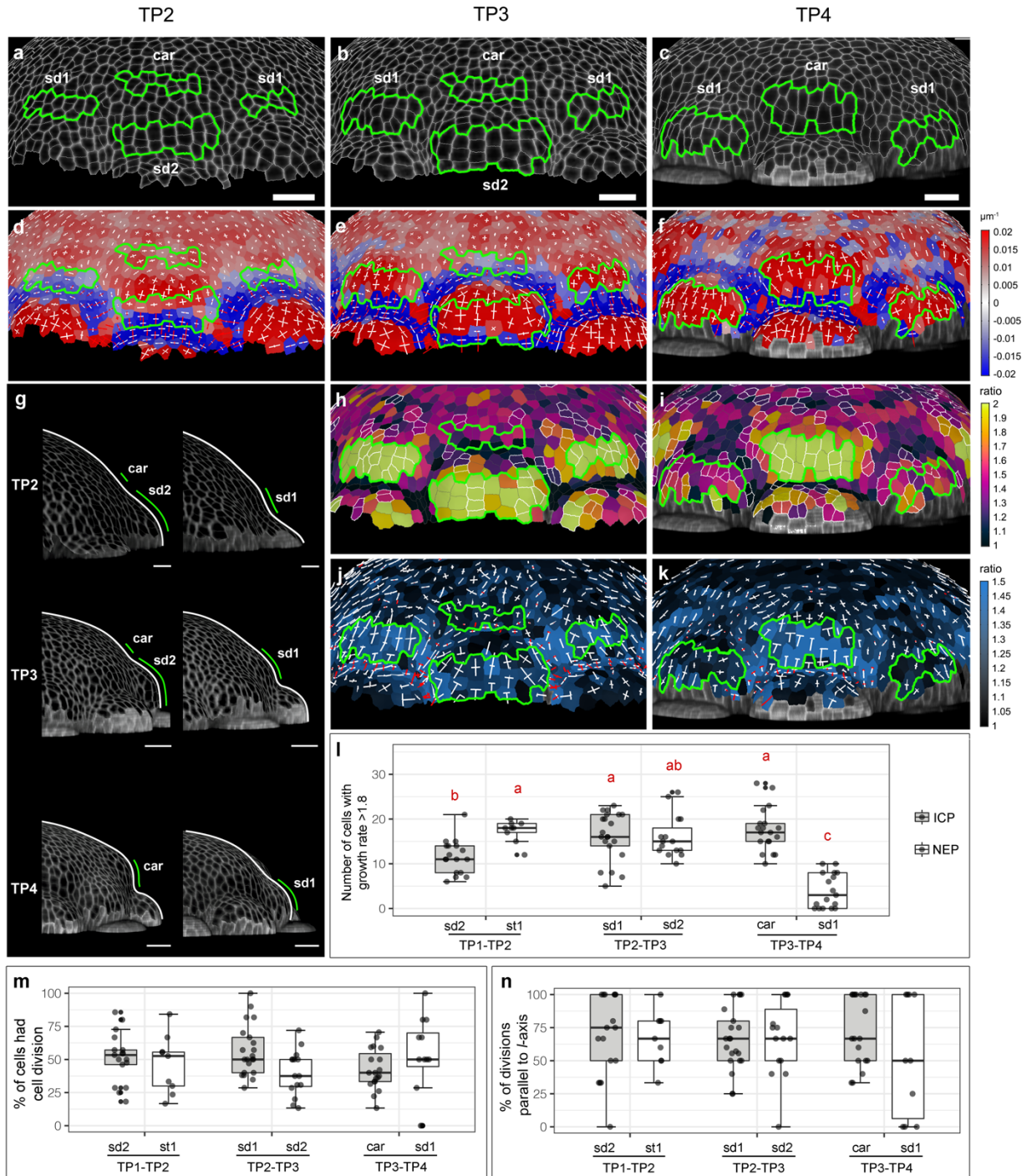


Figure 3.5. Initiation of staminode and carpel primordia. (a-c) Front view of the sd1, sd2, and car primordia at TP2, TP3, and TP4, respectively. The cells outlined in green are the abaxial cells of interest of the initiating primordia, as defined by high growth rates during TP2-TP3 (h) or TP3-TP4 (i). (d-e) Surface curvature heatmaps of A, B, and C, respectively. (g) Side views of the FM at different TPs. The white line outlines the overall morphology of the FMs and the green line indicates the position of the primordia of interest. (h, i) Cell area expansion heatmaps between TP2 to TP3, and TP3 to TP4, overlaid on B and C, respectively. Cells outlined in white resulted from cell division during the interval. (j, k) Cell expansion anisotropy heatmap between TP2 to TP3, and TP3 to TP4, overlaid on b and c, respectively. The color of a cell represents the value of the ratio between the changes in

(Continued) the longest axis and the shortest axis during the interval, and lines inside of the cell represent the degree and direction of cell expansion. White and red lines show the expansion, or compression, of the cell shape along the indicated axis, respectively. **(l)** Comparisons of the number of cells with growth rates > 1.8 in primordia of different stages and developmental windows. Different letters above the boxplots represent significant differences between different primordia ($p < 0.05$, using ANOVA followed by Tukey's pairwise multiple comparisons). **(m)** Comparisons of percentages of cells that had growth rates > 1.8 and also experienced cell division during different time points. No significant difference was detected between different primordia using ANOVA. **(n)** Comparisons of the orientation of cell division among the cells that both had growth rates > 1.8 and experienced cell divisions. No significant difference was detected between different primordia using ANOVA. For (l-m), each data point is a primordium, and for each developmental window, at least three FMs were quantified. Note that for each time period, the identity of the ICP and NEP shift. For instance, sd2 are the ICP at TP1-TP2 but become the NEP at TP2-TP3. Scale bars: A, B, C = 20 μm ; G = 50 μm .

that they quickly made up half of the primordium (e.g., sd1 in Fig. 3.5h, j and car in Fig. 3.5i, k).

Subsequently, the cells on the adaxial side started to exhibit relatively strong growth, and the direction of expansion of most of the cells in the primordium became more isotropic (e.g., sd1 in Fig. 3.5k).

In addition, we observed that after the initial strong growth phase in the abaxial cells, the primordia of sd1 displayed a lower overall growth rate than other NEP; for instance, sd1 in Fig. 3.5h vs. sd2 in Fig. 3.5i. This observation was confirmed by quantifying the number of cells that exhibited growth rates above 1.8 in ICP and NEP of different developmental windows (Fig. 3.5l). During the developmental window TP2 to TP3, in which the sd1 was the ICP, these primordia had similar numbers of cells exhibiting high growth compared to ICP and NEP of other stages. However, once the floral buds enter the TP3 to TP4 window, in which the carpels were the ICP and sd1 was the NEP, the number of sd1 cells exhibiting high growth decreased significantly (Fig. 3.5l).

Among the cells that exhibited high growth rates in the ICP and NEP of different developmental windows, we asked what percentage of these cells experienced cell division during the interval. We did not observe any significant difference between primordia of different windows (Fig. 3.5m) and, on average, about 50% of the cells exhibited both high growth and experienced cell division. We also examined the orientations of the division planes among these cells, and found that

while there was no significant difference between primordia of different stages and developmental windows, most of the cell divisions occurred parallel to the lateral axis (Fig. 3.5n).

Early carpel development

We then analyzed the initial development of the carpel primordia, with a particular focus on three regions: the distal edge, the primordial boundary, and the adaxial fold (Fig. 3.6a). From TP4 to TP6, the width of the distal edge increased both along the lateral axis and the radial axis, and the curvature of most cells increased (Fig. 3.6b-d). Over the same period, the primordial boundary became more folded towards the center of the apex (Fig. 3.6e-g). At TP4 and TP5, the regions that would become the adaxial folds transition from having positive surface curvature to having close to zero (i.e. flat) surface curvature (Fig. 3.6h, i). At TP6, invagination of the adaxial fold appeared to initiate at the base of the primordium and propagate outward such that the proximal region was more deeply folded than the distal at this stage (Fig. 3.6j).

Once the five carpel primordia were initiated, two processes occurred simultaneously to achieve the flat star shape (Fig. 3.6). First, cells at the distal edges of the carpel primordia continued to display relatively high growth rates (Fig. 3.6c'), while cells at the center of the floral apex exhibited much lower overall growth rates (Fig. 3.3). This had the effect of elevating the carpel primordia to the same level as the center of the floral apex. However, unlike the early initiation of the carpel primordia, during which growth was mainly driven by the strong anisotropic expansion from the abaxial cells (Fig. 3.5i, k), the overall anisotropy of the cells on the carpel primordia distal edges was lower and less directional (Fig. 3.6c''). Meanwhile, numerous cells underwent cell division during this developmental window, suggesting that growth was mainly driven by cell division (Fig. 3.6c'). Second, cells at the primordial boundaries experienced strong compression along the lateral axis (Fig. 3.6f''), which helped to define the primordial boundary regions of the flat star shape.

Interestingly, at this stage, although the floral apex was flat and the adaxial folds were not yet physically visible (Fig. 3.6i), minor compression of cells in the future location of the adaxial fold can already be observed (Fig. 3.6i'').

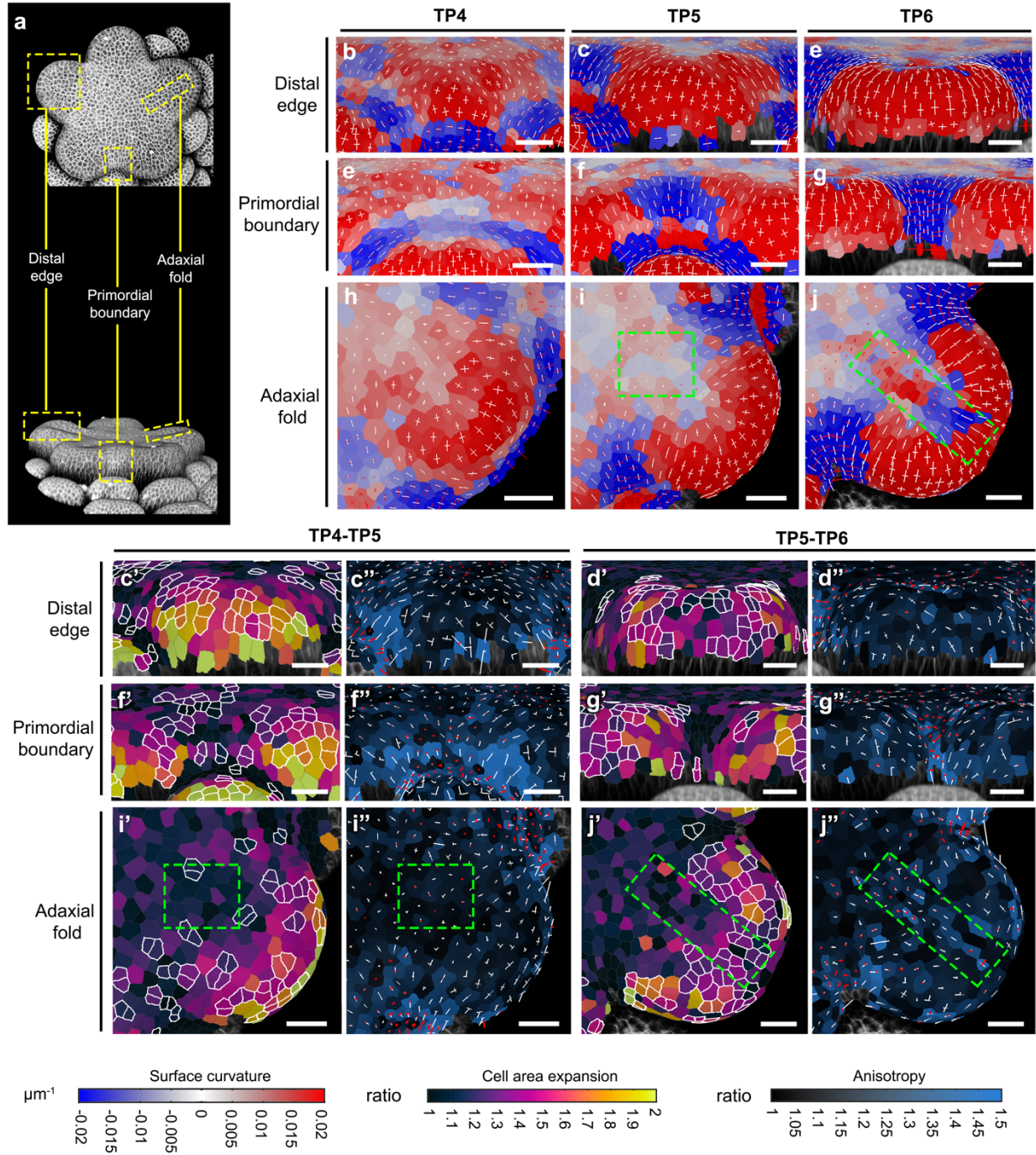


Figure 3.6. Early carpel primordia development. (a) Front view and side view of an *A. coerulea* FM at TP6 to indicate different regions of interest. **(b-d)** Side views of the surface curvature heatmaps of the distal edges of

(Continued) carpel primordia at TP4, TP5, TP6, respectively. **(e-g)** Side views of the surface curvature heatmaps of the primordial boundaries between carpels at TP4, TP5, TP6, respectively. **(h-j)** Front view of the surface curvature heatmaps of the adaxial folds of carpel primordia at TP4, TP5, TP6, respectively. **(c', c'')** Heatmaps of cell area expansion and anisotropy of distal edges between TP4 to TP5, respectively, overlaid onto TP5. **(d', d'')** Heatmaps of cell area expansion and anisotropy of distal edges between TP5 to TP6, respectively, overlaid onto TP6. **(f', f'')** Heatmaps of cell area expansion and anisotropy of primordial boundaries between TP4 to TP5, respectively, overlaid onto TP5. **(g', g'')** Heatmaps of cell area expansion and anisotropy of primordial boundaries between TP5 to TP6, respectively, overlaid onto TP6. **(i', i'')** Heatmaps of cell area expansion and anisotropy of adaxial folds between TP4 to TP5, respectively, overlaid onto TP5. **(j', j'')** Heatmaps of cell area expansion and anisotropy of adaxial folds between TP5 to TP6, respectively, overlaid onto TP6. Cells outlined in white in all cell area expansion heatmaps were cells that experienced cell divisions during the intervals. Green dashed boxes in i, i', i'', j, j', j'' indicate the adaxial folds. All distal edge panels are the side view of the distal edge, all primordial boundary panels are the side views of the primordial boundary, and all adaxial fold panels are the front view of the adaxial fold. Scale bars = 20 μm .

After formation of the flat star apex, the carpel primordia began to elevate along their distal ridges, which was mainly achieved by concentrated cell divisions on the ridges (Fig. 3.6d', j') while the anisotropic expansion rates of cells on the ridges remained low (Fig. 3.6d''). The growth alignment graphs in Fig. 3 also support this observation of concentrated cell divisions in the peripheral region relative to the earlier developmental windows (Fig. 3.3). Meanwhile, the cells at the primordial boundaries continued to experience strong compression along their lateral axis. We did not observe any further cell division in the primordial boundaries (Fig. 3.6g', g''). In addition, the adaxial folds of the carpels have become morphologically visible (Fig. 3.6j), exclusively achieved by modifications in cell shape since no cell division occurred in the region (Fig. 3.6j'). Specifically, cells of the adaxial fold located closer to the center of the floral apex experienced strong compression, while those in the distal region of the adaxial fold exhibited strong anisotropic expansion along the radial axis (Fig. 3.6j'').

DISCUSSION

Cellular dynamic change during FMT in *A. coerulea*

Despite its essential role in floral development, little is known about meristem dynamics during FMT at a cellular level, and the molecular basis of FMT has only been investigated in *A. thaliana* and tomato (Sun *et al.*, 2009, 2014; Bollier *et al.*, 2018). In *A. thaliana*, FMT is marked by down-regulation of the gene *WUS*, which determines stem cell identity; this shift also coincides with the initiation of carpel primordia (Sun *et al.*, 2009, 2014). Therefore, FMT defines the transition from being pluripotent to organogenic for the cells in the central zone, and thus the precise timing of *WUS* repression is considered a key factor that determines the number of cells produced for carpel development (Sun *et al.*, 2014; Sun & Ito, 2015).

Previous transcriptomic sequencing in young *A. coerulea* FMs indicated that the expression of *AqWUS* is maintained during the developmental stages equivalent to TP1 through TP3 in the current study, with expression dropping rapidly to undetectable levels during the developmental stages equivalent to TP4 to TP6 (Min & Kramer, 2020). If we examine the central region of the FM (i.e., bin1 and bin2 in the growth alignment graphs, Fig. 3.3f), which roughly corresponds to the central zone, we did observe similarly low numbers of cell divisions between TP1 to TP3 (Fig. 3.3f; Table B1), with bin2 being higher than bin1. During TP4 to TP6, which corresponds to the early stages of carpel development, the average number of cell divisions in the center of the floral apex was close to zero (Fig. 3.3f; Table B1). However, most strikingly, we observed a higher number of cell divisions in the center of the floral apex between TP3 to TP4, during which the carpel primordia are initiated (Fig. 3.3c, c', f), with the bin1 values being statistically significantly higher than all other stages (Fig. 3.3f; Table B1).

This observation raises some intriguing questions: Why is there an increase in cell division in the central zone when the carpel primordia are initiating, and what is responsible for the pattern? This period also appears to correspond with the onset of FMT based on the decline in *AqWUS* expression, so is this the last flush of CZ cell divisions or are the divisions related more directly to

initiation of the carpel primordia? Answering these questions will require a better understanding of how *AqWUS* down-regulation is controlled in *Aquilegia*, particularly the nature of any “timer mechanism” regulating the number of cell divisions before FMT. In the FMs of *A. thaliana* and tomato, the gene *KNUCKLES* (*KNU*) is activated in a cell division-dependent manner, which determines the temporal control of FMT, since once *KNU* is activated, it terminates the expression of *WUS*. Manipulation of cell cycles in the FM can accelerate or delay the activation of *KNU*, which results in the premature or delayed termination of the FM, respectively (Sun *et al.*, 2014). We currently do not know whether the *KNU-WUS* pathway is conserved in other angiosperm systems, especially taxa with more than one whorl of stamens and unfused carpels but, even if it is not conserved, it will be interesting to examine whether a division-dependent timing mechanism is used for FMT in general. Overall, the combined patterns of cell behavior we observe at the center of the meristem during TP3-TP4 then transitioning into TP4-TP5, which include a sudden uptick in divisions during TP3-TP4 and a sharp decline in cell expansion following this phase, appear to be markers for a loss of stem cell identity in this zone in conjunction with the FMT.

Floral organ primordia initiation in *A. coerulea*

In examining the initiation of the stamen, staminode, and carpel primordia, we observed interesting dynamics in the relative growth behavior of the adaxial and abaxial cells (Fig. 3.4; Fig. 3.5). First, only some of the cells that initially exhibited positive curvature in the NEP end up as adaxial cells in the primordium proper, with the adaxial-most cells being incorporated into the primordium boundary. Second, cells with negative surface curvature that were mainly located in the boundary region below the initial bulge ultimately become the cells exhibiting the highest growth rates. These high growth rates were mainly driven by the high anisotropic cell expansion, which coupled with later cell division quickly promotes outgrowth of the abaxial surface of the

primordium. This pattern is consistent with a previous study of expression of the abaxial polarity gene *AqFIL*, which is detected broadly across the entire ICP and most of the NEP (Fig. 3.1f), similar to the expression patterns of *FIL* in *A. thaliana* FMs (Meaders *et al.*, 2020; Zhao & Traas, 2021). It is curious that cells exhibiting the highest growth rates are along the extreme abaxial margin of the primordium, representing only a portion of the typical abaxial domain, a pattern that has also been observed during leaf and sepal primordium initiation in *A. thaliana* (Zhao & Traas, 2021). A close examination of the spatial-temporal expression patterns of other polarity genes in *A. coerulea* will be a good starting point to decipher any potential difference in the abaxial cells, as well as the transition of cells that were originally in the adaxial surface but ended up in the organ boundary regions.

The observed difference in the growth dynamics between sd1 and sd2 was more surprising. Once the primordia initiate as NEP, the growth rates of sd1 appeared to be lower than other NEP and ICP in other developmental intervals (Fig. 3.5l). Although the sd1 and sd2 whorls have the same staminode identity (Kramer *et al.*, 2007; Sharma & Kramer, 2013), a previous study has observed subtle morphological differences that are apparent when the primordia are as small as 1-2 mm in length, most notably lateral marginal curling that facilitates late-stage adhesion between the organs (Meaders *et al.*, 2020). In that study, the authors raised the question of whether these differences were developmentally determined from the earliest stages or were due to some kind of inductive interaction of the tissues. Our observation of differences from inception may suggest that they do harbor distinct developmental trajectories from their earliest stages, possibly implicating identity-based differences.

In addition, we examined the early developmental processes of the carpel primordia in detail, capturing a transition from growth that is mainly driven by strong anisotropic cell expansion to one that is promoted by concentrated cell divisions (Fig. 3.6). The initial cell expansion phase helps to lift

the carpel primordia up, while the cell division phase appears to sculpt their shape (Fig. 3.5i, k; Fig. 3.6). The first phase of cell expansion seems to be very similar to the initiation of the stamen and staminodes, which was likewise driven by strong anisotropic expansion by a small number of abaxial cells (Fig. 3.5). However, the second phase of carpel growth is quite different from the other organs in that there is a much stronger reliance on accumulation of cell divisions while the cell areas did not expand significantly (e.g., st1 in Fig. 3.4 compared to Fig. 3.6). This observation could suggest that we observed a transition between two sets of molecular programs during early carpel primordia growth: one for the earliest phase of primordia initiation that is common to all floral organs and the subsequent program that is specific to sculpting carpel primordia.

AUTHOR CONTRIBUTIONS

YM and EMK conceived of the study. YM and SJC imaging, data processing and analysis, and EMK provided oversight of the study. YM wrote the manuscript with input from SJC and EMK.

ACKNOWLEDGEMENT

The authors would like to thank Mingyuan Zhu, Daniel Kierzkowski, Anne-Lise Routier-Kierzkowska, Richard Smith, and Soeren Strauss for patiently answering all the questions about MorphoGraphX, and Weilin Meng for generously lending his PC during the entire Covid19 pandemic, on which we conducted all the image processing and analysis. This study was funded by the Emerging Models Award to Ya Min from the Society of Developmental Biology.

REFERENCES

- Barbier de Reuille P, Routier-Kierzkowska A-L, Kierzkowski D, Bassel GW, Schüpbach T, Tauriello G, Bajpai N, Strauss S, Weber A, Kiss A, *et al.* 2015. MorphoGraphX: A platform for quantifying morphogenesis in 4D. *eLife* 4: e05864.
- Bartlett ME, Thompson B. 2014. Meristem identity and phyllotaxis in inflorescence development. *Frontiers in Plant Science* 5.
- Bollier N, Sicard A, Leblond J, Latrasse D, Gonzalez N, Gévaudant F, Benhamed M, Raynaud C, Lenhard M, Chevalier C, *et al.* 2018. At-MINI ZINC FINGER2 and SI-INHIBITOR OF MERISTEM ACTIVITY, a Conserved Missing Link in the Regulation of Floral Meristem Termination in Arabidopsis and Tomato. *The Plant Cell* 30: 83–100.
- Endress PK. 1990. Patterns of floral construction in ontogeny and phylogeny. *Biological Journal of the Linnean Society* 39: 153–175.
- Filiault DL, Ballerini ES, Mandáková T, Aköz G, Derieg NJ, Schmutz J, Jenkins J, Grimwood J, Shu S, Hayes RD, *et al.* 2018. The *Aquilegia* genome provides insight into adaptive radiation and reveals an extraordinarily polymorphic chromosome with a unique history. *eLife* 7: e36426.
- Hamant O, Das P, Burian A. 2019. Time-Lapse Imaging of Developing Shoot Meristems Using A Confocal Laser Scanning Microscope. *Methods in Molecular Biology (Clifton, N.J.)* 1992: 257–268.
- Harrison CJ, Roeder AHK, Meyerowitz EM, Langdale JA. 2009. Local Cues and Asymmetric Cell Divisions Underpin Body Plan Transitions in the Moss *Physcomitrella patens*. *Current Biology* 19: 461–471.
- Heisler MG, Ohno C. 2014. Live-Imaging of the *Arabidopsis* Inflorescence Meristem. In: Riechmann JL, Wellmer F, eds. *Methods in Molecular Biology. Flower Development*. New York, NY: Springer New York, 431–440.
- Hill JP, Lord EM. 1989. Floral development in *Arabidopsis thaliana*: a comparison of the wild type and the homeotic *pistillata* mutant. *Canadian Journal of Botany* 67: 2922–2936.
- Kierzkowski D, Runions A, Vuolo F, Strauss S, Lymbouridou R, Routier-Kierzkowska A-L, Wilson-Sánchez D, Jenke H, Galinha C, Mosca G, *et al.* 2019. A Growth-Based Framework for Leaf Shape Development and Diversity. *Cell* 177: 1405-1418.e17.
- Kirchoff BK, Claßen-Bockhoff R. 2013. Inflorescences: concepts, function, development and evolution. *Annals of Botany* 112: 1471–1476.

- Kramer EM. 2009. *Aquilegia*: A New Model for Plant Development, Ecology, and Evolution. *Annual Review of Plant Biology* 60: 261–277.
- Kramer EM, Holappa L, Gould B, Jaramillo MA, Setnikov D, Santiago PM. 2007. Elaboration of B Gene Function to Include the Identity of Novel Floral Organs in the Lower Eudicot *Aquilegia*. *The Plant Cell* 19: 750–766.
- Kuchen EE, Fox S, Reuille PB de, Kennaway R, Bensmihen S, Avondo J, Calder GM, Southam P, Robinson S, Bangham A, *et al.* 2012. Generation of Leaf Shape Through Early Patterns of Growth and Tissue Polarity. *Science* 335: 1092–1096.
- Laux T, Mayer KF, Berger J, Jürgens G. 1996. The *WUSCHEL* gene is required for shoot and floral meristem integrity in *Arabidopsis*. *Development (Cambridge, England)* 122: 87–96.
- Lenhard M. 2003. Stem cell homeostasis in the *Arabidopsis* shoot meristem is regulated by intercellular movement of *CLAVATA3* and its sequestration by *CLAVATA1*. *Development* 130: 3163–3173.
- Marc J, Palmer JH. 1982. Changes in Mitotic Activity and Cell Size in the Apical Meristem of *Helianthus Annuus* L. During the Transition to Flowering. *American Journal of Botany* 69: 768–775.
- Mayer KFX, Schoof H, Haecker A, Lenhard M, Jürgens G, Laux T. 1998. Role of *WUSCHEL* in Regulating Stem Cell Fate in the *Arabidopsis* Shoot Meristem. *Cell* 95: 805–815.
- Meaders C, Min Y, Freedberg KJ, Kramer E. 2020. Developmental and molecular characterization of novel staminodes in *Aquilegia*. *Annals of Botany* 126: 231–243.
- Min Y, Kramer EM. 2020. Transcriptome profiling and weighted gene co-expression network analysis of early floral development in *Aquilegia coerulea*. *Scientific Reports* 10: 19637.
- Monniaux M, Pieper B, McKim SM, Routier-Kierzkowska A-L, Kierzkowski D, Smith RS, Hay A. 2018. The role of *APETALA1* in petal number robustness. *eLife* 7: e39399.
- O'Connor DL. 2018. Live Confocal Imaging of *Brachypodium* Spikelet Meristems. *Bio-protocol* 8: e3026–e3026.
- Prunet N, Duncan K. 2020. Imaging flowers: a guide to current microscopy and tomography techniques to study flower development (F Wellmer, Ed.). *Journal of Experimental Botany* 71: 2898–2909.
- Prunet N, Jack TP, Meyerowitz EM. 2016. Live confocal imaging of *Arabidopsis* flower buds. *Developmental Biology* 419: 114–120.
- Prunet N, Yang W, Das P, Meyerowitz EM, Jack TP. 2017. *SUPERMAN* prevents class B gene expression and promotes stem cell termination in the fourth whorl of *Arabidopsis thaliana* flowers. *Proceedings of the National Academy of Sciences* 114: 7166–7171.

- Rahni R, Birnbaum KD. 2019. Week-long imaging of cell divisions in the *Arabidopsis* root meristem. *Plant Methods* 15: 30.
- Reddy GV, Roy-Chowdhury A. 2009. Live-imaging and image processing of shoot apical meristems of *Arabidopsis thaliana*. *Methods in Molecular Biology (Clifton, N.J.)* 553: 305–316.
- Roeder AHK, Chickarmane V, Cunha A, Obara B, Manjunath BS, Meyerowitz EM. 2010. Variability in the Control of Cell Division Underlies Sepal Epidermal Patterning in *Arabidopsis thaliana*. *PLOS Biology* 8: e1000367.
- Sappl PG, Heisler MG. 2013. Live-imaging of plant development: latest approaches. *Current opinion in plant biology* 16(1): 33-40.
- Schoof H, Lenhard M, Haecker A, Mayer KFX, Jürgens G, Laux T. 2000. The Stem Cell Population of Arabidopsis Shoot Meristems Is Maintained by a Regulatory Loop between the *CLAVATA* and *WUSCHEL* Genes. *Cell* 100: 635–644.
- Sharma B, Kramer E. 2013. Sub- and neo-functionalization of *APETALA3* paralogs have contributed to the evolution of novel floral organ identity in *Aquilegia* (columbine, Ranunculaceae). *New Phytologist* 197: 949–957.
- Steeves TA, Sussex IM. 1989. *Patterns in Plant Development*. Cambridge University Press.
- Stewart RN, Dermen H. 1970. Determination of Number and Mitotic Activity of Shoot Apical Initial Cells by Analysis of Mericlinal Chimeras. *American Journal of Botany* 57: 816–826.
- Sun B, Ito T. 2015. Regulation of floral stem cell termination in *Arabidopsis*. *Frontiers in Plant Science* 6.
- Sun B, Looi L-S, Guo S, He Z, Gan E-S, Huang J, Xu Y, Wee W-Y, Ito T. 2014. Timing Mechanism Dependent on Cell Division Is Invoked by Polycomb Eviction in Plant Stem Cells. *Science* 343: 1248559–1248559.
- Sun B, Xu Y, Ng K-H, Ito T. 2009. A timing mechanism for stem cell maintenance and differentiation in the *Arabidopsis* floral meristem. *Genes & Development* 23: 1791–1804.
- Tucker SC, Hodges SA. 2005. Floral Ontogeny of *Aquilegia*, *Semiaquilegia*, and *Enemion* (Ranunculaceae). *International Journal of Plant Sciences* 166: 557–574.
- Whitewoods CD, Cammarata J, Venza ZN, Sang S, Crook AD, Aoyama T, Wang XY, Waller M, Kamisugi Y, Cuming AC, et al. 2020. *CLAVATA* Was a Genetic Novelty for the Morphological Innovation of 3D Growth in Land Plants. *Current Biology* 30: 2645–2648.
- Yadav RK, Perales M, Gruel J, Girke T, Jonsson H, Reddy GV. 2011. WUSCHEL protein movement mediates stem cell homeostasis in the Arabidopsis shoot apex. *Genes & Development* 25: 2025–2030.
- Zhang T, Cieslak M, Owens A, Wang F, Broholm SK, Teeri TH, Elomaa P, Prusinkiewicz P. 2021. Phyllotactic patterning of gerbera flower heads. *Proceedings of the National Academy of Sciences* 118: e2016304118.

Zhao F, Traas J. 2021. Stable establishment of organ polarity several plastochrons before primordium outgrowth in *Arabidopsis*. *Development*: dev.198820.

CHAPTER 3.

Genetic architecture underlying variation in floral meristem termination in *Aquilegia*

The following authors contributed to this chapter:

Min, Y., Ballerini, E. S., Edwards, M., B., Hodges, S., A., & Kramer, E. M.

ABSTRACT

Floral meristem termination (FMT) is one of the defining features of a floral meristem (FM). Unlike vegetative meristems, which possess persistent stem cell activity and can generate new leaves continuously throughout the lifespan of a plant, the stem cell activity in a FM will always terminate at a specific time point during primordia initiation, since each flower only has a finite number of organs. Variation in the timing of FMT is an essential source of generating floral morphological diversity, but how this process is fine-tuned at a developmental and evolutionary level is still poorly understood. *Aquilegia* is a well-suited system for investigating this fundamental process, since flowers from different *Aquilegia* species have identical numbers of all floral organs except for stamens. Therefore, variation in the timing of FMT can be represented by consistent differences in stamen whorl numbers between species. We conducted quantitative trait loci (QTL) mapping of this phenotype by crossing two sister species, *A. canadensis* and *A. brevistyla*. Our results reveal a complex genetic architecture with seven major QTL underlying variation in FMT. Each QTL has a small effect, which together account for 46.5% of the phenotypic variation. Utilizing previously published RNA-sequencing data, we identified potential candidate genes under every QTL, and used *in situ* hybridization to reveal novel expression patterns of select candidate genes. To our knowledge, this is the first study to attempt to dissect the genetic basis of how natural variation in the timing of FMT is regulated, and our results provide critical insight into the regulation of FMT and how floral morphological diversity can be generated at the meristematic level.

INTRODUCTION

Indeterminate growth is the foundation of development in all vascular plants and is achieved by the persistent activity of stem cells in the meristems (Steeves & Sussex, 1989). Apical meristems in the shoots and roots are highly organized structures that maintain a delicate yet robust balance between the production of cells that give rise to organs and the renewal of the stem cell population. In the flowering plants, when a plant enters the reproductive phase, the vegetative meristem transitions from producing leaves to reproductive identity, which results in the production of floral organs. Although the overall cellular organization of the vegetative meristem and the floral meristem (FM) is highly similar, the transition to the FM identity is accompanied by a number of changes in the properties of the meristem, including changes in the rate of organ production, the patterns of primordia initiation, and an eventual loss of indeterminacy.

The establishment of determinacy in the FM is a well-regulated process, termed floral meristem termination (FMT), which is crucial and universal in the development of all flowers (Fig. 4.1). A typical flower has four types of floral organs: sepals, petals, stamens, and carpels, which are arranged from the outermost to the innermost positions of a flower (Fig. 4.1). Although the central stem cells stay active in the initial phase of floral organ primordia initiation, this activity will cease at a specific time point, after which all cells will be incorporated into the development of the terminal carpels (Steeves & Sussex, 1989). The precise control of FMT is critical to ensuring that the flower has the correct number of organs, but it is also important to note that variation in the timing of FMT is an important source of floral morphological diversity and novelty. For some species, such as *Arabidopsis thaliana*, FMT occurs relatively quickly, and only four whorls of floral organs are produced. In many other taxa, FM activity is maintained for a more extended period; species from the Magnoliaceae, Monimiaceae, Nelumbonaceae, Nymphaeaceae, Papaveraceae, and Ranunculaceae, for instance, can have hundreds of spirally-arranged or whorled floral organs (Endress, 1990; Fig. 4.1). Moreover, increased numbers of floral organs can create the raw materials for the evolution of new organ types, such as the sterile staminodes observed in *Aquilegia* (Ranunculaceae) or *Mentzelia* (Loasaceae) (Walker-Larsen & Harder, 2000). Understanding how FMT is regulated in different angiosperm lineages is, therefore, interesting from both developmental and evolutionary perspectives. The diversity in floral morphology of the ~400,000 angiosperm species is seemingly infinite, but one of the few major evolutionary trends from the early-diverging angiosperms to both the core eudicot and monocot lineages is the transition from variable to stable whorl numbers in a flower (Endress, 1990), which is directly determined by the timing of FMT.

Currently, we have relatively good knowledge of the genes that are responsible for maintaining and terminating stem cell activities in the *A. thaliana* FM, but how the timing of FMT is fine-tuned at the developmental and evolutionary level is poorly understood. In the FM, the

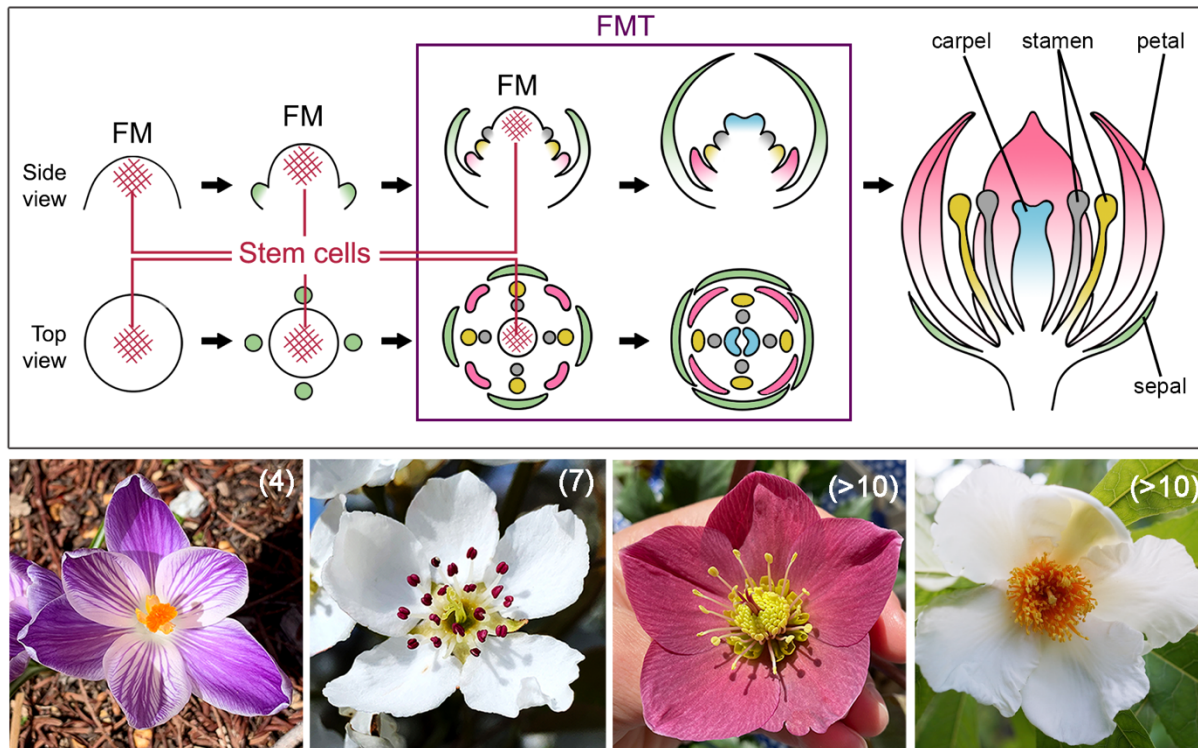


Figure 4.1: FMT is an important and fine-tuned developmental process that occurs in all flowers. Upper panel: diagram of floral organ initiation and FMT during flower development. Organs of the same whorl share the same colors. Lower panel: example of four flowers with different whorl numbers. From left to right: *Crocus vernus* 'Pickwick', *Pyrus communis*, *Helleborus orientalis*, and *Franklinia alatamaha*. Numbers in the parentheses indicate the number of whorls of floral organs in each flower. Photos of *Crocus* and *Pyrus* were taken by Ya Min, and photos of *Helleborus* and *Franklinia* were taken by Evangeline S. Ballerini and Jacob Suissa, respectively.

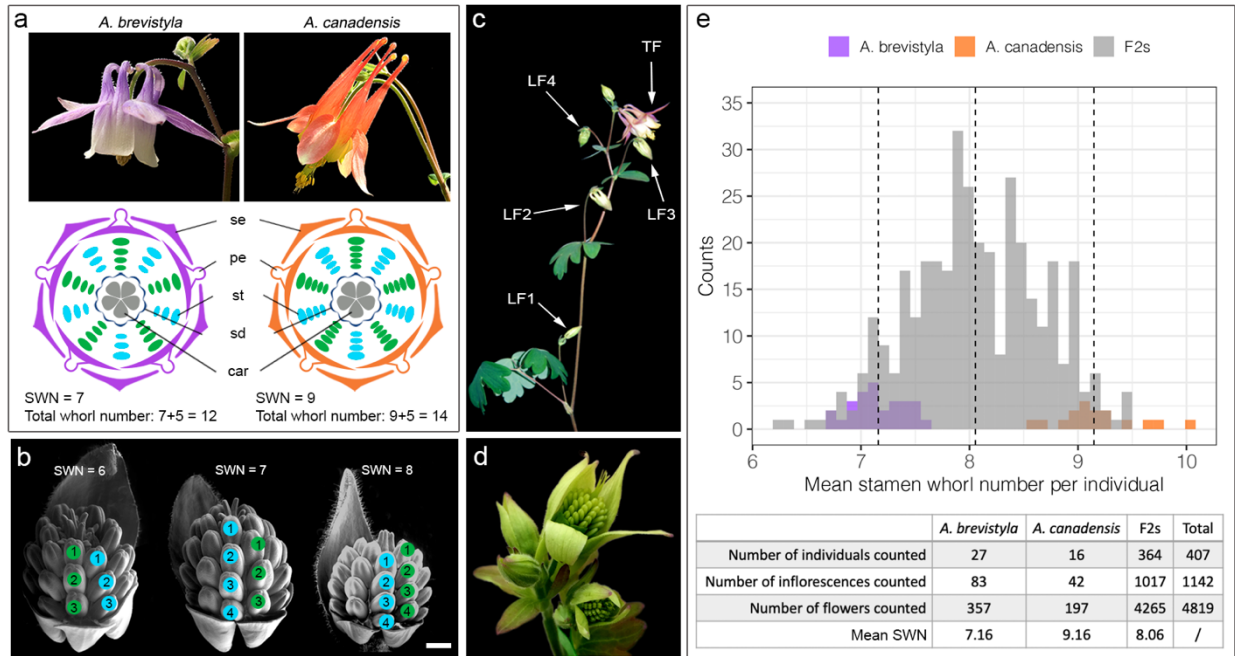
maintenance of the stem cell population is achieved by a feedback loop between the homeodomain protein WUSCHEL (WUS) and the CLAVATA (CLV) ligand-receptor system, in which WUS promotes central stem cell activity and induces the expression of the CLV3 peptide, while activation of the CLV signaling pathway, in turn, represses the expression of WUS (Schoof *et al.*, 2000; Lenhard, 2003; Müller *et al.*, 2006). In the early developing FM, the expression of the C class organ identity gene *AGAMOUS* (*AG*) is induced by WUS acting as a co-factor with the FM identity gene *LEAFY*. *AG*, in turn, specifies the identity of stamens and carpels in the inner whorls of a flower and is also responsible for the down-regulation of WUS expression (Lenhard *et al.*, 2001). While the broad conservation of the WUS-CLV and WUS-AG feedback loops have been demonstrated in

diverse plant taxa (Nardmann & Werr, 2006; Litt & Kramer, 2010; Whitewoods *et al.*, 2020), the exact mechanisms by which AG controls the precise timing of *WUS* down-regulation have only been investigated in *A. thaliana* and tomato (*Solanum lycopersicum*). Specifically, AG activates the expression of a C2H2 zinc-finger transcription factor, *KNUCKLES (KNU)*, which directly represses *WUS* together with adaptor proteins from the MINI ZINC FINGER (MIF) protein family (Payne, 2004; Sun *et al.*, 2009; Bollier *et al.*, 2018). Accurate timing of FMT is achieved in *A. thaliana* because the activation of *KNU* by AG takes approximately two rounds of cell divisions, during which the stamen primordia are initiated. After FMT is achieved, all of the cells remaining in the center of the FM are incorporated into the carpel primordia (Sun *et al.*, 2009).

However, integral to the precise mechanism of *KNU* activation is that it only allows for the production of one whorl of stamens and one whorl of carpels in a flower. This begs the question of whether this pathway is conserved in systems that have more than just four whorls of floral organs. Nonetheless, all currently established model systems (and their close relatives) belong to lineages in the core eudicots or monocot grasses that exhibit no variation in their floral whorl numbers, while most of the plant taxa exhibiting variation in whorls do not have the genomic or genetic resources nor functional tools. Thus, they cannot provide a useful starting point for the investigation of the degree of conservation in this known pathway, or how natural variation in the timing of FMT is regulated in general.

To that end, *Aquilegia* from the buttercup family (Ranunculaceae) is exceptionally well-suited for investigating this fundamental developmental process. There are approximately 70 *Aquilegia* species, which share a low interspecific sequence variation and a high degree of inter-fertility due to a recent adaptive radiation (Filiault *et al.*, 2018). All *Aquilegia* species but one (*A. jonesii*, which lacks staminodes; Munz, 1946) have the same floral organ arrangement, consisting of one whorl of five sepals, one whorl of five petals, many whorls of stamens, two whorls of five staminodes (i.e., 10 in

total), and one whorl of five carpels (Fig. 4.2a). These floral organs are arranged in 10 orthostichies (vertical rows of organs), with alternate orthostichies either positioned directly above the sepals or the petals (Fig. 4.2a).



Figures 4.2: Phenotyping SWN in the parental and F2s populations. (a) Photos of flowers and floral diagrams of *A. brevistyla* and *A. canadensis*. (b) Examples of three F2 flower buds with different SWN. (c) Flowers that were sampled per inflorescence. (d) Developmental stages for which SWN were counted. (e) Histogram and summary statistics of SWN distribution in parental species and the F2s. In (a) and (b), stamen whorls positioned above the sepals are colored in blue while stamen whorls positioned above the petals are colored in green. Scale bar in (b) = 100 μ m. se: sepals; pe: petals; st: stamens; sd: staminodes; car: carpels.

Aquilegia brevistyla and *A. canadensis* are North American sister species (Bastida *et al.*, 2010; Fior *et al.*, 2013; Fig. 4.2a) and, based on previous empirical field observation, their flowers differ in their number of stamen whorls (Munz, 1946). Given that the number of whorls of all the non-stamen floral organs (i.e., sepals, petals, staminodes, and carpels) is identical in these two species, the variation in what we term Stamen Whorl Number (SWN) can be directly translated into variation in the timing of FMT: if the FM is terminated earlier, it will have a smaller SWN compared to a flower of which the FM stays active longer. Using SWN as a quantitative trait, we crossed *A. brevistyla* and *A. canadensis* and conducted quantitative trait locus (QTL) mapping in the resultant F2 generation.

Our results reveal a complex genetic architecture with seven major QTL underlying the variation of FMT. To our knowledge, this is the first study to attempt to dissect the genetic bases of how the natural variation in the timing of FMT is regulated, and our results highlight several potential candidate genes and molecular pathways that may contribute to the regulation of FMT in *Aquilegia*.

MATERIALS AND METHODS

Plant material and growth conditions

A. brevistyla and *A. canadensis* seeds were collected from wild populations in Alberta (Canada) and Ithaca (NY, USA), respectively. One *A. canadensis* (pollen recipient) was crossed with one *A. brevistyla* (pollen donor) to generate the F1 generation. Five F1s were self-fertilized to generate the F2 population. All F2 seeds were stratified at 4 °C in the dark for two to four weeks, germinated in wet soil, and transplanted in individual pots. All plants were vernalized at 4°C for two months to induce flowering. The parental and F1 individuals were grown in the greenhouse of the University of California Santa Barbara, and the F2 populations were grown in the greenhouses of Harvard University. All greenhouses used the same light and temperature conditions to achieve a 16h/8h (day/night) photoperiod at 18°C and 13°C.

Seeds of *Aquilegia x coerulea* 'Kiragami' were purchased from Swallowtail Garden Seeds (Santa Rosa, CA, USA), germinated in wet soil, and grow under the same 18°C /13°C (day/night) condition as described above. Once the plants developed approx. six true leaves, they were transferred into vernalization conditions (16 h daylight at 6 °C and 8 h dark at 6 °C) for three to four weeks, and then moved back to the regular growth conditions to promote flowering.

Meristem size measurement

The entire inflorescences of at least six individuals of each parental species were collected and fixed in FAA (10% formaldehyde, 50% ethanol, 5% acetic acid), and stored at 4°C. Samples were then dehydrated through a graded ethanol series to 100%, transferred to 100% CitriSolv, and embedded in Paraplast Plus (Sigma-Aldrich). Embedded tissues were sectioned to 8 µm thick ribbons with a rotary microtome, stained in 0.1% Toluidine Blue O solution following the protocol described in Ruzin (1990), and mounted in Permount Mounting Medium (Fisher Scientific). Sections were then imaged using the Axio Zoom Microscope at the Harvard Center for Biological Imaging. The width of each floral meristem section was measured using ImageJ. Three to six serial sections were measured for each FM, and at least three FMs were measured for each developmental stage of each species. All FMs that were measured were non-terminal flowers. Early developmental stages were divided into five stages based on the number of stamen whorls that had initiated in the FM. During very early stages, it was not possible to morphologically distinguish the petal and stamen primordia based on the histological sections. Therefore, the stages were defined with a range of numbers to include the possibility of including zero to one whorls of petals.

Phenotyping

For each plant, the SWN of the terminal flower and lateral flowers 1 to 4 from the first three inflorescences were counted (Fig. 4.2c). If flowers of these positions in an inflorescence were damaged/undeveloped, flowers at other positions were counted to achieve a total number of five flowers per inflorescence. If an inflorescence produced less than five flowers, all flowers were counted. SWN were counted when the flowers reached approx.1-2 cm in length (Fig. 4.2d) because at that developmental stage, all the stamens were arranged in vertical rows, which simplified counting.

Genotyping

Detailed genotyping information can be found in (Edwards *et al.*, 2021). Briefly, the DNA of the two parents that generated the cross was extracted from flash-frozen young leaves using NEBNext Ultra II kit (NEB) and sequenced to ~40x coverage as 150 bp reads on an Illumina MiSeq at the Biological Nanostructures Lab in the California NanoSystem Institute at UC Santa Barbara. DNA of F2s was extracted from silica dried young leaves using Qiagen DNEasy reagents and Magattract beads (Qiagen, Inc.), libraries were prepared following the protocol of RipTide High Throughput Rapid DNA Library Preparation kit (iGenomX, CA, USA). The F2 libraries were pooled and sequenced at the Vincent J. Coates Genomics Sequencing Laboratory (UC Berkeley) using NovaSeq 6000 platform to generate 150bp paired-end reads. Samples were multiplexed to generate about 1-2x coverage. All sequence data are deposited in the Sequence Read Archive under BioProject ID PRJNA720109. Scripts and genotype/phenotype data are available at: <https://github.com/anjiballerini/can.x.brev/>.

Sequences were aligned to the *A. coerulea* 'Goldsmith' v3.1 reference genome (<https://phytozome.jgi.doe.gov>) using the Burrows-Wheeler aligner (Li & Durbin, 2009) and variable sites in the parents were identified using SAMtools 0.1.19 (Li *et al.*, 2009a) with custom scripts were used to identify the positions and genotypes at which the parents were homozygous for different alleles. These sites were used to assign reads in the F2s as having either *A. canadensis* or *A. brevistyla* ancestry. To determine the genotypes of the F2s, the genome sequences were binned into 0.5 Mb regions with moderate to high recombination frequencies and 1 Mb in regions with low or no recombination, and the frequency of reads with ancestry for each F0 parent was used to determine the genotype of the bin. These bins and genotypes were used as markers to construct a genetic map and conduct QTL mapping. This genotyping method has been implemented in Filiault *et al.*, 2018, Ballerini *et al.*, 2020, and Edwards *et al.*, 2021.

Mapping

After filtering out individuals and markers with more than 10% of information missing due to sequencing quality, we retained a total of 366 individuals and 620 markers. A genetic map of the seven chromosomes was then constructed following the protocol of the R/qtl package v1.46-2 (Broman *et al.*, 2003), with an error probability rate of 0.001 and “kosambi” map function. Standard interval mapping with Haley-Knott regression (function *scanone*) was used for the initial mapping searching for potential QTL. The best multi-QTL models are produced and selected by using function *stepwiseqtl*, which implement penalties on different interactions and drop one of the current main effects or interactions in each round of model comparison. Interactions among potential QTL and between QTL and covariance were detected with a two-dimensional genome scan (function *scantwo*). Using the estimated positions of QTL from *scanone*, *stepwiseqtl*, and *scantwo* as the input, the positions of QTL were refined by using the function *makeqtl* and *refineqtl*, which then fit with a defined multiple-QTL model (function *fitqtl*) with all detected interactions. F1-parent-of-origin was used as covariance in all the tested mapping models. Position and effect size of QTL were estimated using drop-one-term ANOVA in the best-fitting model. Chromosome diagram with candidate genes (Fig. 4.4) was produced by using the LinkageMapView (Ouellette *et al.*, 2018).

In situ hybridization of candidate genes

Variable regions of the genes of interest were amplified by PCR (primers in Table C6) from young inflorescence cDNA of *Aquilegia x coerulea* ‘Kiragami’. The PCR products were cloned into the pCRTM4-TOPO vectors, sequenced to confirm identity, and reverse transcribed using T3 or T7 RNA polymerase and DIG RNA labeling mix (Sigma-Aldrich). Probe qualification and *in situ* hybridization steps followed (Kramer, 2005). Slides were stained in calcofluor white for 5 min before

imaging, and pictures were taken using the ZEISS Axio Zoom at the Harvard Center for Biological Imaging.

Statistical analysis

All statistical analyses (e.g. ANOVA, Tukey's HSD) were performed using R (version 1.1.456).

Gene trees

Homologs of *AqROXYa* and *AqATH1* from various taxa were obtained by using BLAST on Phytozome (<https://phytozome-next.jgi.doe.gov/>). Multiple sequence alignments and neighbor-joining phylogenetic trees were constructed using Geneious Prime (v2021.1.1). We did not construct phylogenetic trees for other candidate genes because their homologs in *A. coerulea* and *A. thaliana* were each other's reciprocal top BLAST hits.

RESULTS

SWN variation in the parental species and the F2s

We counted the SWN from 357, 197, and 4265 flowers from 27, 16, and 364 *A. brevistyla*, *A. canadensis*, and F2 individuals, respectively (Fig. 4.2). The SWN per individual of the parental species did not overlap: the mean SWN of *A. brevistyla* ranges from 6.69 to 7.57; that of *A. canadensis*, from 8.54 to 10; and that of the F2s, which overlapped with the range of both parental species, from 6.20 to 9.50 (Fig. 4.2e). The mean SWN for all *A. brevistyla*, *A. canadensis*, and F2s were 7.16, 9.16, and 8.06, respectively. Subsequently, we analyzed whether the position of flowers on the inflorescence is associated with their SWN (Fig. 4.2c). Flower position had a significant effect on the SWN for both

parental species but not for the F2s (Fig. C1). Post hoc tests revealed that only the SWN of the terminal flower (TF) vs. first lateral flower (LF1) were significantly different for both parental species, suggesting that the significant positional effect was mainly driven by the difference in SWN between the TF and the LF1 (Fig. C1). Moreover, due to the severe inbreeding depression of *Aquilegia* species (Montalvo, 1994; Yang & Hodges, 2010), each F1 individual only produced a limited number of viable seeds. Therefore, the 364 F2s individuals were the progenies of five self-pollinated F1 individuals. One-way ANOVA revealed that the SWN of the F2s differed significantly between the F1 parents (Fig. C2). Lastly, we also analyzed the variation of SWN among flowers of the same plants. Interestingly, a small portion of *A. brevistyla* (7.4%), *A. canadensis* (18.8%), and F2s (6%) showed no variance in the SWN across all flowers counted within an individual, and this phenomenon was dependent on neither the number of flowers counted per individual plant (Fig. C3; Pearson's correlation = 0.052, $t = 0.98418$, $df = 345$, $p = 0.3257$) nor the F1-parent-of-origin of the F2s (Fig. C3). No significant correlation between the mean SWN per individual and the standard deviation of SWN per individual was detected (Pearson's correlation = 0.035, $t = 0.70438$, $df = 404$, $p = 0.4816$).

Floral meristem size

To determine whether the initial FM sizes were different between the parental species, we measured the widths of FMs of the parental species at their earliest developmental stages (Fig. 4.3). In general, the FMs of *A. canadensis* appeared to be slightly, but significantly wider, than those of *A. brevistyla* throughout the early developmental stages (Fig. 4.3; Table C1). The average FM widths of *A. canadensis* and *A. brevistyla* before the initiation of carpel primordia were 174.68 μm and 191.67 μm , respectively (Table C1). Interestingly, the developmental windows for significant FM size expansion seemed to be longer in *A. canadensis* than *A. brevistyla* (Fig. 4.3; Table C1). The significant

increase in widths of *A. brevistyla* FMs occurred when there were 0 to 4 whorls of non-sepal floral organs initiating, while the significant increase in the widths of *A. canadensis* FMs encompassed a larger developmental period, ranging from the stages that there were 0 to 6 whorls of non-sepal floral organs initiating (Table C1).

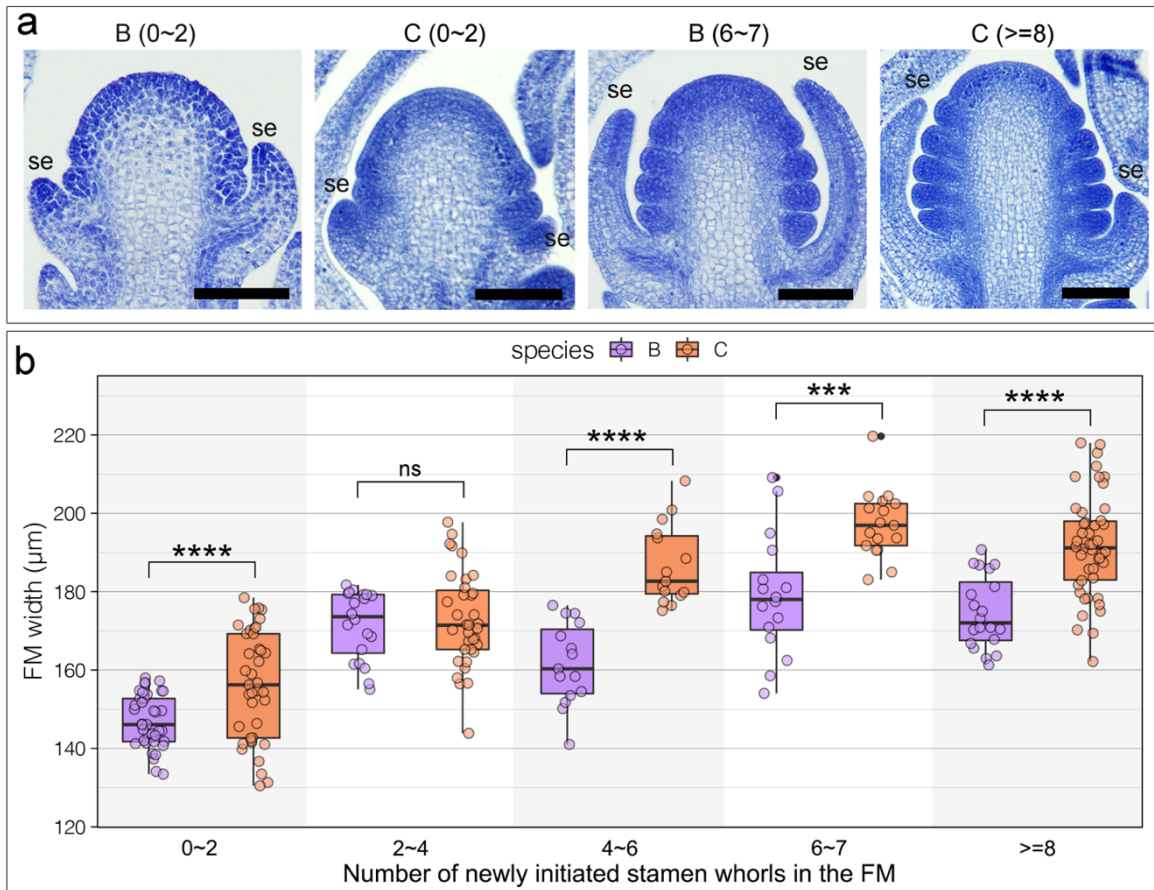


Figure 4.3. FM widths measurements of the parental species during the early developmental stages. (a) Examples of FM morphologies in *A. brevistyla* and *A. canadensis* at early developmental stages. Numbers in the parenthesis indicate the number newly initiated stamen whorls in each FM. Scale bars = 100 µm. **(b)** Comparison of FM width of difference developmental stages between *A. brevistyla* and *A. canadensis*. Each data point represents a measurement of a FM width from a section. Three to six continuous sections were measured for each FM, and at least three FMs were measured for each developmental stage of each species. Comparison of FM widths of each stage between the parental species was done using Tukey's HSD. ns: not significant; ***: p-value < 0.001; ****: p-value < 0.0001; se: sepal; B: *A. brevistyla*; C: *A. canadensis*.

Genetic architecture underlying stamen whorl variation

The genetic map was constructed using a total of 620 genetic markers, which fell into seven linkage groups (Fig. C4). We recovered seven major QTL using the mean SWN per individual as a

phenotype and the F1-parent-of-origin as a covariate, with one QTL on each chromosome (Fig. 4.4a; Table 3.1). The difference in LOD scores between models that included or excluded the covariate are diminutive on all chromosomes (ranging from -0.3 to 0.49; Fig. C5a), indicating no significant interaction between the QTL and the covariate. We also performed a two-dimensional genome scan to search for evidence of the presence of more than one QTL on each chromosome but did not obtain any significant evidence (Table C2). Although the initial standard interval mapping seemed to indicate the presence of two QTL, the presence of only one true QTL on chromosome 2 was further confirmed by controlling the two potential QTL: when the true QTL (i.e., Q2) was controlled, the presence of the second peak also disappeared (Fig. C5b). We did detect significant interactions between two pairs of QTL: Q3 and Q7, and Q1 and Q6 (Fig. C5c), and thus incorporated these interactions in the full QTL model (Table 3.1).

The full QTL model had a total LOD score of 48 and explained 46.5% of the observed phenotypic variation (Table 3.1). Q3, Q4, and Q5 exhibit larger additive effects than dominant effects, while the remaining QTL have larger dominant effects on the phenotypic variation (Fig. 4.4a, C6; Table 3.1). The phenotypic variation explained by each QTL and the QTL interactions was very similar, with Q4 and Q6 having the largest additive and dominant effects, respectively, and each explained 8.8% of the phenotypic variation (Table 3.1). This suggested the genetic architecture of SWN is a complex trait controlled by multiple loci, each with small effect.

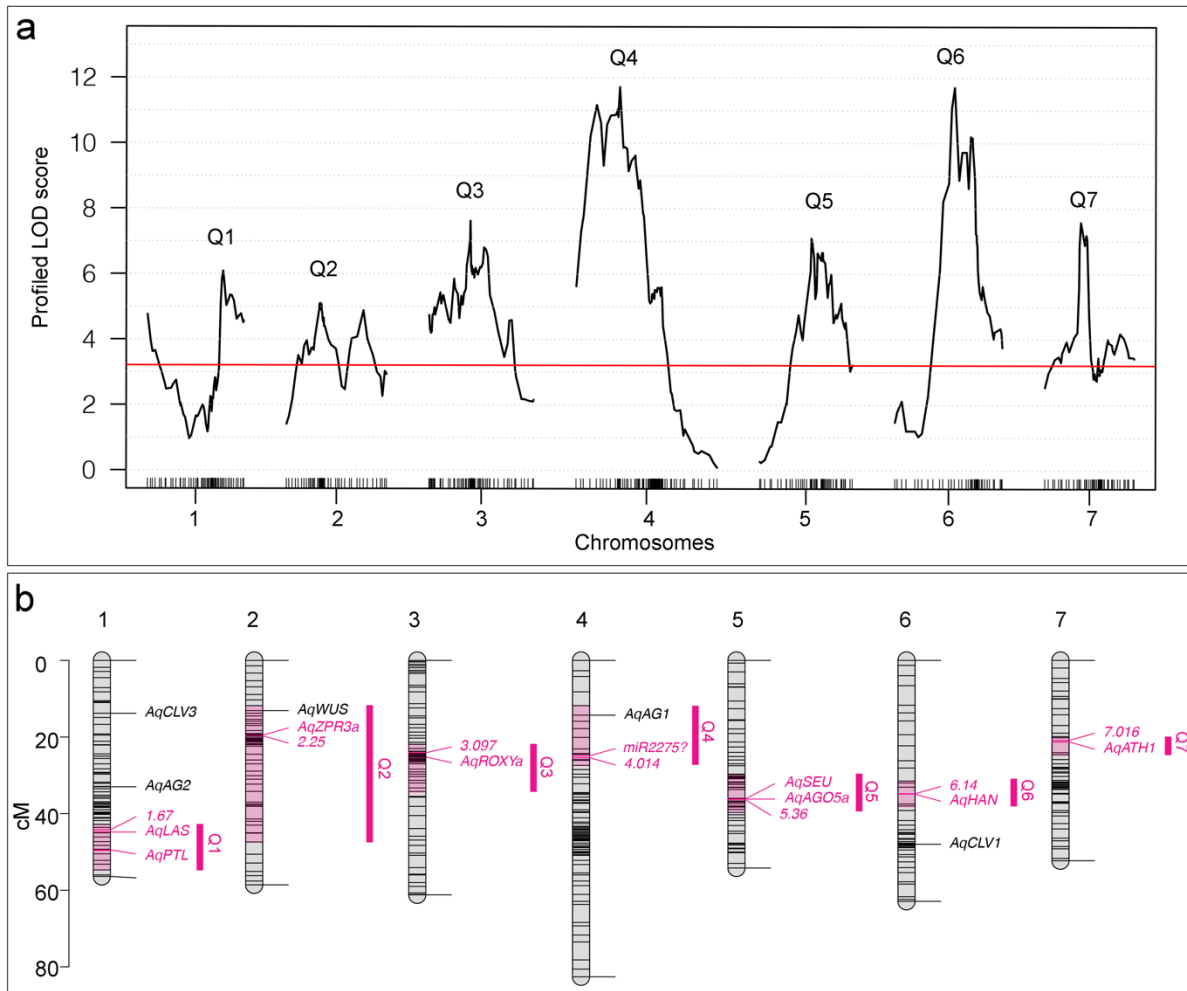


Figure 4.4: Genetic architecture and candidate genes. (a) LOD scores across seven chromosomes. Red line: $\alpha = 0.05$ genome-wide significance cutoff based on 1000 permutations. (b) Locations of QTL interval (pink regions on the chromosomes and magenta vertical bars), candidate genes, and genetic markers. All the genetic markers were named in numeric forms (e.g., 1.67 and 2.25) and only markers with the highest LOD scores under each QTL are shown.

Table 4.1: Summary statistics for QTL. Chr: chromosome; PVE: percent variance explained; Add./(a): additive affects; Dom./(d): dominant effects.

Full model result:						
$y \sim Q1 + Q2 + Q3 + Q4 + Q5 + Q6 + Q7 + Q1:Q6 + Q3:Q7$						
	df	SS	MS	LOD	PVE	Pvalue(F)
Model	22	61.87	2.81	48.04	44.47	0
Error	331	71.27	0.22			
Total	353	133.14				

Drop one QTL at a time ANOVA table										
	Chr	Position (cM)	df	Type III SS	LOD	PVE	F value	Pvalue (F)	Add.	Dom.
Q1	1	44.233	6	5.87	6.1	4.4	4.6	<0.001	0.05	-0.16
Q2	2	19.676	2	4.89	5.1	3.7	11.4	<0.001	-0.07	0.2
Q3	3	24.050	6	7.43	7.6	5.6	5.7	<0.001	-0.11	-0.01
Q4	4	25.406	2	11.73	11.7	8.8	27.3	<0.001	-0.27	0.07
Q5	5	30.155	2	6.89	7.1	5.2	16.0	<0.001	-0.25	0.17
Q6	6	34.828	6	11.72	11.7	8.8	9.1	<0.001	-0.14	-0.27
Q7	7	20.944	6	7.38	7.6	5.6	5.7	<0.001	0	0.15
Q1 * Q6			4	5.45	5.7	4.1	6.3	<0.001		
Q3 * Q7			4	5.39	5.6	4.1	6.3	<0.001		

Estimated effects for QTL interactions			
Q1 (a) * Q6 (a): 0.01	Q1 (d) * Q6 (a): -0.23	Q1 (a) * Q6 (d): -0.38	Q1 (d) * Q6 (d): 0.45
Q3 (a) * Q7 (a): 0.19	Q3 (d) * Q7 (a): 0.09	Q3 (a) * Q7 (d): -0.16	Q3 (d) * Q7 (d): -0.24

Candidate genes

In order to identify potential candidate genes underlying these QTL, we examined the genomic regions defined by markers that flanked the 95% Bayesian credible interval of each QTL, which was calculated by using the posterior distribution of $10^{\wedge}LOD$ on a given chromosome. The genomic regions of Q1, Q4, Q6, and Q7 were less than 6 Mb in size, while those of Q2, Q3, and Q5 were more than 20 Mb (Table C3). Among all the QTL, Q6 and Q2 had the smallest (1.5 Mb) and the largest (36.5 Mb) intervals, containing 226 and 3242 genes, respectively (Table C3). We narrowed down the list of candidate genes by using a previously published RNA-sequencing (RNAseq) data for early FMs of *A. coerulea*, which sampled developmental stages covering the FMT window (Min & Kramer, 2020). We found that all of the QTL intervals, with the exception of Q4, had approx. 70%

of their total genes expressed in at least one of the RNAseq developmental stages; only 46.21% of the total Q4 genes were expressed in early developmental stages (Table C3).

Subsequently, we sought to identify candidate genes under each QTL based on 1) the locations of the candidate genes relative to the location of the markers with the highest LOD scores, 2) gene expression levels during early FM developmental stages, and 3) homology to previously studied loci related to meristem function (i.e., not just restricted to FM). Because our genotyping method used 0.5 Mb or 1Mb binned genomic regions as the genetic markers rather than single nucleotide markers (see details in Materials and Methods), we gave the highest priority to genes located in the region of the marker with the highest LOD scores.

Within the highest LOD bin of Q1, we identified a homolog of *LATERAL SUPPRESSOR* (*LAS*), *AqLAS*. *LAS* encodes a member of the GRAS family of putative transcriptional regulators, and mutations in the *LAS* orthologs in *A. thaliana* and tomato lead to a loss of axillary meristems (Schumacher *et al.*, 1999; Greb, 2003; Wang *et al.*, 2014). Moreover, one additional gene within the interval that was located 3 Mb away from *AqLAS* also caught our attention: *AqPETAL LOSS* (*AqPTL*). *PTL* is a floral organ boundary gene in *A. thaliana* that controls cell proliferation in a non-cell autonomous fashion (Griffith *et al.*, 1999; Brewer *et al.*, 2004; Lampugnani *et al.*, 2012). We considered *AqPTL* interesting for two reasons. First, *PTL* has been shown to physically interact with and be transcriptionally regulated by C2H2 transcription factor JAGGED (*JAG*) (Sauret-Güeto *et al.*, 2013). In addition, silencing of *AqJAG* led to early FM arrest in *A. coerulea*, indicating that it is an important gene in maintaining the *Aquilegia* FM (Min & Kramer, 2017). Second, *PTL* and the gene product of *HANABA TANARU* (*HAN*) interact by sharing *JAG* as direct protein partners to regulate floral morphogenesis in *A. thaliana* (Ding *et al.*, 2015), and the homolog of *HAN* is a candidate gene under our Q6 (Fig. 4.4b).

br = bracts; c = carpels; * = sepals; → = petals; ► = axillary meristems

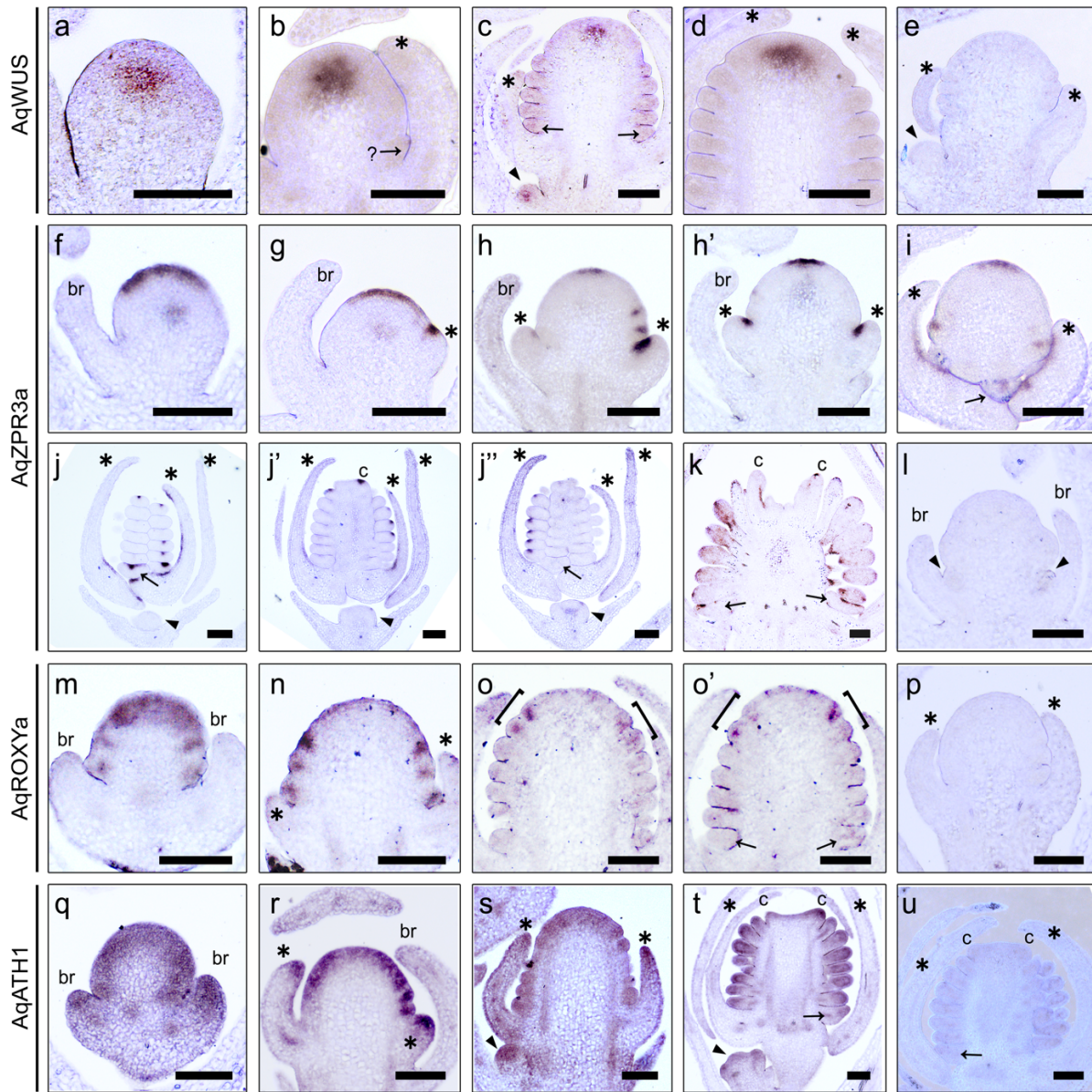


Figure 4.5. *In situ* hybridization of *AqWUS* and candidate genes. (a-e) Expression patterns of *AqWUS* (a-c) and its negative control (e). **(a)** A young FM that has not produced any floral organs. **(b)** A young FM that is in the process of initiating either a petal primordium or the outer most stamen primordia (and thus indicated by an arrow with a question mark). **(c)** A FM that has at least eight whorls of stamens initiated; *AqWUS* expression can also be seen at the axillary meristem below this FM (arrowhead). **(d)** A FM that has at least 11 whorls of stamens produced. **(e)** Sense probe on a FM with 3-4 whorls of stamens. **(f-l)** Expression patterns of *AqZPR3a* (f-k) and its negative control probe (l). **(f)** A young FM that has not produced any floral organs. **(g)** A young FM that has just started to produce sepal primordia (asterisk). **(h, h')** Serial sections through the same young FM that has only produced sepal primordia (asterisks). **(i)** A slightly tangential section through a FM that has produced 1-2 whorls of stamens. **(j, j', j'')** Serial sections through the same young floral bud that has initiated all floral organs. Expression of *AqZPR3a* is also seen in the central zone of the axillary meristem in (j'') (arrowhead). **(k)** A young floral bud in which all floral organs are differentiating. **(l)** Meristem at same stage as (f) hybridized with sense probe. **(m-p)** Expression of *AqROXYa* (m-o') and its negative control (p). **(m)** A young FM that has not produced any floral organs. **(n)** A young FM that is in the process of initiating petal or the outer-most stamen primordia. **(o, o')** Serial

(Continued) sections through the same FM showing *AqROXYa* is only expressed on the abaxial side of the newly emerging primordia (brackets). **(p)** Meristem at the same stage as (p) hybridized with sense probe. **(q-u)** Expression of *AqATH1* (q-t) and its negative control (u). **(q)** A young FM that has not produced any floral organs. **(r)** A young FM that is in the process of initiating petal and stamen primordia. **(s)** A FM initiating stamen primordia and an associated axillary meristem (arrowhead). **(t)** A floral bud with carpel primordia just initiated and an axillary meristem, which has just initiated the sepal primordia. **(u)** Meristem at the same stage as (t) hybridized with sense probe. All scale bars = 100 μ m.

Interestingly, *AqWUS* is within the 95% Bayesian credible intervals of Q2, located at the edge of the interval (Fig. 4b). Since the expression of *AqWUS* has not been examined *in situ*, we analyzed its expression pattern during the early developmental stages of *A. coerulea* FM (Fig. 4.5a-e). *AqWUS* is expressed in a small population of cells in the center of the FM from the earliest stages (Fig. 4.5a-e). The expression in these central zone cells persists during the initiation of floral organs and disappears when carpel primordia start to initiate. These observations are consistent with the expression of *WUS* orthologs in all taxa examined to date (Nardmann & Werr, 2006; Galli & Gallavotti, 2016), suggesting functional conservation of *AqWUS* as well. However, the marginal position of *AqWUS* in Q2 makes it a less compelling candidate.

Under Q2, 8.7 Mb away from *AqWUS* within the highest LOD interval, we identified another candidate, the gene *AqLITTLE ZIPPER 3a* (*AqZPR3a*) (Fig. 4.4). *AqZPR3a* encodes a small-leucine zipper-containing protein and is the homolog of the previously identified gene *ZPR3* in *A. thaliana* (Weits *et al.*, 2019). Homologs of the *ZPR* genes have been shown to regulate leaf polarity and shoot apical meristem maintenance in *A. thaliana* and tomato (Wenkel *et al.*, 2007; Kim *et al.*, 2008; Weits *et al.*, 2019; Xu *et al.*, 2019), but little is known about whether they are involved in any FM-specific functions in these plant systems. In *Aquilegia*, *AqZPR3a* exhibits very intriguing and dynamic expression patterns during early FM development (Fig. 4.5f-l). At the earliest stages of the FM, before floral organ primordium is initiated, concentrated expression of *AqZPR3a* is detected across the central epidermal layer of the FM, and moderate expression is found in the central zone (Fig. 4.5f). This strong expression in the FM epidermal layer persists until the FM has initiated

several whorls of floral organs, but the width of the domain seems to contract as FM development proceeds (Fig. 4.5f-i). On the other hand, the expression in the central zone disappears rapidly after initiation of the sepal primordia (Fig. 4.5f, g, h', j'). Strong expression of *AqZPR3a* is also detected at the adaxial boundary of all initiating floral organ primordia (Fig. 4.5h-j'). However, these adaxial expression domains are restricted to the median region of the primordia, rather than the entire abaxial surface, which can be seen in serial sections through the same FM in Fig. 4.5h, h', as well as in Fig. 4.5j, j', j'. Moreover, strong but patchy expression of *AqZPR3a* is detected in the adaxial epidermal layer of slightly older lateral organs, such as the sepals (Fig. 4.5i, j, j'), petals (Fig. 4.5k), stamens (Fig. 4.5k) and carpels (Fig. 4.5k). Intriguingly, expression of the ZRP genes across the epidermal layer of the early meristems has never been observed in any other plant systems.

Under Q3, we identified the candidate gene *AqROXYa* which codes for a thioredoxin superfamily protein and is a homolog of *A. thaliana* genes *ROXY1* and *ROXY2* (Fig. 4.4; Fig. C7). In *A. thaliana*, *ROXY1* appears to be a negative regulator of *AG* and functions to regulate petal initiation (Xing *et al.*, 2005; Quon *et al.*, 2017), and *ROXY2* with other members of the thioredoxin family members have been shown to regulate both floral organ development and stress responses (Xing & Zachgo, 2008; Murmu *et al.*, 2010; Li *et al.*, 2019). However, the homolog of *ROXY* in maize has been shown to regulate shoot meristem size and phyllotaxy (Yang *et al.*, 2015). In *Aquilegia*, expression of *AqROXYa* is detected across the FM at the earliest developmental stages (Fig. 4.5m), but this broad expression disappears once the primordia begin initiating. Likewise, *AqROXYa* is detected in a restricted abaxial region of emerging floral organ primordia but quickly declines once they are initiated (Fig. 4.5m-o'). For instance, in a FM with several whorls of initiated stamen primordia, the expression of *AqROXYa* is only detected in the abaxial side of the innermost two whorls of emerging organ primordia (Fig. 4.5o, o').

The confidence interval of Q4 spanned 3.8 Mb but only contained 176 annotated genes that were expressed in the RNAseq dataset (Table C3, C4). The only loci with homologs that are likely to function in meristems are two closely related tandem duplicates of the *AGAMOUS* homolog *AqAG1* (Fig. 4.4b). However, *AqAG1* is located at the edge of the genomic interval, quite distant from the marker with the highest LOD score (Fig. 4.4b). Within the 1Mb region (4,800,000...5,800,000) that contained the marker with the highest LOD, there were only 40 expressed genes, eight of which are *Aquilegia*-specific without any annotated *A. thaliana* homologs, with most of the remaining genes annotated to be involved in plant defense and basic metabolic functions (Table C4). We also searched for potential microRNA-encoding loci and found that within the region with the highest LOD, there are three of the 11 annotated clusters of microRNA2275 (miR2275) precursors in the *Aquilegia* genome (Pokhrel *et al.*, 2021). MiR2275 is the only known microRNA that triggers phased, secondary, small interfering RNAs (phasiRNAs) of 24 nucleotides in length, and the production of 24-nt phasiRNAs requires both miR2275 copies and 24-*PHAS* loci as their targets (Liu *et al.*, 2020). We also found that the 3.8 Mb region of Q4 is enriched in 24-*PHAS* loci, containing 91 24-*PHAS* loci in total, comprising 31.7% of all 24-*PHAS* loci on chromosome 4 (~45.8 Mb) and 14.1% of such loci in entire genome (~300 Mb) (Pokhrel *et al.*, 2021). Almost half of the 24-*PHAS* loci in Q4 are targeted by miR2275 copies in the same interval.

For Q5, there are two genes located within the highest LOD interval that have homologs that are known to function as FM regulators: *AqSEUSS* (*AqSEU*) and *AqARGONAUTE 5a* (*AqAGO5a*). In *A. thaliana*, *SEU* is known to repress *AG* to regulate FM and organ patterning (Pfluger & Zambryski, 2004; Grigorova *et al.*, 2011; Wynn *et al.*, 2014), while in *Aquilegia*, *AqAGO5a* has been identified as a core hub gene associated with early FM development (Min & Kramer, 2020).

Q6 spans 1.5 Mb with only 226 genes in total, 170 of which are expressed in the RNAseq dataset (Fig. 4.4; Table C4). Within the bin of the highest LOD score, there is one gene for which a

homolog has been functionally studied: *HANABA TANARU* (*AqHAN*). *HAN* codes for a GATA type zinc finger transcription factor, and in *A. thaliana*, *HAN* is expressed at the organ boundaries, is known to regulate *WUS* expression, and directly interacts with a number of key genes in FM regulation and primordia initiation (Zhao *et al.*, 2004; Ding *et al.*, 2015). As mentioned above, we have detected significant interaction between Q1 and Q6 (Fig. C5). We found it intriguing that *HAN* and *PTL* interact through *JAG* to control FM morphogenesis in *A. thaliana* (Ding *et al.*, 2015), since their *Aquilegia* homologs are located within the confidence interval of Q1 and Q6, respectively.

Lastly, Q7 also has a very narrow interval of only 2.5 Mb in the genome with 242 expressed genes in the RNAseq dataset. *AqHOMEBOX GENE 1* (*AqATH1*) is the only gene with a homolog that has been functionally studied that is also located within the highest LOD interval. *AqATH1* is the ortholog of gene *ATH1* in *A. thaliana* (Fig. C8) and belongs to the *BELL1*-like homeodomain gene family. *ATH1* regulates the boundary between the stem and the lateral organs, but is also involved in stem cell regulation in meristems by maintaining the expression of the meristem marker gene *SHOOT MERISTEMLESS* via a self-activation loop (Gómez-Mena & Sablowski, 2008; Li *et al.*, 2012; Cao *et al.*, 2020). *AqATH1* is broadly expressed across the *Aquilegia* FM throughout the early developmental stages (Fig. 4.5q-t), in all early floral organ primordia (Fig. 4.5r-t), and at the distal tip of the young lateral organs such as the bracts (Fig. 4.5q), sepals (Fig. 4.5r, s), and petals (Fig. 4.5t).

DISCUSSION

***Aquilegia* is an ideal system for studying FM regulation and termination**

Over recent decades, we have gained significant insight into various aspects of plant meristem development and function, but the regulation of FMT remains a poorly studied subject.

This is despite the fact that FMT is an indispensable process in floral development and variation in FMT timing is a key component of the generation of floral morphological diversity. Progress in understanding the regulation and evolution of FMT is hampered due to the lack of natural variation in floral organ whorl numbers in all of our currently established model systems (and their close relatives), while taxa with such a variation generally lack the genomic and molecular resources to investigate this question further. To this end, *Aquilegia* can be an ideal system for studying FMT thanks to its recent adaptive radiation, which means that *Aquilegia* species share relatively low interspecific sequence variation combined with a high degree of inter-fertility (Hodges & Arnold, 1994; Filiault *et al.*, 2018). At the same time, they all share a consistent floral bauplan that only varies in SWN (Munz, 1946), and possess a fully sequenced and well-annotated genome along with RNAi-based methods for functional studies (Kramer, 2009; Filiault *et al.*, 2018). Recognizing that floral SWN is the best available quantitative trait to represent the timing of FMT, we utilized a genetic cross between two sister species differing in SWN and sought to take the first step to explore the molecular basis of naturally occurring variation in the FMT timing. The interfertile *A. brevistyla* and *A. canadensis* species pair are highly suited to this study since their respective mean SWN of 7.16 and 9.16 do not overlap. Further, the mean SWN of their F2 progeny was found to encompass the entire range of the parental species (Fig. 4.2e).

One question we sought to explore was whether the differences in ultimate floral size between the two sister species is reflected by differences in early FM growth dynamics. By analyzing developmental histological series of FMs in the parental species, we detected a subtle yet significant difference. Although the FMs of both species exhibit similar growth dynamics - increasing in size during their earliest developmental stages and then staying relatively constant during the later stage - the FMs of *A. canadensis* tend to be larger at inception and grow to a larger size, even before differences in SWN are evident (Fig. 4.3; Table C1). Overall, we observe that 1) the *A. canadensis*

FMs are larger in general, 2) have a longer developmental window to increase FM size, and yet, 3) still make five stamens per whorl. There are numerous previous studies showing that an increase in FM size is often associated with an increase in floral organ number *per whorl*, rather than an increase in the number of whorls (e.g., Carles *et al.*, 2004; Fan *et al.*, 2014; Chu *et al.*, 2019). Of course, these studies typically rely on mutagenesis or gene over-expression rather than natural variation. This suggests that natural variation in meristem size relies on a greater degree of coordination such that meristem size changes in conjunction with the size of primordia inhibition fields, allowing merosity to stay constant. The current data does not allow us to distinguish between whether the *A. canadensis* FM is growing for a longer period (e.g., perhaps plastochrons are slower, allowing more mass to be accumulated between subsequent whorls) or proliferating at a faster rate. Given what we know about the role of cell division timing in influencing FMT, answering this question is important to understanding the FMT mechanism in *Aquilegia*. Future studies using a recently developed live imaging technique in *Aquilegia* (Chapter 2), may allow us to compare growth rates between the initiation of successive whorls in these two species and better characterize this phenomenon.

Another curious observation regarding SWN is that we observed a small portion of individuals in both parental species as well as the F2s that exhibited no variation in SWN, regardless of how many flowers were counted on the plants. In contrast, most other individuals exhibited variation in SWN within an individual plant (Fig. C3). This seems to suggest that there is variation in the robustness of this trait between different individuals. Unfortunately, the fact that there was no significant divergence in this pattern between the parent species meant that we could not map it in the current study, but we hope that examination of within-inflorescence SWN canalization in other *Aquilegia* species will allow the identification of suitable models and the dissection of its genetic basis.

Variation in the timing of *Aquilegia* FMT is controlled by multiple loci of small effects

We recovered seven major QTL that are responsible for variation in SWN, with one QTL located on each chromosome and the percent of phenotypic variance explained by each QTL ranging from 3.7% to 8.8% (Fig. 4.4; Table 3.1). These results are comparable to previous studies in meristem-related traits of domesticated crops, particularly maize, which also revealed multiple QTL of small effects (Vlăduțu *et al.*, 1999; Upadyayula *et al.*, 2006; Bommert *et al.*, 2013; Thompson *et al.*, 2014, 2015). Interestingly, although all the meristem-related traits measured in maize were highly heritable, the total percentage of variance explained by all the QTL was never higher than 50% (e.g., Bommert *et al.*, 2013; Thompson *et al.*, 2014, 2015), suggesting there are other loci with even smaller effects that were not picked up by the QTL mapping, which is a likely scenario for our current study as well.

We have identified a number of candidate genes under the QTL (Fig. 4.4; Table C5) and, further, uncovered novel FM expression patterns of *AqZPR3a* and *AqROXYa*, which were the candidate genes under Q2 and Q3, respectively (Fig. 4.4, 4.5). In *A. thaliana* and tomato, expression of the *ZPR* genes is restricted to the adaxial region of lateral organs and the central zone of the shoot meristem, and the *ZPR* genes function in both establishing organ polarity and restricting the stem cell domain in the meristems by acting as post-translational suppressors of the class III HD-ZIP abaxial identity genes by inhibiting their homodimerization (Wenkel *et al.*, 2007; Kim *et al.*, 2008; Weits *et al.*, 2019; Xu *et al.*, 2019). However, we have also observed strong expression of *AqZPR3a* in the central epidermal layer of FMs throughout their early developmental stages (Fig. 4.5f-i), which has not been observed in any previous studies. It will be very interesting to determine whether this novel expression pattern indicates a novel function or related to known *ZPR* functions in modulating meristem regulation. In the case of *ROXY* homologs in other models, expression has been found to be restricted to incipient and newly emerged organ primordia (Xing *et al.*, 2005; Li *et*

al., 2009b; Yang *et al.*, 2015), but abaxialized expression such as what was found for *AqROXYa* has not been observed before. In *A. thaliana*, *ROXY1* is known to interact with *PTL* to regulate floral primordium initiation, while in maize, a *ROXY* homolog controls meristem size primordia (Xing *et al.*, 2005; Li *et al.*, 2009b; Yang *et al.*, 2015); either of these functions could be important for controlling FMT in *Aquilegia*.

The Q4 locus is of particular interest because it explains the highest relative percentage of phenotypic variation, but it is also the QTL with the fewest obvious candidate genes to investigate (Table C3, C4). Chromosome 4 of *Aquilegia* appears to have followed a distinct evolutionary path from the rest of the genome and displays many unique features compared to the remaining six chromosomes, including having a higher proportion of genes arrayed in tandem and segmental duplicates, more genetic polymorphism and transposable elements, lower gene density, and reduced gene expression (Filiault *et al.*, 2018; Aköz & Nordborg, 2019). Although the *AqAG1* tandem duplication is included in the 95% Bayesian credible interval, it may be less likely to be the causative gene compared to other genes that were located closer to the highest LOD score marker. The lack of potential candidate genes under Q4 led us to consider other factors besides protein coding genes, yielding the finding that the highest Q4 LOD interval harbors a large number of miR2275 precursors and 24-*PHAS* loci. As the only microRNA that triggers 24-nt phasiRNA, a pathway that is conserved across the angiosperms, miR2275 has been shown to be expressed in the reproductive tissues of various monocot and dicot lineages, particularly in developing anthers (Zhai *et al.*, 2015; Fei *et al.*, 2016; Kakrana *et al.*, 2018; Pokhrel *et al.*, 2020, 2021). However, besides their functions in anthers, relatively little is known about 24-nt phasiRNAs in general.

Certainly, it is also possible that the causal gene underlying Q4 is one of the *Aquilegia*-specific loci that did not have a direct *A. thaliana* homolog, which equally applies to the other QTL as well. Next steps in evaluating these candidate genes will include comparative expression between *A.*

canadensis and *brevistyla*, functional studies, and population-based allelic analyses to identify fixed differences. The current study is a key first step in identifying a promising list of candidate genes for regulating natural variation in FMT, which will provide insight into both the developmental and evolutionary mechanisms underlying FMT.

AUTHOR CONTRIBUTIONS

YM and EK conceived of and designed the study. EB collected seeds, crossed and sequenced the parental species, and grew and pollinated the F1 individuals. ME and YM grew the F2s. YM conducted all phenotyping. EB, ME and YM prepared the libraries for sequencing of the F2 individuals and constructed the genetic map. YM did all the data analysis and *in situ* hybridization. EK and SH provided oversight of the study. YM wrote the manuscript with input from the co-authors.

ACKNOWLEDGEMENT

The authors would like to thank Nicole Bedford, Olivia Meyerson, and Rubén Rellán-Álvarez for discussing QTL mapping analysis; Suresh Pokhrel for providing information on miRNA in *Aquilegia*; Pierre Baduel and Rebecca Povilus for discussing data analysis strategies; the graduate students at the Harvard Statistics Department who volunteered their time for professional and free statistics consultation; Karl Broman for actively answering questions about the R/qtl package on online forums. Funding has been provided by a Simmon's Award to YM from the Harvard Center for Biological Imaging; a National Science Foundation Graduate Research Fellowship under grant no. DGE1745303 to MBE; and both a NIH Ruth L. Kirschstein National Research Service Award (F32GM103154) and a UC Santa Barbara Harvey Karp Discovery award to ESB. Sequencing was carried out by the DNA Technologies and Expression Analysis Cores at the UC Davis Genome

Center, supported by NIH Shared Instrumentation Grant 1S10OD010786-01 and the Biological Nanostructures Lab at UC Santa Barbara.

REFERENCE

- Aköz G, Nordborg M. 2019. The *Aquilegia* genome reveals a hybrid origin of core eudicots. *Genome Biology* 20: 256.
- Ballerini ES, Min Y, Edwards MB, Kramer EM, Hodges SA. 2020. *POPOVICH*, encoding a C2H2 zinc-finger transcription factor, plays a central role in the development of a key innovation, floral nectar spurs, in *Aquilegia*. *Proceedings of the National Academy of Sciences* 117: 22552–22560.
- Bastida JM, Alcántara JM, Rey PJ, Vargas P, Herrera CM. 2010. Extended phylogeny of *Aquilegia*: the biogeographical and ecological patterns of two simultaneous but contrasting radiations. *Plant Systematics and Evolution* 284: 171–185.
- Bollier N, Sicard A, Leblond J, Latrasse D, Gonzalez N, Gévaudant F, Benhamed M, Raynaud C, Lenhard M, Chevalier C, *et al.* 2018. At-MINI ZINC FINGER2 and SI-INHIBITOR OF MERISTEM ACTIVITY, a Conserved Missing Link in the Regulation of Floral Meristem Termination in Arabidopsis and Tomato. *The Plant Cell* 30: 83–100.
- Bommert P, Nagasawa NS, Jackson D. 2013. Quantitative variation in maize kernel row number is controlled by the *FASCIATED EAR2* locus. *Nature Genetics* 45: 334–337.
- Brewer PB, Howles PA, Dorian K, Griffith ME, Ishida T, Kaplan-Levy RN, Kilinc A, Smyth DR. 2004. *PETAL LOSS*, a trihelix transcription factor gene, regulates perianth architecture in the *Arabidopsis* flower. *Development* 131: 4035–4045.
- Broman KW, Wu H, Sen S, Churchill GA. 2003. R/qtl: QTL mapping in experimental crosses. *Bioinformatics* 19: 889–890.
- Cao X, Wang J, Xiong Y, Yang H, Yang M, Ye P, Bencivenga S, Sablowski R, Jiao Y. 2020. A Self-Activation Loop Maintains Meristematic Cell Fate for Branching. *Current Biology* 30: 1893-1904.e4.
- Carles CC, Lertpiriyapong K, Reville K, Fletcher JC. 2004. The *ULTRAPETALA1* gene functions early in Arabidopsis development to restrict shoot apical meristem activity and acts through *WUSCHEL* to regulate floral meristem determinacy. *Genetics* 167: 1893–1903.
- Chu Y, Jang J, Huang Z, van der Knaap E. 2019. Tomato locule number and fruit size controlled by natural alleles of *lc* and *fas*. *Plant Direct* 3.
- Ding L, Yan S, Jiang L, Zhao W, Ning K, Zhao J, Liu X, Zhang J, Wang Q, Zhang X. 2015. *HANABA TARANU* (*HAN*) Bridges Meristem and Organ Primordia Boundaries through *PINHEAD*, *JAGGED*, *BLADE-ON-PETIOLE2* and *CYTOKININ OXIDASE 3* during Flower Development in *Arabidopsis* (XW Deng, Ed.). *PLOS Genetics* 11: e1005479.

- Edwards MB, Choi GPT, Derieg NJ, Min Y, Diana AC, Hodges SA, Mahadevan L, Kramer EM, Ballerini ES. 2021. Genetic architecture of floral traits in bee- and hummingbird-pollinated sister species of *Aquilegia* (columbine). *bioRxiv*. 2021.04.12.439277.
- Endress PK. 1990. Patterns of floral construction in ontogeny and phylogeny. *Biological Journal of the Linnean Society* 39: 153–175.
- Fan C, Wu Y, Yang Q, Yang Y, Meng Q, Zhang K, Li J, Wang J, Zhou Y. 2014. A novel single-nucleotide mutation in a *CLAVATA3* gene homolog controls a multilocular silique trait in *Brassica rapa* L. *Molecular Plant* 7: 1788–1792.
- Fei Q, Yang L, Liang W, Zhang D, Meyers BC. 2016. Dynamic changes of small RNAs in rice spikelet development reveal specialized reproductive phasiRNA pathways. *Journal of Experimental Botany* 67: 6037–6049.
- Filiault DL, Ballerini ES, Mandáková T, Aköz G, Derieg NJ, Schmutz J, Jenkins J, Grimwood J, Shu S, Hayes RD, *et al.* 2018. The *Aquilegia* genome provides insight into adaptive radiation and reveals an extraordinarily polymorphic chromosome with a unique history. *eLife* 7: e36426.
- Fior S, Li M, Oxelman B, Viola R, Hodges SA, Ometto L, Varotto C. 2013. Spatiotemporal reconstruction of the *Aquilegia* rapid radiation through next-generation sequencing of rapidly evolving cpDNA regions. *New Phytologist* 198: 579–592.
- Galli M, Gallavotti A. 2016. Expanding the Regulatory Network for Meristem Size in Plants. *Trends in Genetics* 32: 372–383.
- Gómez-Mena C, Sablowski R. 2008. *ARABIDOPSIS THALIANA* HOMEBOX GENE1 Establishes the Basal Boundaries of Shoot Organs and Controls Stem Growth. *The Plant Cell* 20: 2059–2072.
- Greb T. 2003. Molecular analysis of the *LATERAL SUPPRESSOR* gene in *Arabidopsis* reveals a conserved control mechanism for axillary meristem formation. *Genes & Development* 17: 1175–1187.
- Griffith ME, da Silva Conceição A, Smyth DR. 1999. *PETAL LOSS* gene regulates initiation and orientation of second whorl organs in the *Arabidopsis* flower. *Development (Cambridge, England)* 126: 5635–5644.
- Grigorova B, Mara C, Hollender C, Sijacic P, Chen X, Liu Z. 2011. *LEUNIG* and *SEUSS* co-repressors regulate *miR172* expression in *Arabidopsis* flowers. *Development* 138: 2451–2456.
- Hepworth SR, Pautot VA. 2015. Beyond the Divide: Boundaries for Patterning and Stem Cell Regulation in Plants. *Frontiers in Plant Science* 6.
- Hodges SA, Arnold ML. 1994. Columbines: a geographically widespread species flock. *Proceedings of the National Academy of Sciences* 91: 5129–5132.

- Kakrana A, Mathioni SM, Huang K, Hammond R, Vandivier L, Patel P, Arikat S, Shevchenko O, Harkess AE, Kingham B, *et al.* 2018. Plant 24-nt reproductive phasiRNAs from intramolecular duplex mRNAs in diverse monocots. *Genome Research* 28: 1333–1344.
- Kim Y-S, Kim S-G, Lee M, Lee I, Park H-Y, Seo PJ, Jung J-H, Kwon E-J, Suh SW, Paek K-H, *et al.* 2008. HD-ZIP III Activity Is Modulated by Competitive Inhibitors via a Feedback Loop in *Arabidopsis* Shoot Apical Meristem Development. *The Plant Cell* 20: 920–933.
- Kramer EM. 2005. Methods for studying the evolution of plant reproductive structures: comparative gene expression techniques. *Methods in Enzymology* 395: 617–636.
- Kramer EM. 2009. *Aquilegia*: A New Model for Plant Development, Ecology, and Evolution. *Annual Review of Plant Biology* 60: 261–277.
- Lampugnani ER, Kilinc A, Smyth DR. 2012. *PETAL LOSS* is a boundary gene that inhibits growth between developing sepals in *Arabidopsis thaliana*: *PTL* controls sepal boundaries. *The Plant Journal* 71: 724–735.
- Lenhard M. 2003. Stem cell homeostasis in the *Arabidopsis* shoot meristem is regulated by intercellular movement of *CLAVATA3* and its sequestration by *CLAVATA1*. *Development* 130: 3163–3173.
- Lenhard M, Bohnert A, Jürgens G, Laux T. 2001. Termination of Stem Cell Maintenance in *Arabidopsis* Floral Meristems by Interactions between *WUSCHEL* and *AGAMOUS*. *Cell* 105: 805–814.
- Li H, Durbin R. 2009. Fast and accurate short read alignment with Burrows–Wheeler transform. *Bioinformatics* 25: 1754–1760.
- Li H, Handsaker B, Wysoker A, Fennell T, Ruan J, Homer N, Marth G, Abecasis G, Durbin R, 1000 Genome Project Data Processing Subgroup. 2009a. The Sequence Alignment/Map format and SAMtools. *Bioinformatics (Oxford, England)* 25: 2078–2079.
- Li S, Lauri A, Ziemann M, Busch A, Bhave M, Zachgo S. 2009b. Nuclear Activity of *ROXY1*, a Glutaredoxin Interacting with TGA Factors, Is Required for Petal Development in *Arabidopsis thaliana*. *The Plant Cell* 21: 429–441.
- Li N, Muthreich M, Huang L, Thurow C, Sun T, Zhang Y, Gatz C. 2019. TGACG-BINDING FACTORS (TGAs) and TGA-interacting CC-type glutaredoxins modulate hyponastic growth in *Arabidopsis thaliana*. *New Phytologist* 221: 1906–1918.
- Li Y, Pi L, Huang H, Xu L. 2012. *ATH1* and *KNAT2* proteins act together in regulation of plant inflorescence architecture. *Journal of Experimental Botany* 63: 1423–1433.

- Litt A, Kramer EM. 2010. The ABC model and the diversification of floral organ identity. *Seminars in Cell & Developmental Biology* 21: 129–137.
- Liu Y, Teng C, Xia R, Meyers BC. 2020. PhasiRNAs in Plants: Their Biogenesis, Genic Sources, and Roles in Stress Responses, Development, and Reproduction. *The Plant Cell* 32: 3059–3080.
- Min Y, Kramer EM. 2017. The *Aquilegia* JAGGED homolog promotes proliferation of adaxial cell types in both leaves and stems. *New Phytologist* 216: 536–548.
- Min Y, Kramer EM. 2020. Transcriptome profiling and weighted gene co-expression network analysis of early floral development in *Aquilegia coerulea*. *Scientific Reports* 10: 19637.
- Montalvo AM. 1994. Inbreeding Depression and Maternal Effects in *Aquilegia Caerulea*, a Partially Selfing Plant. *Ecology* 75: 2395–2409.
- Müller R, Borghi L, Kwiatkowska D, Laufs P, Simon R. 2006. Dynamic and Compensatory Responses of *Arabidopsis* Shoot and Floral Meristems to *CLV3* Signaling. *The Plant Cell* 18: 1188–1198.
- Munz PA. 1946. *Aquilegia: the cultivated and wild columbines*. Ithaca. NY.
- Murmu J, Bush MJ, DeLong C, Li S, Xu M, Khan M, Malcolmson C, Fobert PR, Zachgo S, Hepworth SR. 2010. *Arabidopsis* Basic Leucine-Zipper Transcription Factors TGA9 and TGA10 Interact with Floral Glutaredoxins ROXY1 and ROXY2 and Are Redundantly Required for Anther Development. *Plant Physiology* 154: 1492–1504.
- Nardmann J, Werr W. 2006. The Shoot Stem Cell Niche in Angiosperms: Expression Patterns of *WUS* Orthologues in Rice and Maize Imply Major Modifications in the Course of Mono- and Dicot Evolution. *Molecular Biology and Evolution* 23: 2492–2504.
- Ouellette LA, Reid RW, Blanchard SG, Brouwer CR. 2018. LinkageMapView—rendering high-resolution linkage and QTL maps. *Bioinformatics* 34: 306–307.
- Payne T. 2004. *KNUCKLES (KNU)* encodes a C2H2 zinc-finger protein that regulates development of basal pattern elements of the *Arabidopsis* gynoecium. *Development* 131: 3737–3749.
- Pfluger J, Zambryski P. 2004. The role of *SEUSS* in auxin response and floral organ patterning. *Development* 131: 4697–4707.
- Pokhrel S, Huang K, Bélanger S, Caplan JL, Kramer EM, Meyers BC. 2020. Pre-meiotic, 21-nucleotide Reproductive PhasiRNAs Emerged in Seed Plants and Diversified in Flowering Plants. *bioRxiv*: 2020.10.16.341925.
- Pokhrel S, Huang K, Meyers BC. 2021. Conserved and non-conserved triggers of 24-nt reproductive phasiRNAs in eudicots. *bioRxiv*: 2021.01.20.427321.

- Quon T, Lampugnani ER, Smyth DR. 2017. *PETAL LOSS* and *ROXY1* Interact to Limit Growth Within and between Sepals But to Promote Petal Initiation in *Arabidopsis thaliana*. *Frontiers in Plant Science* 8.
- Sauret-Güeto S, Schiessl K, Bangham A, Sablowski R, Coen E. 2013. *JAGGED* Controls *Arabidopsis* Petal Growth and Shape by Interacting with a Divergent Polarity Field (O Leyser, Ed.). *PLoS Biology* 11: e1001550.
- Schoof H, Lenhard M, Haecker A, Mayer KFX, Jürgens G, Laux T. 2000. The Stem Cell Population of *Arabidopsis* Shoot Meristems Is Maintained by a Regulatory Loop between the *CLAVATA* and *WUSCHEL* Genes. *Cell* 100: 635–644.
- Schumacher K, Schmitt T, Rossberg M, Schmitz G, Theres K. 1999. The *Lateral suppressor (Ls)* gene of tomato encodes a new member of the VHIID protein family. *Proceedings of the National Academy of Sciences* 96: 290–295.
- Steeves TA, Sussex IM. 1989. *Patterns in Plant Development*. Cambridge University Press.
- Sun B, Xu Y, Ng K-H, Ito T. 2009. A timing mechanism for stem cell maintenance and differentiation in the *Arabidopsis* floral meristem. *Genes & Development* 23: 1791–1804.
- Thompson AM, Crants J, Schnable PS, Yu J, Timmermans MCP, Springer NM, Scanlon MJ, Muehlbauer GJ. 2014. Genetic Control of Maize Shoot Apical Meristem Architecture. *G3 Genes | Genomes | Genetics* 4: 1327–1337.
- Thompson AM, Yu J, Timmermans MCP, Schnable P, Crants JE, Scanlon MJ, Muehlbauer GJ. 2015. Diversity of Maize Shoot Apical Meristem Architecture and Its Relationship to Plant Morphology. *G3 Genes | Genomes | Genetics* 5: 819–827.
- Upadyayula N, da Silva HS, Bohn MO, Rocheford TR. 2006. Genetic and QTL analysis of maize tassel and ear inflorescence architecture. *Theoretical and Applied Genetics* 112: 592–606.
- Vlăduțu C, McLaughlin J, Phillips RL. 1999. Fine Mapping and Characterization of Linked Quantitative Trait Loci Involved in the Transition of the Maize Apical Meristem From Vegetative to Generative Structures. *Genetics* 153: 993–1007.
- Walker-Larsen J, Harder LD. 2000. The evolution of staminodes in angiosperms: patterns of stamen reduction, loss, and functional re-invention. *American Journal of Botany* 87: 1367–1384.
- Wang Q, Kohlen W, Rossmann S, Vernoux T, Theres K. 2014. Auxin Depletion from the Leaf Axil Conditions Competence for Axillary Meristem Formation in *Arabidopsis* and Tomato. *The Plant Cell* 26: 2068–2079.
- Weits DA, Kunkowska AB, Kamps NCW, Portz KMS, Packbier NK, Nemeček V, Z. Gaillochot C, Lohmann JU, Pedersen O, van Dongen JT, et al. 2019. An apical hypoxic niche sets the pace of shoot meristem activity. *Nature* 569: 714–717.

- Wenkel S, Emery J, Hou B-H, Evans MMS, Barton MK. 2007. A Feedback Regulatory Module Formed by *LITTLE ZIPPER* and *HD-ZIPIII* Genes. *The Plant Cell* 19: 3379–3390.
- Whitewoods CD, Cammarata J, Venza ZN, Sang S, Crook AD, Aoyama T, Wang XY, Waller M, Kamisugi Y, Cuming AC, *et al.* 2020. *CLAVATA* Was a Genetic Novelty for the Morphological Innovation of 3D Growth in Land Plants. *Current Biology* 30: 2645–2648.
- Wynn AN, Seaman AA, Jones AL, Franks RG. 2014. Novel functional roles for *PERLANTHIA* and *SEUSS* during floral organ identity specification, floral meristem termination, and gynoecial development. *Frontiers in Plant Science* 5.
- Xing S, Rosso MG, Zachgo S. 2005. *ROXY1*, a member of the plant glutaredoxin family, is required for petal development in *Arabidopsis thaliana*. *Development* 132: 1555–1565.
- Xing S, Zachgo S. 2008. *ROXY1* and *ROXY2*, two *Arabidopsis* glutaredoxin genes, are required for anther development. *The Plant Journal* 53: 790–801.
- Xu Q, Li R, Weng L, Sun Y, Li M, Xiao H. 2019. Domain-specific expression of meristematic genes is defined by the *LITTLE ZIPPER* protein *DTM* in tomato. *Communications Biology* 2: 134.
- Xu Y, Prunet N, Gan E-S, Wang Y, Stewart D, Wellmer F, Huang J, Yamaguchi N, Tatsumi Y, Kojima M, *et al.* 2018. *SUPERMAN* regulates floral whorl boundaries through control of auxin biosynthesis. *The EMBO Journal*: 14.
- Yang F, Bui HT, Pautler M, Llaca V, Johnston R, Lee B, Kolbe A, Sakai H, Jackson D. 2015. A Maize Glutaredoxin Gene, *Abphy12*, Regulates Shoot Meristem Size and Phyllotaxy. *The Plant Cell* 27: 121–131.
- Yang JY, Hodges SA. 2010. Early Inbreeding Depression Selects for High Outcrossing Rates in *Aquilegia formosa* and *Aquilegia pubescens*. *International Journal of Plant Sciences* 171: 860–871.
- Žádníková P, Simon R. 2014. How boundaries control plant development. *Current Opinion in Plant Biology* 17: 116–125.
- Zhai J, Zhang H, Arikat S, Huang K, Nan G-L, Walbot V, Meyers BC. 2015. Spatiotemporally dynamic, cell-type-dependent premeiotic and meiotic phasiRNAs in maize anthers. *Proceedings of the National Academy of Sciences* 112: 3146–3151.
- Zhao Y, Medrano L, Ohashi K, Fletcher JC, Yu H, Sakai H, Meyerowitz EM. 2004. *HANABA TARANU* Is a GATA Transcription Factor That Regulates Shoot Apical Meristem and Flower Development in *Arabidopsis* [W]. *The Plant Cell* 16: 2586–2600.

CONCLUSION

In this dissertation, I sought to promote *Aquilegia* as a model system for studying FM development and lay the groundwork for understanding how FMT is regulated in *Aquilegia* from three different perspectives: Chapter 1 provided us with broad transcriptomic data covering the period before, during and after FMT; Chapter 2 generated a cellular description of the FMT process at unprecedented resolution; and Chapter 3 revealed the complex nature of the genetic architecture underlying variation in the timing of FMT by utilizing the natural variation in the floral structures of different *Aquilegia* species, yielding a promising list of candidate genes that potentially contribute to the regulation of FMT variation. In addition to this wealth of novel information regarding FMT in *Aquilegia*, my dissertation also revealed that several key aspects of FMT appear to be different in *Aquilegia* relative to what has previously been shown in *A. thaliana*, which also emphasizes the necessity of pursuing a diverse set of model systems for studying FMT.

First, based on the transcriptomic profiling in Chapter 1, we found that several key genes that are involved in the regulation of the *AG-KNU-WUS* pathway in *A. thaliana* either do not have orthologs in the *Aquilegia* genome, or have expression profiles during early FM developmental stages that are inconsistent with their functions in *A. thaliana*, suggesting that the pathway is not conserved in *Aquilegia*. We have also observed a much longer expression window of *AqWUS* relative to *WUS* in *A. thaliana* at the comparable developmental stages, which may be related to *Aquilegia*'s apocarpous gynoecium.

Second, detailed observation of cell proliferation and expansion dynamics in Chapter 2 revealed that there is an increase in cell division in the center of the floral apex after the physical initiation of the carpel primordia. This is inconsistent with what has been observed in *A. thaliana* - that cell divisions cease in the center of the floral apex before the initiation of carpels (Sun & Ito, 2015). Such a difference could again be due to the difference in gynoecial structures, that carpels form a syncarpous gynoecium in *A. thaliana* but an apocarpous gynoecium in *Aquilegia*. Further

investigations in more taxa with apocarpous gynoecia are necessary to examine the connection between gynoecia structures and the regulation of FMT.

Furthermore, in *A. thaliana*, it has been shown that the size of the FM will enlarge when the vegetative meristem transitions to FM identity, but that then the size of the FM will rapidly decrease over the course of organ initiation and eventually be consumed by the initiation of carpel primordia (Kwiatkowska, 2004, 2008). This notion that the FM will only enlarge upon identity transition and then be consumed has sometimes been assumed to be a general phenomenon (e.g., Remizowa, 2019). A previous study has shown that meristem size also increases in *Aquilegia* upon the transition from being vegetative to reproductive identity (Ballerini & Kramer, 2011), but careful measurements of FM sizes in *A. brevistyla* and *A. canadensis* in Chapter 3 showed that these FMs continue to enlarge rapidly during the early FM developmental stages, and then stay at a relatively constant size until the production of carpels. Although the *A. canadensis* FMs were significantly larger, they also appeared to need a longer developmental window (as measured in plastochron, time interval between two successive whorls) to increase in size. In fact, ontogenetic studies of taxa that produce numerous floral organs have also documented significant increases in FM size during organ production. For instance, in *Pulsatilla chinensis* (Ranunculaceae), which produces more than 250 stamens and 250 carpels in a flower, the FM enlarged to a degree that was described as “exceedingly convex and becomes almost spherical” during the initiation of stamens (Ren *et al.*, 2010). All of these observations clearly suggest that FM behavior varies depending on the number of whorls in a flower and that likewise, regulation of FM proliferation and the eventual termination could also vary widely.

Last but not least, different degrees of variation in the timing of FMT in *Aquilegia* reveal both flexibility and complexity in the FMT program. QTL mapping in Chapter 3 demonstrated that stamen whorl number is a quantitative trait and a good representation of the timing of FMT. The mean stamen whorl number of both parental species and the F2 population showed a relatively

normal distribution, indicating variability in the timing of FMT, but also a tight crosstalk between the FMT program and other molecular programs controlling the floral morphogenesis, since organ identity was consistently coordinated across these flowers. Moreover, perhaps the most surprising was the observed patterns of variation within an individual. The systematic counting of stamen whorl numbers in *A. brevistyla*, *A. canadensis*, and their F2 progeny showed an intriguing phenomenon that has not been observed before: for each group, there was a small portion of individuals that showed no variation in stamen whorl numbers, regardless of how many flowers were counted in a plant, while the remaining members of the cohorts displayed a range in stamen whorl number variation among the flowers of the same individual. This intriguing observation suggests variation in the robustness of FMT timing between different individuals.

The results from this dissertation offer us many exciting directions for future research. Together Chapters 1 and 3 have provided a list of candidate genes for FM and FMT regulation that are worthy of further functional studies. The quantitative live-imaging technique in Chapter 2 is likely applicable to other *Aquilegia* species or taxa from closely related genera, and comparative studies of FMs with different whorl numbers and different gynoecial structures will provide us with valuable information regarding cell behavior during FMT. In addition, detailed allelic analysis is necessary for the candidate genes from Chapter 3 to dissect the regulation of FMT. It will also be interesting to analyze the heritability of variation in stamen whorl number within an individual to determine the relative contribution from environmental vs. genetic factors to this phenotype. If it is a highly heritable trait, I will be particularly keen to perform a genetic cross between plants that show no individual variation in stamen whorl number and those that show large variation, which could uncover the mechanisms of canalization in FMT timing. Furthermore, the development of stable transgenic transformation methods will also help to greatly accelerate and expand the scope of future research. For instance, with the combination of live-imaging and stable transformation, we

will be able to observe the expression patterns of key genes and quantify their functions in cellular behavior in real-time, while chromatin immunoprecipitation sequencing will reveal the direct targets of key genes and help us to construct the regulatory network in FMT.

REFERENCES

- Ballerini ES, Kramer EM. 2011. Environmental and molecular analysis of the floral transition in the lower eudicot *Aquilegia formosa*. *EvoDevo* 2: 4.
- Kwiatkowska D. 2004. Surface growth at the reproductive shoot apex of *Arabidopsis thaliana pin-formed 1* and wild type. *Journal of Experimental Botany* 55: 1021–1032.
- Kwiatkowska D. 2008. Flowering and apical meristem growth dynamics. *Journal of Experimental Botany* 59: 187–201.
- Remizowa MV. 2019. One Upward, Two Steps Down: Order of Floral Organ Initiation. *Russian Journal of Developmental Biology* 50: 325–340.
- Ren Y, Chang H-L, Endress PK. 2010. Floral development in Anemoneae (Ranunculaceae). *Botanical Journal of the Linnean Society* 162: 77–100.
- Sun B, Ito T. 2015. Regulation of floral stem cell termination in *Arabidopsis*. *Frontiers in Plant Science* 6.

Appendix A.

Quantitative live confocal imaging of *Aquilegia* floral meristems

The following authors contributed to this appendix:

Min, Y.*, Conway, S. J.*, & Kramer, E. M. (*co-first authors)

BACKGROUND

Meristems are groups of pluripotent stem cells typically located at the tips of shoots. Many fundamental features of meristems are shared across all vascular plants, e.g. the maintenance of a pool of undifferentiated cells, regulated cell proliferation and expansion, and control of post-embryonic organogenesis. However, there remains a great deal of unexplored variation in meristem structure and behavior across land plants. Exploring this diversity is hampered by the reliance on common developmental techniques, such as fixed tissue sectioning and imaging that do not allow processes such as spatial and temporal patterns of cell division and expansion to be directly observed. In model systems such as *Arabidopsis thaliana*, genetic and molecular tools have been coupled with advancements in live imaging techniques that allow analyses of both cell behaviors and gene expression in real time, and these tools have provided considerable progress in our understanding of meristem development. However, these advancements are currently limited to a small number of model species and there is a pressing need to develop quantitative live imaging techniques in non-model systems, and specifically, approaches that may be broadly practical across a range of plant taxa. Here we present a detailed protocol for live imaging and analysis of floral meristems in *Aquilegia coerulea*, a member of the buttercup family (Ranunculaceae). This protocol provides a powerful tool to study the development of the meristem and initiation of floral organs and should be easily adaptable to many plant lineages, including other emerging model systems. This protocol will allow researchers to explore questions outside the scope of our common model systems.

MATERIALS AND REAGENTS

1. Petri dishes (35 x 10 mm; Corning, NY, USA)

2. Agar (Invitrogen, catalog number: 16500-100)
3. Linsmaier & Skoog medium (Caisson Labs, catalog number: L2P03)
4. Sucrose (Macron Fine Chemicals, catalog number: 57-50-1)
5. NaOH (Sigma-Aldrich, catalog number: 221465)
6. Kinetin (Sigma, catalog number: K0753-1G)
7. Gibberillic Acid (Sigma, catalog number: G7645-1G)
8. Eppendorf tubes
9. Parafilm
10. 100% EtOH
11. Aluminum foil
12. Microscope slides
13. Razor blades
14. Propidium Iodide (Sigma-Aldrich, catalog number: P4864)

EQUIPMENT

1. Scalpel with No. 10 blade (BioQuip Products, #2723A)
2. Straight dissecting needle (Carolina, #627201)
3. Precision Watchmaker's Forceps, Extra-Fine Point (Carolina, #624791)
4. Glass beads (Sigma-Aldrich, # 18406)
5. Microscope (Zeiss Stemi DV4 Stereo)
6. Microscope (LSM 980 NLO Multi-photon with a water immersion lens W Plan-Apochromat 20x/1.0 DIC UV-IR M27 75mm)

SOFTWARE

1. MorphographX (MGX) <https://morphographx.org/software/>.

RECIPES

Culture medium

1. To make up 1L of the culture medium, dissolve 2.375 g of Linsmaier & Skoog medium (Fisher Scientific; final strength: 0.5X) and 30 g of sucrose (final concentration: 3%) in 1L of ddH₂O. The Linsmaier & Skoog medium should provide buffering capacity such that the pH of the solution should be about 5.8. If the pH is too high, adjust it with 1N NaOH solution. Then add 8 g of agar (final concentration: 0.8%) and autoclave.
2. Once the autoclaved medium has cooled to a degree that is not too hot to be touched by a bare hand, add in 10⁻⁶ M kinetin (Sigma) and 10⁻⁷ M gibberellic acid (GA3, Sigma). Mix well and pour the plates in a fume hood to avoid contamination. 10⁻⁶ M kinetin and 10⁻⁷ M GA3 can be diluted as follows:
 - a. 10⁻⁶ M kinetin
 - Make 10⁻¹ M stock solution: dissolve 21.52 mg kinetin in 1ml of 1N NaOH in an Eppendorf tube. Seal the tube tightly with parafilm. This stock solution can be stored at 4°C for a few months.
 - Add 1 µl of the stock solution in 100 µl ddH₂O to reach the concentration of 10⁻³ M
 - Add 1 µl of 10⁻³ M solution in every 1 ml of culture medium to reach the concentration of 10⁻⁶ M
 - b. 10⁻⁷ M GA3:

- Make 10^{-1} M stock solution: dissolve 34.64 mg GA3 in 1ml 100% EtOH in a 1.6 ml Eppendorf tube. Seal the tube tightly with parafilm. This stock solution can be stored at 4°C for a few months.
- Add 1 μ l of the stock solution in 1 ml ddH₂O to reach the concentration of 10^{-4} M
- Add 1 μ l of 10^{-4} M solution in every 1 ml of culture medium to reach the concentration of 10^{-7} M

PROCEDURE

A. Plant materials and growth conditions

1. Seeds of *Aquilegia x coerulea* 'Kiragami' can be purchased from Swallowtail Garden Seeds (Santa Rosa, CA, USA) and germinated in wet soil in plug trays, which generally takes two to three weeks.
2. When the seedlings develop their first two true leaves, they are transplanted from plug trays to five-inch pots. Seedlings and young plants are grown in growth chambers with 16 h daylight at 18 °C, 8 h dark at 13 °C, and humidity under 40%. In these regular growth conditions, the plants are watered twice per week.
3. Once the plants develop five to six true leaves, they are transferred into the vernalization chamber which is set at 16 h daylight at 6 °C and 8 h dark at 6 °C. They should be well watered (i.e., the soil is fully hydrated) before being moved into cold conditions and are generally not watered during the vernalization period.
4. Plants stay in vernalization for three to four weeks and then are moved back into regular growth chambers for flowering. We usually put a small amount of controlled-release

fertilizer in each pot post vernalization. Inflorescences generally start to develop three weeks after vernalization.

5. Dead leaves should be actively removed to prevent fungal or pest infections.

B. Preparation of culture/imaging plates

1. Take an empty 1000 μ L pipette rack and gently press each foil square into one of the holes to create a round well (Fig. A1a-c). Cut small squares of aluminum foil (1x1cm). Carefully store foil squares in an autoclavable container (such as a glass petri dish) and autoclave (Fig. A1c).
2. Autoclave glass beads and ddH₂O.
3. Prepare the media according to Recipe 1.
4. While still molten, fill petri dishes half way with agar, quickly place one foil square in the center of the petri dish, concave side up. With sterile tweezers place a glass bead into the depression in the foil square (Fig. A1d). This is sufficient to ensure that the convex side of the foil is pressing into the agar. Once the bead is put on the foil square, the foil will automatically gravitate to the center of the plate. Let the plates cool and solidify inside of the sterile hood. Once solid, using tweezers, remove the glass beads and carefully peel off the foil square. This leaves a shallow well in the agar for mounting the meristems (Fig. A1e, 1f).
5. Solidified plates can be stored at 4°C for 2 months.

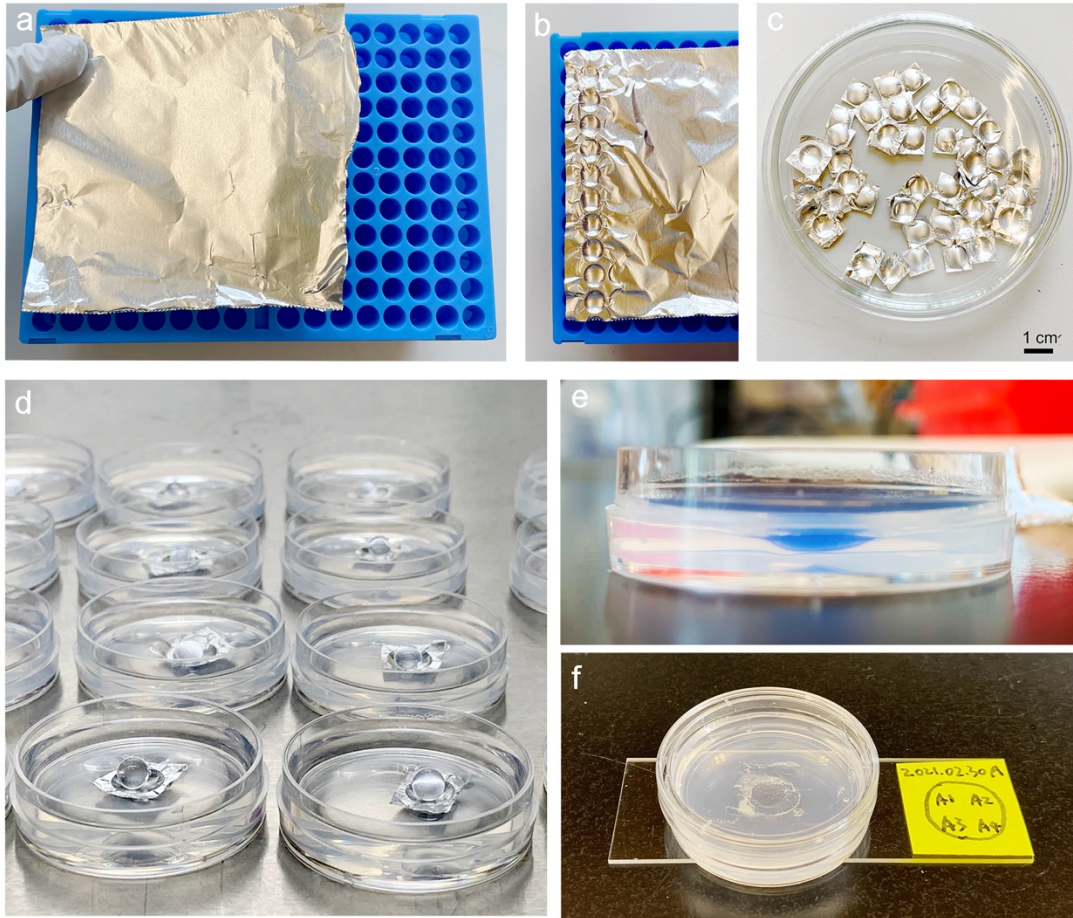


Figure A1. Making plates for live-imaging. (a) Take an empty 1000µL pipette rack and gently press each foil square into one of the holes to create a round well. (b) A strip of wells. (c) Foil squares are autoclaved and stored in a glass petri dish. (d) Examples of plates solidifying in a sterile hood with foil squares and glass beads in place. (e) A plate with blue dye to show the well in the center, where the meristems will be positioned. (f) The plate then will be glued onto a microscope slide. The slide was labelled with dates, while A1-A4 were the meristem labels and their relative locations in the well.

C. Tissue dissection and mounting

1. The forceps, surgical needles, and dissection blades are all sterilized in 10% bleach, washed in ddH₂O, and dried with Kimwipes before dissection.
2. Young axillary inflorescences or whole inflorescences are excised off the plant using forceps or scissors for meristem dissections (Fig. A2).

3. Inflorescences are washed in freshly prepared 10% bleach for 20 min. Any leaves and bracts on the stem should be removed using the forceps, but the attachment points of the petioles should be left on the stem (Fig. A2); if the petiole is completely removed from the stem, we found that the bleach solution will enter the wound and spread through the cells quickly, which kills the axillary meristems as well.
4. The stems are then washed with double-distilled water (ddH₂O) three times to completely remove the bleach residue, after which stems are kept immersed in ddH₂O.
5. When dissecting, put one stem under the microscope (the rest remaining in distilled water), and carefully remove the bracts and sepals of each floral meristem using the tip of a dissecting needle. Then excise the meristem off the branch with the scalpel and transfer it onto a 35 x 10 mm petri dish (Corning, NY, USA) with the culture medium. Make sure the base of the stem (usually there is about 1 mm of stem remaining) holding the meristem is pushed into the agar. We typically mount four floral meristems per dish.
6. Glue the petri dish to a microscope slide and label the date and the meristems on the slide (Fig. A1c).



Figure A2. Developmental stages for dissecting FMs for imaging. Axillary meristems can be obtained from either a lateral inflorescence branch (a, b) or a young inflorescence (c, d). Scale bars = 1 cm. Leaves that should be removed before or after the 10% bleach wash are indicated. Red dash lines indicate the locations where the floral axis will be excised for the bleach wash.

D. Staining

1. Meristems should be stained for 1-3 minutes in the petri dish by applying 50 μ L propidium iodide (0.5mg/mL) directly to the meristems. The mounting well should sufficiently contain the stain so that it creates a dome over the meristems. Take care that there is sufficient stain so that the meristems are fully immersed in stain throughout the whole staining period. It is important to note that the staining time will likely be specific to the plant and tissue being imaged, so here we just give a general time range and it is recommended that the staining time be optimized for each experiment. We would recommend starting with a low concentration for 1 minute and add time only if the tissue seems under-stained. Another important optimization is the staining for subsequent imaging time points. *Aquilegia* meristems were stained for 2.5 minutes for time point 1, then 2 minutes for time point 2 and 3, and 2-3 minutes for timepoint 4.
2. Carefully remove the stain and wash the meristems with ddH₂O three times by pipetting.

E. Imaging

Notes: Imaging will differ depending on the type of confocal and objective lenses available, as well as the type of tissue or stain used.

1. Meristems were imaged immediately after staining using a LSM 980 NLO Multi-photon confocal laser scanning microscope (Zeiss, Germany) equipped with a water immersion objective (W Plan-Apochromat 20x/1.0 DIC UV-IR M27 75mm, Zeiss).

2. The petri dishes were filled with ddH₂O while imaging and the water was immediately removed after imaging.
3. A DPSS 514nm laser was used for excitation and emission was collected between 580-670nm.
4. Scans were frame averaged 2x and z-sections taken at 2 μm intervals. This interval will vary depending on the size of the tissue We found that 2 μm was sufficient for downstream analysis while also minimizing the time the tissue was subjected to the laser.
5. After imaging, the remaining water in the petri dishes was carefully removed by pipetting using a P20 pipette and the petri dishes were returned to the tissue culture growth chamber.
6. Samples were imaged every 48 hours, typically 3-5 timepoints.

IMAGE PROCESSING

*Note: The following protocol for conducting segmentation and lineage tracing of the confocal images are adapted from (de Renille et al., 2014; Strauss et al., 2019) and the user manual at <https://www.mpipz.mpg.de/MorphoGraphX/help>, all of which detailed the structure of MorphoGraphX (MGX), including how the image data are stored, extracted, and processed. Here, we focus on the steps and parameters that are specific to processing confocal images of *Aquilegia floral meristems* and steps to reproduce figures in **Chapter 2**. We will use two original .czi files from our study as an example, which can be downloaded from this google drive link: <https://drive.google.com/drive/folders/1WjaCieLGrnTW7d51143b8HOn-dYmsMU?usp=sharing>*

A. Software installation and equipment setup

Download the newest version of MGX from <https://morphographx.org/software/>. Since the software improvements have mostly been implemented in the Linux versions, installation of the Linux operation system is preferred. To run MGX requires a computer nVIDIA graphics card that

supports CUDA, with at least 2 Gb of video memory and 8 Gb of the main memory of the computer itself. A larger video memory, a larger main computer memory, and/or a multi-core CPU can significantly shorten the processing time of some of the steps.

Processing a large amount of imaging data with MGX can be time-consuming so we strongly recommend readers have a comfortable workstation with proper office ergonomics if possible. An ultrawide monitor, or a dual-monitor setup, can be extremely helpful especially during the parental lineage tracing error correction process.

B. Load image into MorphoGraphX (MGX)

1. Convert the format of the stack image: Open the stack image (e.g. the 20210207_r8_A1.czi files) with FIJI (<https://imagej.net/Fiji>) or ImageJ: (<https://imagej.net/Welcome>), adjust the brightness and contrast, and save the image as 20210207_r8_A1.tif format.

Note: The images we acquired from the confocal microscope can be dim because we wanted to minimize tissue damage from both laser power and laser exposure time (which in turn slows down the growth), and thus the adjustment in brightness and contrast was almost always needed. Slightly over-saturated images usually look very good when loaded in MGX (Fig. A3).

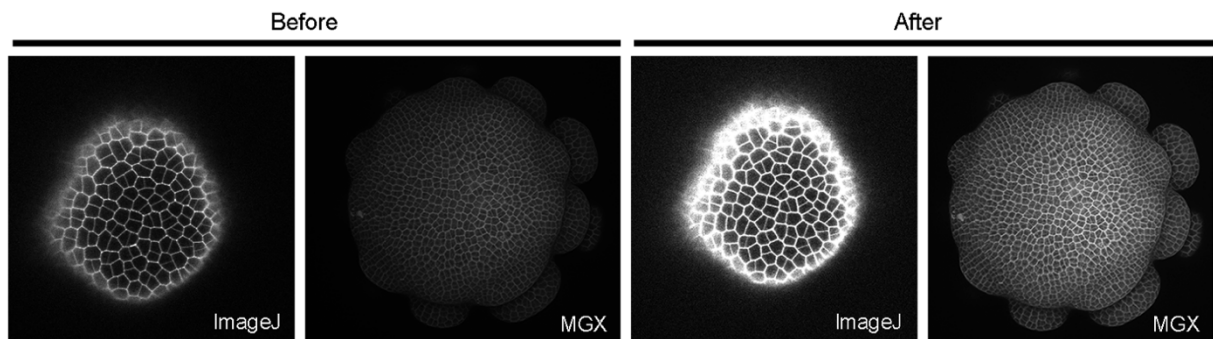


Figure A3. Comparison of how a confocal stack looks in ImageJ and MGX before and after adjusting the brightness and contrast. Images that appear to be slightly over-saturated in ImageJ generally look good in MGX.

2. Load the stack into MorphoGraphX: either drag the 20210207_r8_A1.tif file directly onto the MGX interface (Fig. A4), or Stack1 → open → choose the image.

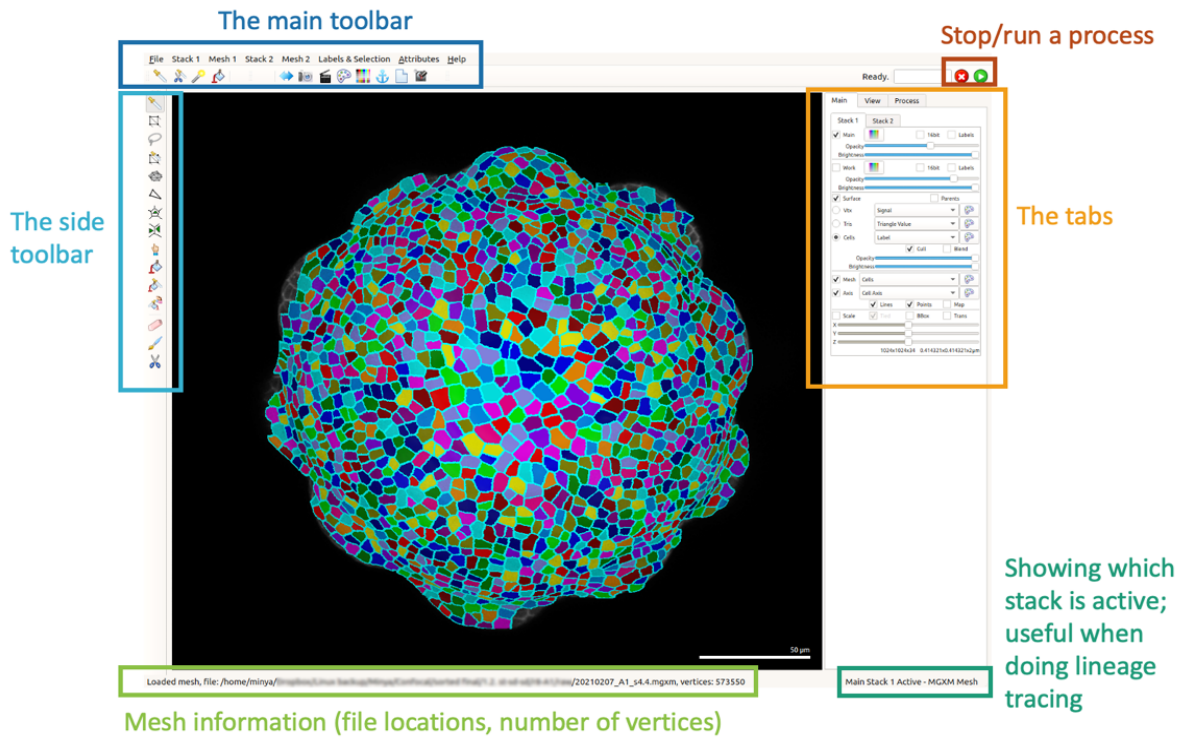





Figure A4. Overall layout of MorphographX interface.

3. If the stack still appears to be dark, there are two ways to directly adjust the brightness in MGX instead of adjusting the brightness/contrast in Fiji and loading the stacks again: 1) under the Main tab, under Work, change Opacity; 2) go to the View tab, and change the brightness and contrast under View Quality.
4. You can rotate the stack by using the left click of your mouse, move the stack to different parts of the screen with the right-click, and zoom in and out with the scroll wheel. By default, Stack 1 will appear green (and Stack 2 will be red), the setting of the colors can be changed using the Main Stack Colormap  under the Main tab.

C. Extract the surface

1. Go to tab, Process → Stack → Filters → Gaussian Blur Stack; change all the X/Y/Z Sigma parameters (appears at the right bottom corner; double click the cell to change) to 1; run the process twice (either by double-clicking the processor or hitting the “Run” arrow  on the upper right corner).

Note: It is important to blur each stack the same number of times, especially when dealing with images for lineage tracing.


2. Run Process → Morphology → Edge Detect, which creates a solid global shape of the object.
3. *Optional:* remove unwanted parts. For example, if we only want the top part of the meristem, we could remove the extra stamen/staminode primordia by clicking on “Voxel Edit ” on the top bar; Press Alt-key and left click of the mouse to erase parts that you don’t want.

Note: 1) If the Alt-key is not working, it is likely due to a conflict in the hotkey setting in your operating system, which already assigned a function to the Alt-key and thus prevents it from being used for selection in MorphoGraphX. You can change this setting in your operating system by assigning other keys to avoid the conflict. 2) Removing unwanted parts using the voxel edit can increase the speed of downstream processes, but the removal of parts is not reversible, so this step is generally not recommended unless there is a significant constraint on the computer capacity.

4. *Optional:* If there are holes on the shape, run Stack → Morphology → Fill Holes. Skip if no hole is observed.

Note: The adjustable parameters in this step are the X/Y-Radius. The bigger they are, the better they can fill the holes. However, the bigger they are, the more possible it is going to change your surface shape.

5. Go to Mesh → Creation → Marching Cubes Surface, change the threshold parameter to 20000, run the process.

6. Trim off the bottom. In the Main tab, ensure that the Mesh checkbox and “View” option are set to “All”. This will enable the visualization of the mesh. Click the “Select points in mesh (Alt+V) ” tool on the left toolbar and hold the Alt-key to select the bottom vertices of the apex. The selected vertices should turn red. Hit the delete key on the keyboard to remove them. To make this easier, it is nice to have the apex in a horizontal position. You can do this by left-double clicking on it. Try to delete the bottom cleanly. Save the mesh as “20210207_r8_A1_s.c6.mgxm”
7. Run Mesh → Structure → Subdivide. Then go to Mesh → Structure → Smooth Mesh, change the Passes number to 10 (the default is 1), and run the process. Repeat this subdivide step and then smooth the process two more times (i.e. three times in total). By now the total vertical number (shown in the bottom left window) in the mesh for an early stage FM should be above 500,000, while for an older stage FM should be about 1,000,000.

Note: Each subdivision increases the total vertical numbers by roughly four times. The last round of subdividing and smoothing can be demanding on computational power.

8. Save the mesh as “20210207_r8_A1_s.c8.mgxm”
9. Go to the Main tab, Unselect “Mesh”. Make sure “Main” and “Surf” are selected, but “Work” is not. Then run Process → Mesh → Signal → Project Signal to project the signals to the surface.

*Note: The default Max Dist (μm): 6.0 is good for *Aquilegia floral meristems* since they have relatively large cells especially compared to *Arabidopsis meristem* cells. If visualizing a tissue with smaller cells, the Max Dist can be decreased accordingly.*

10. Save the mesh as “20210207_r8_A1_s.c10.mgxm”

D. Cell segmentation.

1. Go to Process → Mesh → Segmentation → Auto-segmentation and change the following parameters from default: normalize to “No”, auto-seeding to 3.0, blur cell radius to 3.0, combine to 1.1. Run the process.

*Note: The auto-segmentation process can be demanding to the computational power. For *Aquilegia floral meristems*, depending on the developmental stages, we got good results by changing the auto-seeding and blur cell radius to 2.0, 2.5, or 3.0. The radius for auto-seeding and blur cells should be the same.*



2. Save the mesh as “20210207_r8_A1_s.d2.mgxm”

E. Correct segmentation errors

No matter how good the image stack is, there are likely to be segmentation errors, especially with samples such as *Aquilegia floral meristems* that contain hundreds to thousands of cells in a stack. It is very important to correct as many errors as possible at this step since it will greatly reduce the time that will likely be needed in future processes to correct parental labeling errors (which is relatively more time-consuming compared to correcting segmentation errors). *It is also important to constantly save the newer version of the mesh (e.g. 20210207_r8_A1_s.e0.mgxm).* The two processes with opposite functions, “Watershed Segmentation” and “Segmentation Clear”, are located right next to each other on the list, and it is not impossible to click the wrong button during processing. If the “Segmentation Clear” is run by accident on the whole mesh while the newest version of the corrected mesh has not been saved, it means starting over again.

Checking segmentation errors can be done by zooming in on one part of the mesh and selecting “Vtx” under the Surface panel of the Main tab and then accessing the Mesh panel under the “Cells” option. By toggling back and forth between the checked and unchecked options in the Mesh checkbox, you can compare the cell wall positions and segment boundaries. Correct all the

possible errors in that region, then move to another part of the mesh and repeat the process. There are a few types of common segmentation errors (Figs. A5-A7):

1. If a cell is over-segmented: If cell A is over-segmented into A1 and A2, select “Add label to selection ” on the left toolbar, press Alt-key and click on A1 (or A2). Then select “Fill label (Alt+M) ” on the left toolbar, press Alt-key and click on A2 (or A1) (Fig. A5).

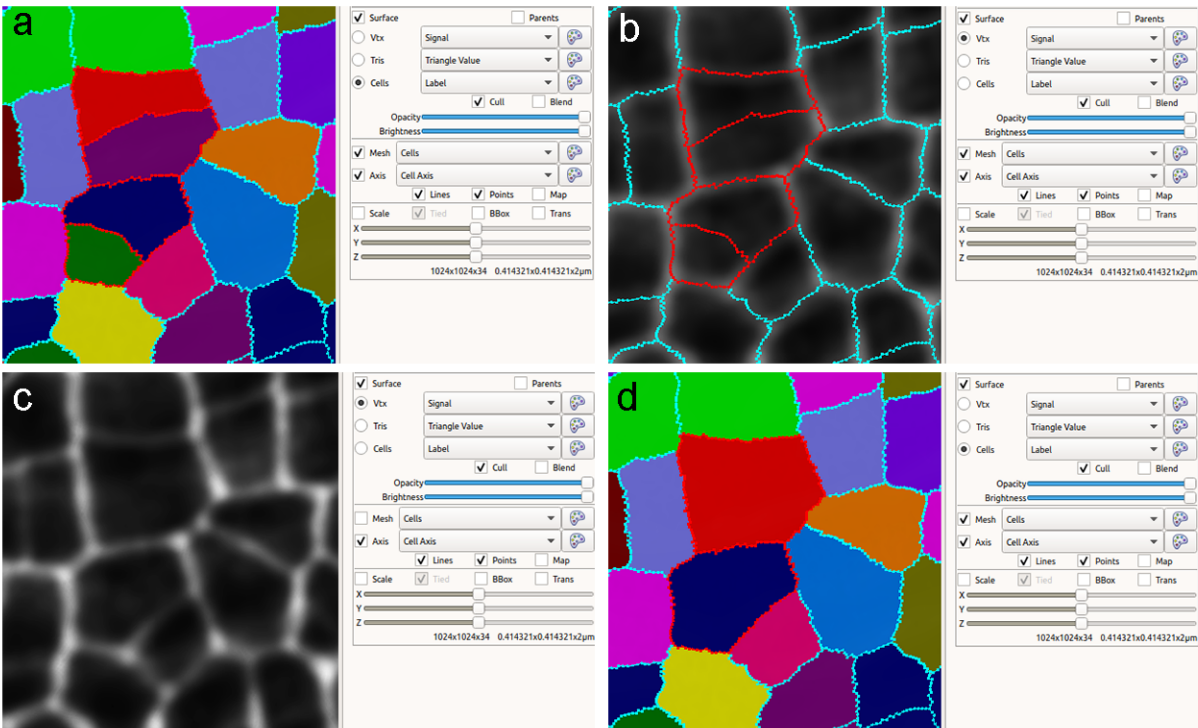





Figure A5. Examples of over-segmented cells. (a) How over-segmented cells (outlined in red) look under the Surface/Cells view. (b) How over-segmented cells (outlined in red) look under the Surface/Vtx view. (c) How the mesh looks. Over-segmented cells can be easily spotted by comparing between (c) and (b). (d) How cells look after over-segmentation has been corrected.

2. If a cell is under-segmented: This is a relatively common situation for cells at the boundary of the stack (due to faint signals) and at the organ boundaries (because the cells at the boundary are much smaller than the auto-segmentation radius). Click “Select points in mesh (Alt+V) ” on the left toolbar, press Alt-Key and select parts of the cell that needs to be

corrected (as long as some vertices in that cell were selected it is fine), then under the Process tab, run Mesh → Selection → Extend to Whole Cells, which selects all the vertices in that target cell (Fig. A6). On the left toolbar, click on “Erase selected ” to remove the labels from the cell. Labels can also be removed by running Mesh → Segmentation → Segmentation Clear under the same Process tab (Fig. A6). Then choose “Add new seed (Alt+B) ” from the left toolbar, press the Alt-key, and the left click of the mouse to draw the outlines of the cells (Fig. A6). Theoretically, the cells can be segmented as long as there is at least one seed inside, but drawing out the rough outlines of the cells can help with correct segmentation because sometimes the cell boundaries are faint. Lastly, under the Process tab, run Mesh → Segmentation → Watershed Segmentation (Fig. A6).

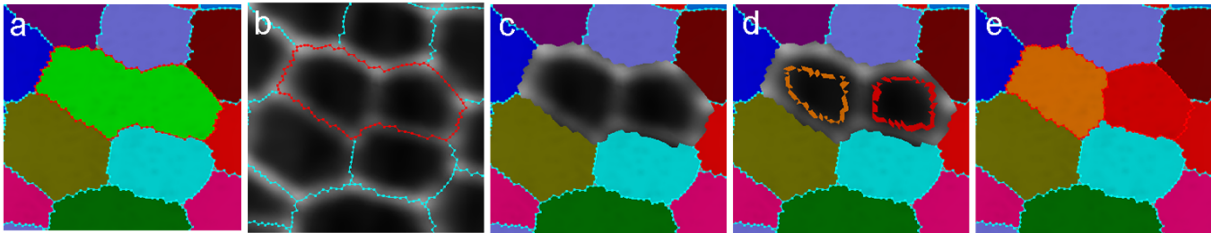


Figure A6. Examples of under-segmented cells. (a) A under-segmented cell outlined in red. **(b)** Under-segmented cells can be easily spotted by comparing the segmented outlines to the original mesh. **(c)** The label of the under-segmented cell being cleared. **(d)** The two cells being re-seeded. **(e)** How the labels look after the under-segmentation is corrected.




3. If the boundary of a cell is incorrect: This is most likely due to a faint signal in the cell wall staining (Fig. A7). On the left toolbar, click “Add label to selection ”, then press the Alt-key and click the cell that needs to be corrected. Then choose “Add current seed (Alt+N) ” from the left toolbar, use the left click of the mouse to fill in the gaps, and draw the correct boundary (Fig. A7). Then under the Process tab, run Mesh → Segmentation → Watershed Segmentation (Fig. A7).



Figure A7. Example of a cell with incorrect boundary. (a) Red arrow pointing to the incorrect boundary of a cell. (b) How the original segmentation looked. (c) How the corrected segmentation looked.

4. Remove the cells on the boundary of the mesh: After all visible errors are corrected on the mesh, run Mesh → Cell Mesh → Fix Corners Classic under the Process tab. Then click “Select points in mesh (Alt+V) ” on the left toolbar, press Alt-key and select cells on the boundary of the mesh, then under the Process tab, run Mesh → selection → Extend to whole cells. After the cells are selected, click “Delete selected” on the left toolbar, then save the mesh as “20210207_r8_A1_s.e4.mgxm”.

This last step is important because the sizes of the cells on the boundary are likely to be inaccurate due to several reasons: 1) the confocal Z-stack may have stopped scanning at this point without including the entire cell on the boundary; and 2) we arbitrarily trimmed off the bottom of the stack in step C6, which may have trimmed off parts of cells located on the boundary (Fig. A8).

After the first layer of cells on the boundary is removed, run Mesh → Cell Mesh → Fix Corners Classic under the Process tab again, and save the mesh again. This will be the mesh (i.e. 20210207_r8_A1_s.e4.mgxm) that is used to conduct lineage tracing.

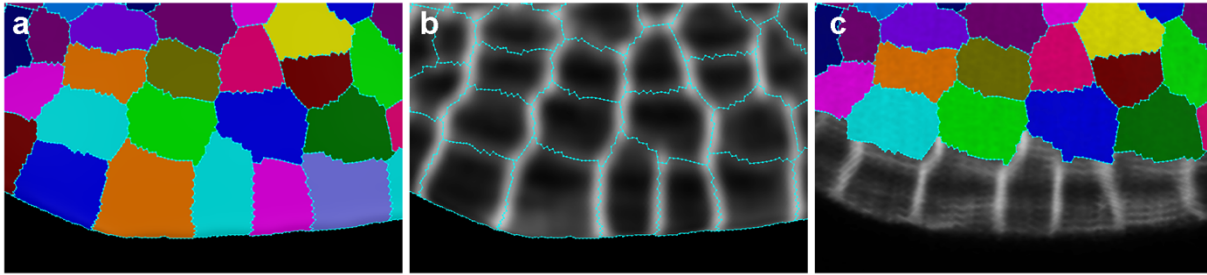



Figure A8. Removing cells on the boundary of the mesh. (a, b) How the labels look before removing the cells on the boundary, which had unnatural shapes. (c) How the labels looked after removing the cells on the boundary.

PARENT LABELING & LINEAGE TRACING


After processing the stacks and meshes from both time-point 1 (20210207_r8_A1_s.e4.mgxm) and time-point 2 (20210209_r8_A1_s.e4.mgxm), they are ready to conduct parental labeling and lineage tracing.

A. Parental labeling

1. Go to the Main toolbar, load the segmented mesh for time point 1 on Mesh 1, and the segmented mesh for time point 2 on Mesh 2. Both meshes are now loaded as meshes of Stack 1 and 2 under the Main tab respectively. The main stacks (i.e., the original .tif files) can also be loaded using the Main toolbar for Stack 1 and 2. It is a personal preference whether or not to load the main stacks because they are not required for the lineage tracing process, but it might look nicer to have the main stack shown when taking pictures.
2. Go to the View tab, and check “Stack1” in the Control-Key-Interaction panel. This allows you to move the meshes separately. Using the right click of the mouse alone will move both meshes together, but using the right click of the mouse while pressing the Control-key on the keyboard will only move the Stack 1. Use the control key and the mouse to move Stack 1 and 2 side by side on the screen.

3. Go to the Main tab Stack 1, next to the Mesh checkbox, click Colors Editor  to change the colors of Mesh 1 and/or Mesh 2 so that they are different from each other.
4. Go to the Main tab Stack 1, make sure the checkboxes of Main, Work, and Surface panels are all unchecked, but the one for Mesh is checked. Make sure that “Cells” is selected as the view option for both the Mesh and the Surface panels, and the view option for Cells is selected as “Label”.
5. Go to the Main tab Stack 2, uncheck Main and Work, but check Surface and Mesh. The view options for Surface and Mesh should be “Label” and “Cells” as well, respectively. Then check the checkbox of Parents to the right of the Surface checkbox. The colored segmented cells of Stack 2 should disappear after this.
6. When the meshes of the meristems are first loaded, we see the front view of the meristems. Use the left click on the mouse and the Control key to adjust the orientations of both meshes so that the side views are shown.
7. Use the left click of the mouse and the Control key to move the Mesh 1 above the Mesh 2. Then use the left click of the mouse alone to rotate both meshes so that the front views are shown again.
8. Look for a few cells on Mesh 1 and 2 that appear to be the same. Usually, the large cells at the center of the meristems are the most easily recognizable. Transfer the Mesh 1 on top of Mesh 2 by pressing the Control-key and using the right click of the mouse to match those recognized cells on both meshes.
9. Adjust the orientation and angles of Mesh 1 using the left click of the mouse and the Control-key to make more cells on both meshes overlap. If the growth between the two time points is rather large, adjust the size of the Mesh 1 by going to the Main tab Stack 1, check

the Scale checkbox, and increase the X values (adjusting Y or Z is also fine since all axes are linked).

10. To transfer labels from Mesh 1 to Mesh 2, go to the Main tab Stack 2 so that Stack 2 is active. Select “Grab Label ” from the left toolbar, hold the Alt-key, and click on the cells that are aligned on both meshes. If a cell at time-point 1 appears to have divided at time-point 2, click both cells and they will appear to be the same color.
11. Transfer labels of all possible cells from Mesh 1 to Mesh 2. Because of the meristem’s 3D structure, it is impossible to grab labels of all matching cells without adjusting the angles and orientation of the meshes. We recommend that users deal with one subregion of the mesh at a time (just like when correcting the segmentation errors): start from the center of the meristem, move down from the center to one edge of the mesh, label all possible cells in that region, then move on to the adjacent region. It is also possible that different regions of the samples require independent adjustments to the mesh sizes, which will require the user to use the Scale function (Step A9) repeatedly. For example, when tracing cells on the newly initiated primordia, the size of Mesh 1 will likely need to be scaled up greatly to match the cells on the Mesh 2; but when tracing cells on the boundary regions, Mesh 1 will most likely not need to be scaled. A video demonstration of lineage tracing can be found on:
<https://www.youtube.com/watch?v=KDiCyGrALYk&t=26s>
12. Save the parents' labels by running Mesh → Lineage Tracking → Save Parents under the Process tab. Make sure Stack 2 is active when saving the parents (otherwise an empty file will be saved). Use caution when saving because the Save Parents option is listed adjacent to Reset Parents, and the consequences of accidentally running the wrong process can be detrimental. Make sure to label the lineage tracing file informatively and identify the version,

since multiple versions may need to be saved when correcting lineage tracing errors (because there is no undo button!). For instance: r8-A1-0207to0209-v1.csv.

B. Correcting lineage tracing errors

Although it is not necessary to correct lineage tracing errors to generate a growth heat map, it is important to correct all errors before running any analysis to ensure the accuracy of the results. To check the correspondence of the traced cells, make sure Stack 1 is active, and under the Process tab, run Mesh → Cell Axis → PDG → Check Correspondence. The cells with errors will be highlighted in red on both meshes. To correct the errors, the original meshes of time-point 1 and time-point 2 need to be opened in two additional, separate MorphoGraphX windows, which is why we have recommended that users have an ultrawide monitor or a dual-monitor setup. Opening the meshes in additional windows is necessary because the meshes in the lineage tracing window have been simplified, so that only the vertices at the junctions between cells are present. Therefore, any modification of the meshes should be done on the original mesh rather than the mesh being checked for correspondence.



The error correction process consists of repetitive steps of 1) zoom in on one region of the meshes of the lineage tracing window, 2) identify the sources of errors, 3) correct the error on the original mesh 1 or 2, 4) save the updated versions of the original mesh and load it in the lineage tracing MorphoGraphX window again, 5) re-run “Check Correspondence” to make sure all the cells in the region are blue, and 6) move on to the next region with errors in the lineage tracing window until all the errors are corrected.

There are a few common types of errors in check correspondence:

1. Parental labeling error or segmentation error on the original meshes. If either kind of error occurs, the area on Mesh 1 will look like (Fig. A9a). Turn on the checkbox for Surface for

both Stack 1 and 2, make sure Cells are selected, and the view option is set to Label.

Compare the colors of the cells in that location to determine whether a cell was wrongly labeled, or the original mesh was wrongly segmented.

- If the cells on Mesh 2 had the wrong parental label, repeat steps 8 to 10 in Part A (Parental labeling) but only for the cells with error. Make sure Stack 2 is active and save the parents' labels by running Mesh → Lineage Tracking → Save parents under the Process tab. We recommend saving the new version of the parental labels as a new file, no matter how trivial the modification may have seemed to be.
 - If the error is due to segmentation error on the original mesh, it would be because either a cell on Mesh 1 is under-segmented or the cell on Mesh 2 is over-segmented. Check the original meshes as described in Step 5, and save the modified mesh as a new, separate file.
2. Errors at the cell junctions. This is likely to be the most common error in Check Correspondence and the junctions in question will be indicated in Mesh 1. They are usually due to tiny differences in how neighboring cells connect to each other in Mesh 1 and 2 (Fig. A9b). Zoom in on the junction in question in both Mesh 1 and 2, compare check and uncheck the Mesh checkbox to identify which mesh should be corrected. Then use “Add label to selection ” on the left tool bar, then press Alt-key and click the cell that needs to be corrected. Then choose “Add current seed (Alt+N) ” from the left toolbar, use the left click of the mouse to fill in the junction. Then under the Process tab, run Mesh → Cell Mesh → Fix Corners Classic, and save the modified mesh as a new, separate file.

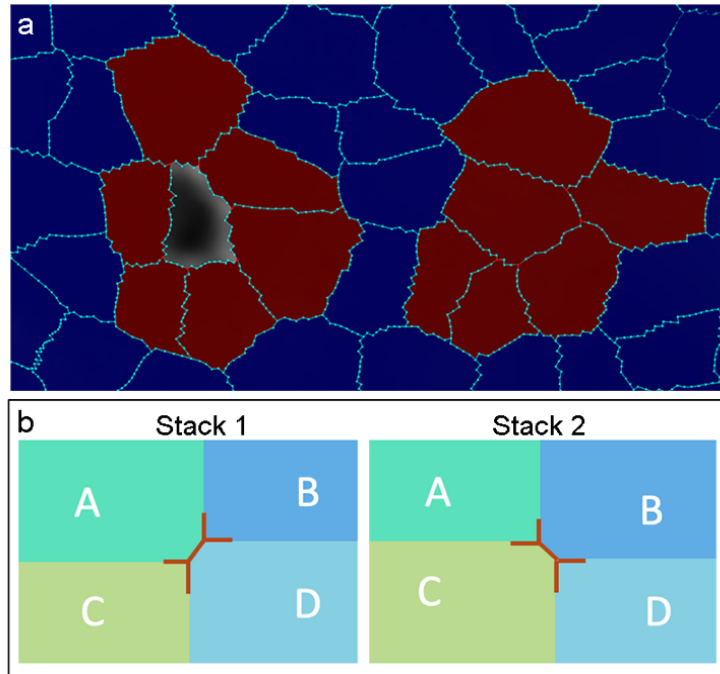

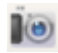



Figure A9. Examples of lineage tracing errors. (a) Two major types of errors. Left: Most likely due to incorrect parental labeling or incorrect segmentation, e.g. Stack 1 is over-segmented, but only one of the cells can be mapped to Stack 2. Right: Most likely due to incorrect cell junctions. (b) An example of why junction error can occur. In Stack 1, Cell A and D were physically connected to each other but C and B were not, while in Stack 2, C and B were physically connected to each other.


DATA ANALYSIS

After all the errors are corrected, reload Mesh 1 and 2 to Stack 1 and 2, respectively. Make sure Stack 2 is active and the Parents box is checked. Under the Process tab, run Mesh → Lineage Tracking → Load parents and load the latest version of the parental tracing file.

For all the heat maps, the scale of the values can be changed in Process → Mesh → Heat Map → Heat Map Range; the styles can be changed by clicking the Colors Editor  next to the view option of Cells in the Surface panel; and screenshots can be taken by clicking the Save screenshot  on the main toolbar. All the original images from Chapter 2 were saved as .PNG in 2700 px (width) x 2500 px (height).

A. Heat maps of cell area expansion and cell proliferation

1. To create a heat map for cell area expansion, under the Process tab, run Process → Mesh → Heat Map → Heat Map Classic. Select “Area” for the heat map type and “Geometry” for the visualization. Differences in various change map options can be found on the MorphoGraphX manual. Also select the “Change map” checkbox. This tells MorphoGraphX to make a heat map comparing Stack1 and Stack2. The heat map can be visualized on either the first (typically, Stack1) or second (Stack2) time point. For the growth sample here, select “Increasing” if Stack 1 (i.e. time-point1) is active or “Decreasing” if Stack 2 (i.e. time-point 2) is active.
2. To create a map of cell proliferation, make sure Stack 2 is active, and run Process → Mesh → Lineage Tracking → Heat Map Proliferation.
3. To create images such as Fig. A3 in Chapter 2, in which divided cells are highlighted on a cell area extension heat map, first run cell area expansion heat map on Stack 2. Check “Report to spreadsheet” so that the values of cell area expansion for each cell can be saved. Give the spreadsheet an informative name, such as “r8-A1-tp1_tp2-growth-allcells.csv”. Then create a map of cell proliferation by running Process → Mesh → Lineage Tracking → Heat Map Proliferation. Subsequently, run Process → Mesh → Heat Map → Heat Map Select, change the range values: Lower Threshold to 2, Upper Threshold to 3 or higher. This step will select all the cells that have experienced cell division. Then go to Process → Mesh → Heat Map → Heat Map Load, load “r8-A1-tp1_tp2-growth-allcells.csv” as the Heat Map file, and make sure the Column to load is set as “Value”.
4. The aesthetics of the growth heat map and cell outlines can be changed in the Main tab. To change the cell outlines, go to Main → Stack 1 → the Colors Editor  by the Mesh

panel. To change the heat map styles, go to Main → Stack 2 (if heat map is displayed on Stack 2) → the Colors Editor  by the Cells in the Surface panel. Sometimes the heatmap color scale appears to be incorrect on the screen. This is most likely to happen when both Stack 1 and Stack 2 are displaying heat maps, and the color scale of Stack 1 will cover the color scale of Stack 2. This can be simply solved by unclicking the Surface panel under Stack 1.

B. Heat maps of principle direction of growth and anisotropy

1. Make sure the parental file has been loaded to Stack 2 and then switch to Stack 1 to designate it as the active stack. Under the Process tab, run Mesh → Cell Axis → PDG → Check Correspondence, No error should show up since the meshes have been corrected. Make sure the active Stack is the stack that you want to display the heat map on, so if you want to display heat map on time-point 2, make Stack 2 as the active stack. Then run Mesh → Cell Axis → PDG → Compute Growth Directions. The PDG values can also be saved by running Mesh → Cell Axis → Cell Axis Save. Detailed explanations of the PDG parameters can be found in the MorphGraphX manual.
2. To change the display of the PDG map, go to Mesh → Cell Axis → PDG → Display Growth Directions. The PDG heat maps in [Chapter 2](#) were displayed as Anisotropy, which is the ratio between StretchMax and StretchMin. A ratio of 1 means no deformation, 2 means an elongation by 100%, 0.8 a shrinkage of 20%. The color and size of the PDG vectors can also be modified. By default, vectors corresponding to expansion (stretch ratio > 1) are displayed in white, while red is used to draw the direction of shrinkage (stretch ratio < 1). The “Threshold” parameter is used to display PDGs axis only in cells for which the

anisotropy is above a given value. Since we save each image at a relatively high resolution (2700 x 2500), we found that a Line Width of at least 10 px is needed for good visualization on the final screenshot.

PERSPECTIVES

In this study, we presented the first quantitative live-imaging protocol of floral buds of *A. coerulea*, which offers considerable potential for application to other non-traditional plant systems. However, there is still room for improvement to obtain higher quality quantitative data. First, our samples were stained with propidium iodide (PI), which generally gave good signal in most of the tissue, but cells in the organ boundary regions were often under-stained. Repetitive long-term staining with PI is known to become toxic to tissues and thus slow growth (Grandjean *et al.*, 2004; Bureau *et al.*, 2018), which was also the primary factor that restricted the length of the analyzed developmental window. Further development of transgenic markers for the plasma membrane would help to solve these issues. Second, our analysis was limited to surface reconstruction of the cells, although the behavior of cells under the epidermal layer is an indispensable part of fully understanding meristem morphogenesis. Third, due to the imaging mechanisms of the available confocal microscope, cell walls perpendicular to the focal axis of the microscope were often not detected. Combined with the fact that cells at the organ boundary were often poorly stained, we were often unable to segment and analyze cells in many boundary regions on the abaxial side of some primordia. Except for the issue with PI staining, all of the other limitations described here are, in fact, challenges faced by similar studies in the established model systems (Rambaud-Lavigne & Hay, 2020; Prunet & Duncan, 2020). Fortunately, rapid development in microscopes that allow long-term, deep-tissue, minimally invasive scanning, as well as software developments that can segment and reconstruct multiple cell layers in 3D from the imaging data, are in progress. A

comprehensive understanding of "the genetics of geometry" (Coen *et al.*, 2004) of morphogenesis in a diverse set of plant systems is hopefully underway.

REFERENCE

- Bureau C, Lanau N, Ingouff M, Hassan B, Meunier A-C, Divol F, Sevilla R, Mieulet D, Dievart A, Périn C. 2018. A protocol combining multiphoton microscopy and propidium iodide for deep 3D root meristem imaging in rice: application for the screening and identification of tissue-specific enhancer trap lines. *Plant Methods* 14: 96.
- Coen E, Rolland-Lagan A-G, Matthews M, Bangham JA, Prusinkiewicz P. 2004. The genetics of geometry. *Proceedings of the National Academy of Sciences* 101: 4728–4735.
- Grandjean O, Vernoux T, Laufs P, Belcram K, Mizukami Y, Traas J. 2004. *In Vivo* Analysis of Cell Division, Cell Growth, and Differentiation at the Shoot Apical Meristem in Arabidopsis. *The Plant Cell* 16: 74–87.
- Prunet N, Duncan K. 2020. Imaging flowers: a guide to current microscopy and tomography techniques to study flower development (F Wellmer, Ed.). *Journal of Experimental Botany* 71: 2898–2909.
- Rambaud-Lavigne L, Hay A. 2020. Floral organ development goes live (F Wellmer, Ed.). *Journal of Experimental Botany* 71: 2472–2478.
- de Reuille PB, Robinson S, Smith RS. 2014. Quantifying Cell Shape and Gene Expression in the Shoot Apical Meristem Using MorphoGraphX. In: Žárský V, Cvrčková F, eds. *Methods in Molecular Biology. Plant Cell Morphogenesis: Methods and Protocols*. Totowa, NJ: Humana Press, 121–134.
- Strauss S, Sapala A, Kierzkowski D, Smith RS. 2019. Quantifying Plant Growth and Cell Proliferation with MorphoGraphX. In: Cvrčková F, Žárský V, eds. *Methods in Molecular Biology. Plant Cell Morphogenesis: Methods and Protocols*. New York, NY: Springer, 269–290.

Appendix B.

Supplemental materials for Chapter 2

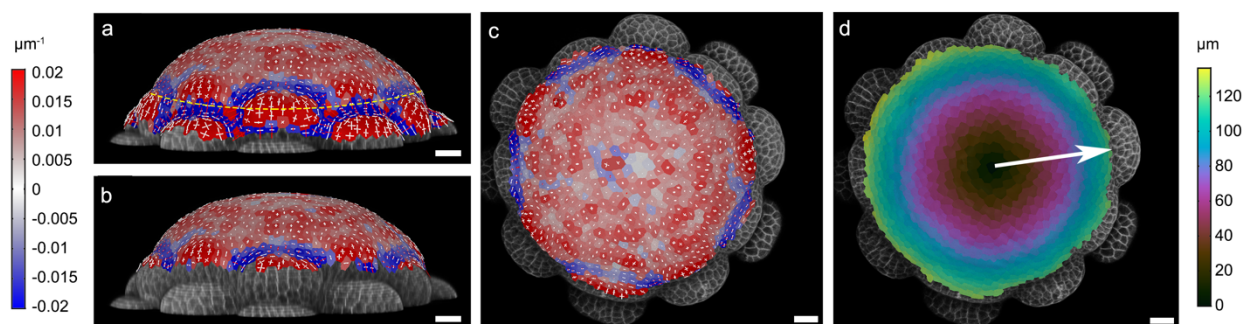


Figure B1. Regions used for constructing growth alignment graphs. (a) Side view of a meristem overlaid with surface curvature heatmap. Dashed yellow line circled the region defined by the boundary of the ITP. **(b)** Side view of a meristem overlaid with surface curvature heatmap only with the regions that will be used to construct the growth alignment graphs. **(c)** Front view of (b). **(d)** Cell distance heatmap that was used to determine the center most cell of the region of interest, and the white arrow represented the axis that would be used to construct the growth alignment graphs. Scale bars = 20 μm .

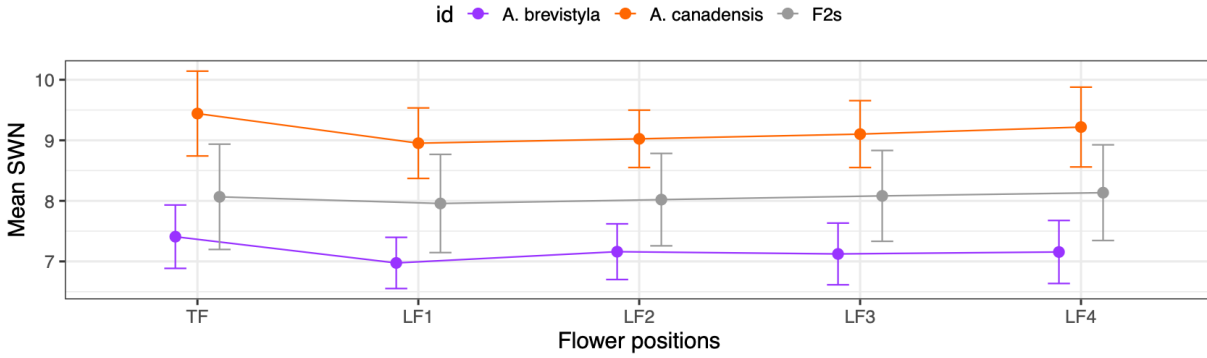
Table B1. Pair-wise Tukey's HSD test for cell area expansion rates and average cell division numbers between different TP intervals for the growth alignment graphs. Each interval is abbreviated as TP(first TP)(second TP): e.g. TP12 stands for the interval between TP1 to TP2. Cells in grey were pairs that have no significant difference.

		Cell area expansion rate				Average cell division			
		pair	Difference	Lower bound	Upper bound	Adjusted P-value	Difference	Lower bound	Upper bound
Bin1	TP12-TP23	-0.1038	-0.1258	-0.0819	0.0000	-0.0004	-0.0291	0.0283	1.0000
	TP12-TP34	-0.1124	-0.1355	-0.0894	0.0000	-0.0308	-0.0610	-0.0006	0.0429
	TP12-TP45	0.1128	0.0906	0.1351	0.0000	0.0369	0.0078	0.0661	0.0050
	TP12-TP56	0.0838	0.0596	0.1079	0.0000	0.0486	0.0170	0.0802	0.0003
	TP23-TP34	-0.0086	-0.0305	0.0134	0.8236	-0.0304	-0.0592	-0.0017	0.0321
	TP23-TP45	0.2167	0.1956	0.2378	0.0000	0.0373	0.0097	0.0650	0.0021
	TP23-TP56	0.1876	0.1645	0.2107	0.0000	0.0490	0.0188	0.0792	0.0001
	TP34-TP45	0.2252	0.2029	0.2476	0.0000	0.0677	0.0385	0.0970	0.0000
	TP34-TP56	0.1962	0.1720	0.2204	0.0000	0.0794	0.0477	0.1111	0.0000
TP56-TP45	0.0291	0.0057	0.0525	0.0064	-0.0116	-0.0423	0.0190	0.8382	
Bin2	TP12-TP23	-0.0640	-0.0880	-0.0400	0.0000	0.0020	-0.0394	0.0435	0.9999
	TP12-TP34	-0.0073	-0.0326	0.0179	0.9331	0.0039	-0.0397	0.0476	0.9992
	TP12-TP45	0.2320	0.2076	0.2563	0.0000	0.0671	0.0250	0.1092	0.0001
	TP12-TP56	0.2083	0.1818	0.2347	0.0000	0.0760	0.0303	0.1217	0.0001
	TP23-TP34	0.0567	0.0326	0.0808	0.0000	0.0019	-0.0396	0.0435	0.9999
	TP23-TP45	0.2960	0.2729	0.3191	0.0000	0.0651	0.0252	0.1050	0.0001
	TP23-TP56	0.2723	0.2470	0.2976	0.0000	0.0740	0.0303	0.1177	0.0000
	TP34-TP45	0.2393	0.2149	0.2637	0.0000	0.0632	0.0210	0.1054	0.0004
	TP34-TP56	0.2156	0.1891	0.2421	0.0000	0.0721	0.0263	0.1179	0.0002
TP56-TP45	0.0237	-0.0019	0.0494	0.0857	-0.0089	-0.0532	0.0354	0.9821	
Bin3	TP12-TP23	-0.0287	-0.0589	0.0015	0.0712	0.0283	-0.0249	0.0816	0.5940
	TP12-TP34	0.0352	0.0034	0.0670	0.0213	0.0762	0.0201	0.1323	0.0020
	TP12-TP45	0.2703	0.2396	0.3009	0.0000	0.1311	0.0771	0.1852	0.0000

	TP12-TP56	0.2411	0.2079	0.2744	0.0000	0.0736	0.0150	0.1322	0.0056
	TP23-TP34	0.0639	0.0337	0.0942	0.0000	0.0479	-0.0055	0.1012	0.1030
	TP23-TP45	0.2990	0.2700	0.3281	0.0000	0.1028	0.0516	0.1541	0.0000
	TP23-TP56	0.2699	0.2381	0.3017	0.0000	0.0453	-0.0108	0.1013	0.1784
	TP34-TP45	0.2351	0.2044	0.2658	0.0000	0.0549	0.0008	0.1091	0.0449
	TP34-TP56	0.2059	0.1726	0.2393	0.0000	-0.0026	-0.0614	0.0561	1.0000
	TP56-TP45	0.0292	-0.0031	0.0614	0.0981	0.0575	0.0007	0.1144	0.0455
Bin4	TP12-TP23	0.0216	-0.0218	0.0650	0.6553	-0.0189	-0.0778	0.0400	0.9058
	TP12-TP34	-0.0166	-0.0624	0.0291	0.8588	0.0258	-0.0362	0.0878	0.7877
	TP12-TP45	0.2234	0.1793	0.2675	0.0000	0.0787	0.0189	0.1385	0.0031
	TP12-TP56	0.1642	0.1163	0.2120	0.0000	-0.0769	-0.1418	-0.0120	0.0108
	TP23-TP34	-0.0382	-0.0818	0.0053	0.1162	0.0447	-0.0143	0.1037	0.2345
	TP23-TP45	0.2018	0.1600	0.2436	0.0000	0.0976	0.0409	0.1542	0.0000
	TP23-TP56	0.1426	0.0968	0.1883	0.0000	-0.0580	-0.1200	0.0040	0.0798
	TP34-TP45	0.2401	0.1959	0.2843	0.0000	0.0529	-0.0070	0.1128	0.1131
	TP34-TP56	0.1808	0.1329	0.2287	0.0000	-0.1027	-0.1677	-0.0377	0.0002
TP56-TP45	0.0593	0.0129	0.1057	0.0045	0.1556	0.0927	0.2184	0.0000	
Bin5	TP12-TP23	0.0216	-0.0218	0.0650	0.6553	0.0176	-0.0399	0.0752	0.9195
	TP12-TP34	-0.0166	-0.0624	0.0291	0.8588	0.0462	-0.0144	0.1068	0.2279
	TP12-TP45	0.2234	0.1793	0.2675	0.0000	0.0652	0.0068	0.1237	0.0197
	TP12-TP56	0.1642	0.1163	0.2120	0.0000	-0.0583	-0.1217	0.0052	0.0892
	TP23-TP34	-0.0382	-0.0818	0.0053	0.1162	0.0286	-0.0290	0.0863	0.6566
	TP23-TP45	0.2018	0.1600	0.2436	0.0000	0.0476	-0.0077	0.1030	0.1303
	TP23-TP56	0.1426	0.0968	0.1883	0.0000	-0.0759	-0.1365	-0.0153	0.0058
	TP34-TP45	0.2401	0.1959	0.2843	0.0000	0.0190	-0.0395	0.0775	0.9021
	TP34-TP56	0.1808	0.1329	0.2287	0.0000	-0.1045	-0.1680	-0.0410	0.0001
TP56-TP45	0.0593	0.0129	0.1057	0.0045	0.1235	0.0620	0.1849	0.0000	
Bin6	TP12-TP23	-0.0409	-0.1025	0.0207	0.3659	0.0002	-0.0545	0.0548	1.0000
	TP12-TP34	-0.0157	-0.0806	0.0492	0.9645	0.0278	-0.0298	0.0853	0.6813
	TP12-TP45	-0.0431	-0.1057	0.0194	0.3274	-0.0081	-0.0636	0.0473	0.9946
	TP12-TP56	0.0883	0.0204	0.1562	0.0036	-0.1079	-0.1681	-0.0476	0.0000
	TP23-TP34	0.0252	-0.0365	0.0869	0.7995	0.0276	-0.0272	0.0823	0.6438
	TP23-TP45	-0.0022	-0.0615	0.0570	1.0000	-0.0083	-0.0609	0.0443	0.9928
	TP23-TP56	0.1292	0.0643	0.1940	0.0000	-0.1080	-0.1656	-0.0505	0.0000
	TP34-TP45	-0.0274	-0.0901	0.0353	0.7557	-0.0359	-0.0915	0.0197	0.3965
	TP34-TP56	0.1040	0.0360	0.1720	0.0003	-0.1356	-0.1959	-0.0753	0.0000
TP56-TP45	-0.1314	-0.1972	-0.0656	0.0000	0.0997	0.0413	0.1581	0.0000	

Appendix C.

Supplemental materials for Chapter 3



	One-way ANOVA						Tukey's HSD				
		Df	Sum Sq	Mean Sq	F value	Pr (>F)		diff	lwr	upr	p-adj
A. brevistyla	flower	4	2.02	0.5049	4.176	0.00325 **	TF-LF1	0.383	0.121	0.645	0.00084 ***
	residuals	130	15.72	0.1209							
A. canadensis	flower	4	2.387	0.5967	2.764	0.0335 *	TF-LF1	0.48	0.02	0.938	0.036 *
	residuals	75	16.191	0.2159							
F2s	flower	4	1.56	0.3909	0.875	0.479					
	residuals	289	125.53	0.4344							

Signif. codes: 0 '****' 0.001 '***' 0.01 '**' 0.05 '.' 0.1 '.' 1

Figure C1: SWN and the position of flowers on inflorescences. Positions of flowers on inflorescences have no significant influence on the SWN among the F2s, but do differ in the parental species, where terminal flowers tend to have higher SWN.

	Df	Sum Sq	Mean Sq	F value	Pr (>F)
F1 parent	4	19.40	4.850	16.32	3.39e-12 ***
Residuals	326	96.89	0.297		

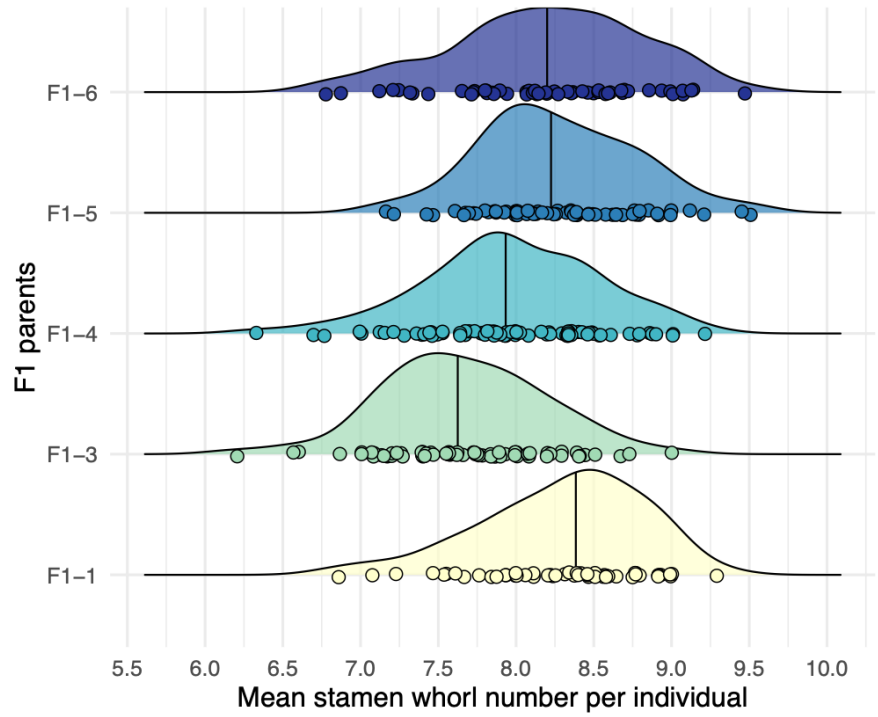


Figure C2: F1-parent-of-origin has a significant impact on the distribution of SWN in their respective F2 progeny. Density ridgeline plots showing the distribution of SWN of F2s of different F1 parents.

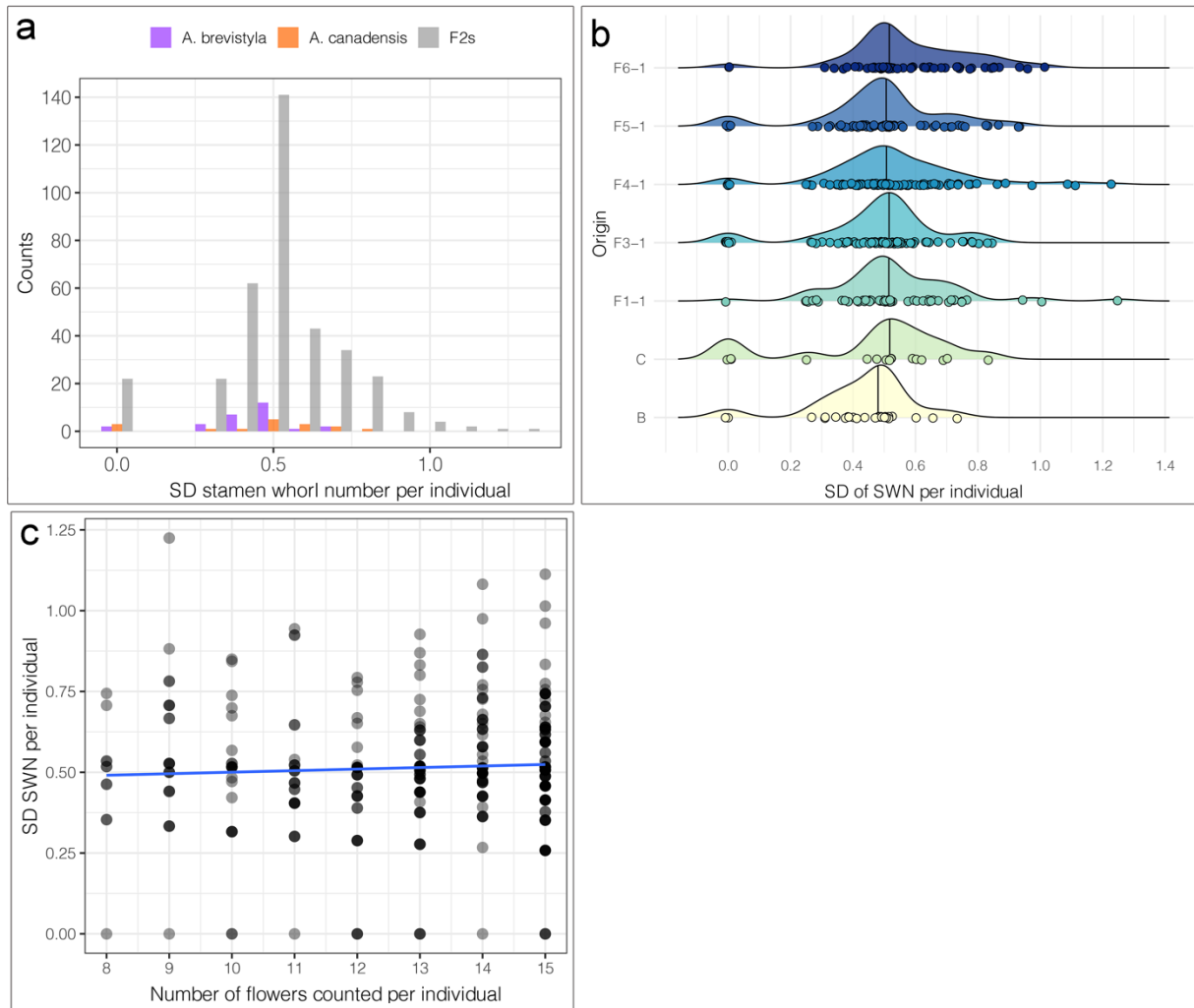


Figure C3: Distribution of the SD of SWN among the parental and F2 populations. (a) Histogram showing that both parents and the F2s had a small number of individuals showing 0 variation (SD=0) in SWN while the remaining individuals display a large variation in SWN. **(b)** Density ridgeline plots showing the same patterns of SD of SWN distribution regardless of F1-parent-of-origin. **(c)** SD=0 is not an artifact of individuals with fewer flowers counted. There are individuals exhibiting SD=0 in SWN regardless of how many flowers were counted per plant.

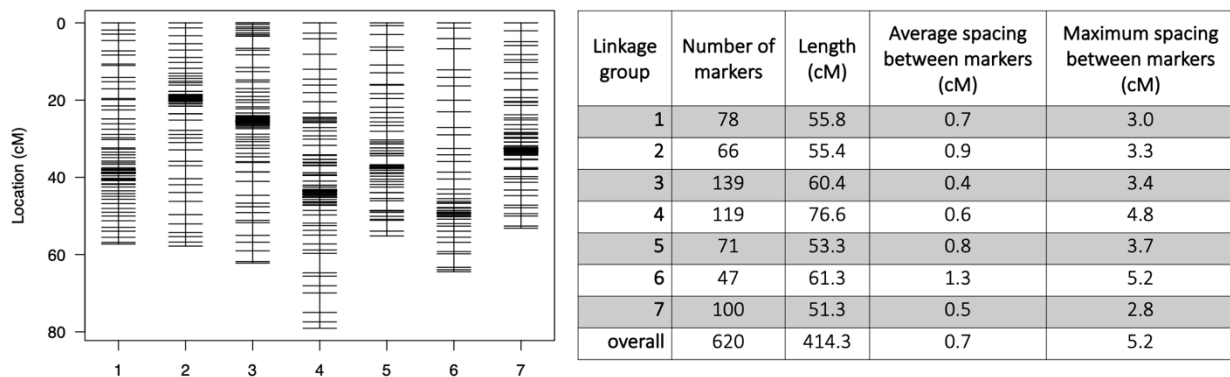


Figure C4: Diagram (left) and summary statistics (right) of the genetic map.

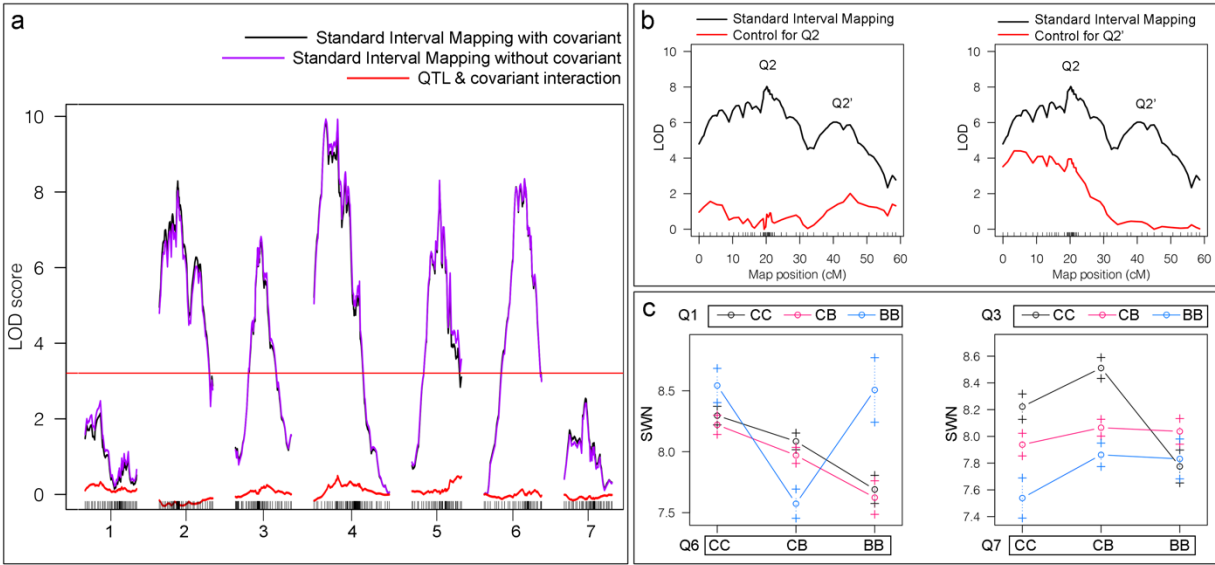


Figure C5: Confirmation of QTL underlying SWN variation. (a) No significant interaction between covariant and QTL was detected. (b) Controlling for potential QTL on chromosome 2 did not provide evidence to support the presence of two unlinked QTL. The real QTL on chromosome 2 was named Q2, the potential second QTL was named Q2'. When Q2 was controlled, the evidence for Q2' disappeared, but when Q2' was controlled, the evidence for Q2 stayed significant. (c) QTL interaction between Q1 x Q6, and Q3 x Q7. C: *A. canadensis* allele; B: *A. brevistyla* allele. In (a) and (b), the LOD scores were from the standard interval mapping rather than the full QTL model, which assumes the presence of a single QTL and could not include QTL interactions. This is the reason why the LOD score distributions appear to be a bit different from Fig. 4a.

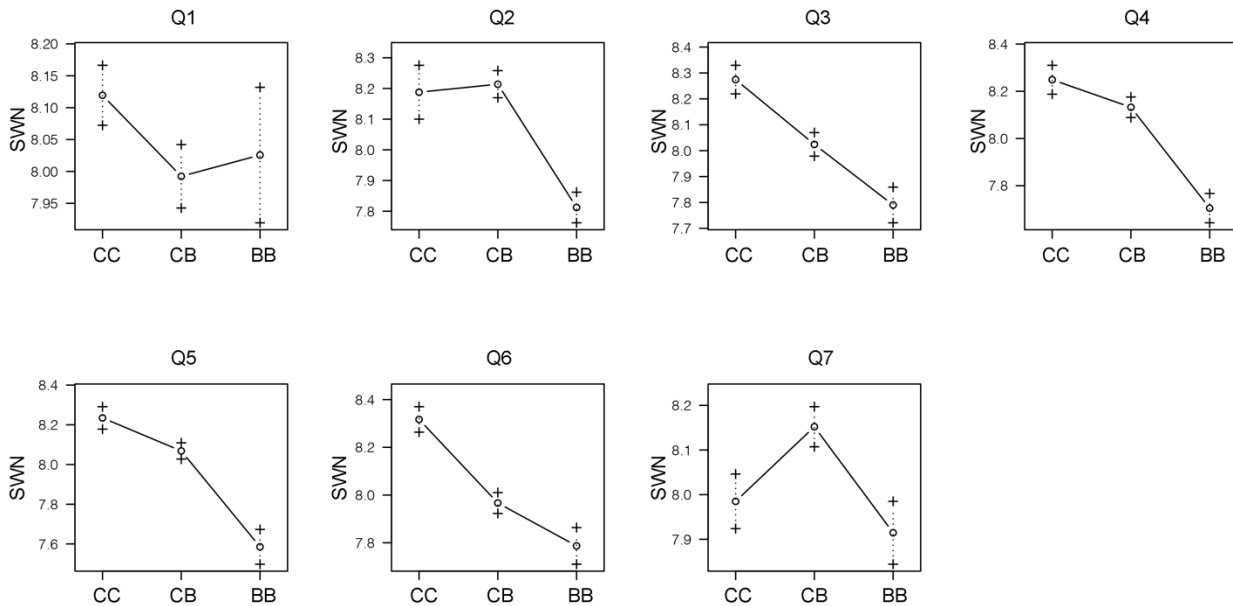


Figure C6: Effect plots of the markers that have the highest LOD score under each QTL. C: *A. canadensis* allele; B: *A. brevistyla* allele

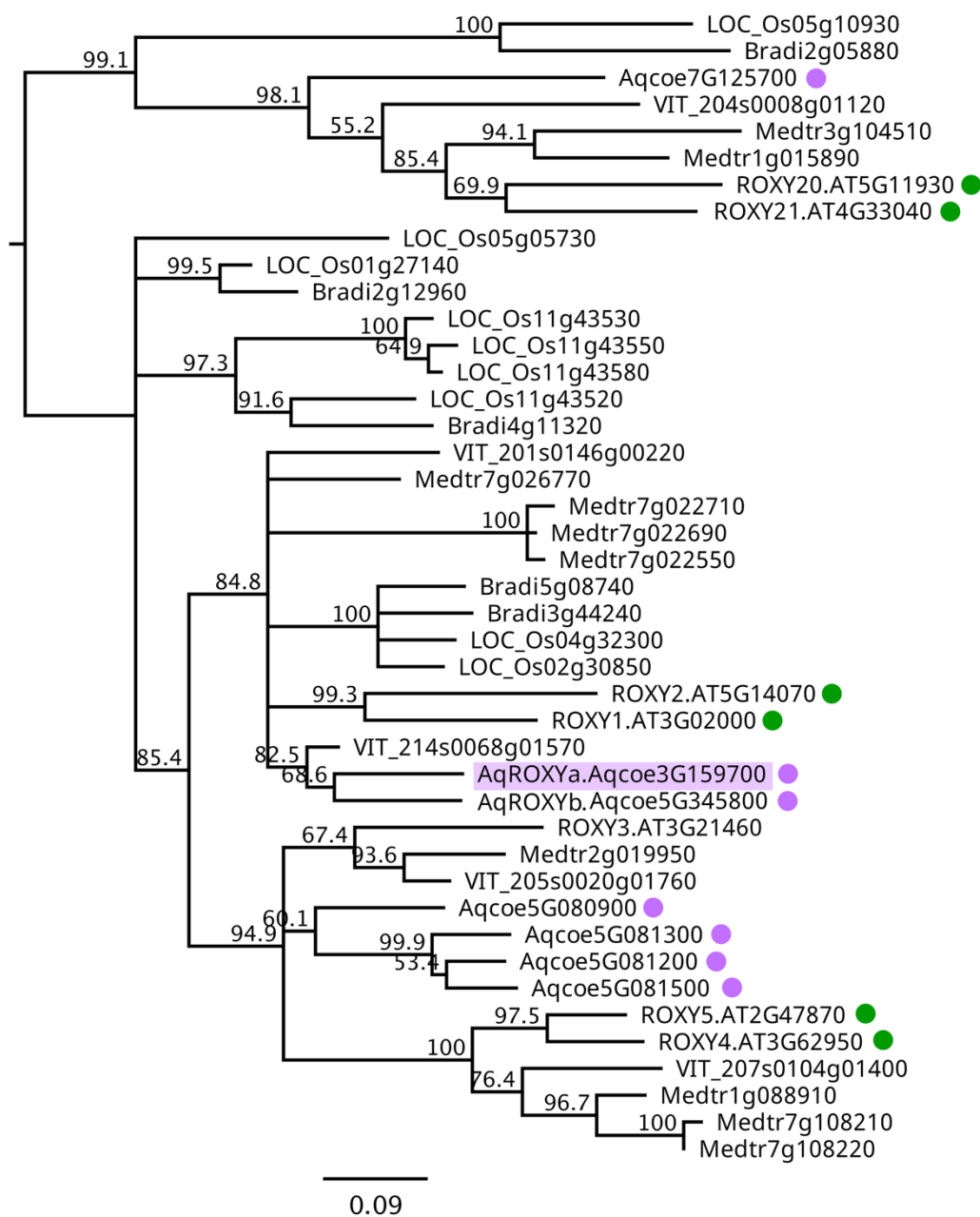


Figure C7: Gene phylogeny for AqROXYa. Neighbor-joining phylogeny of ROXY homologs using amino acid alignment. Species included in this phylogeny and the prefix of their gene identifiers: *A. coerulea* (“Aqcoe”), *Vitis vinifera* (“VIT”), *A. thaliana* (“AT”), *Medicago truncatula* (“Medtr”), *Oryza sativa* (“LOC_Os”), and *Brachypodium distachyon* (“Bradi”). All sequences were obtained from Phytozome (<https://phytozome-next.jgi.doe.gov/>). Homologs in *A. thaliana* and *A. coerulea* are indicated by green and purple dots, respectively. AqROXYa is highlighted in purple. This gene phylogeny is consistent with previously published ROXY homologs in *A. thaliana* (Li *et al.*, 2009).

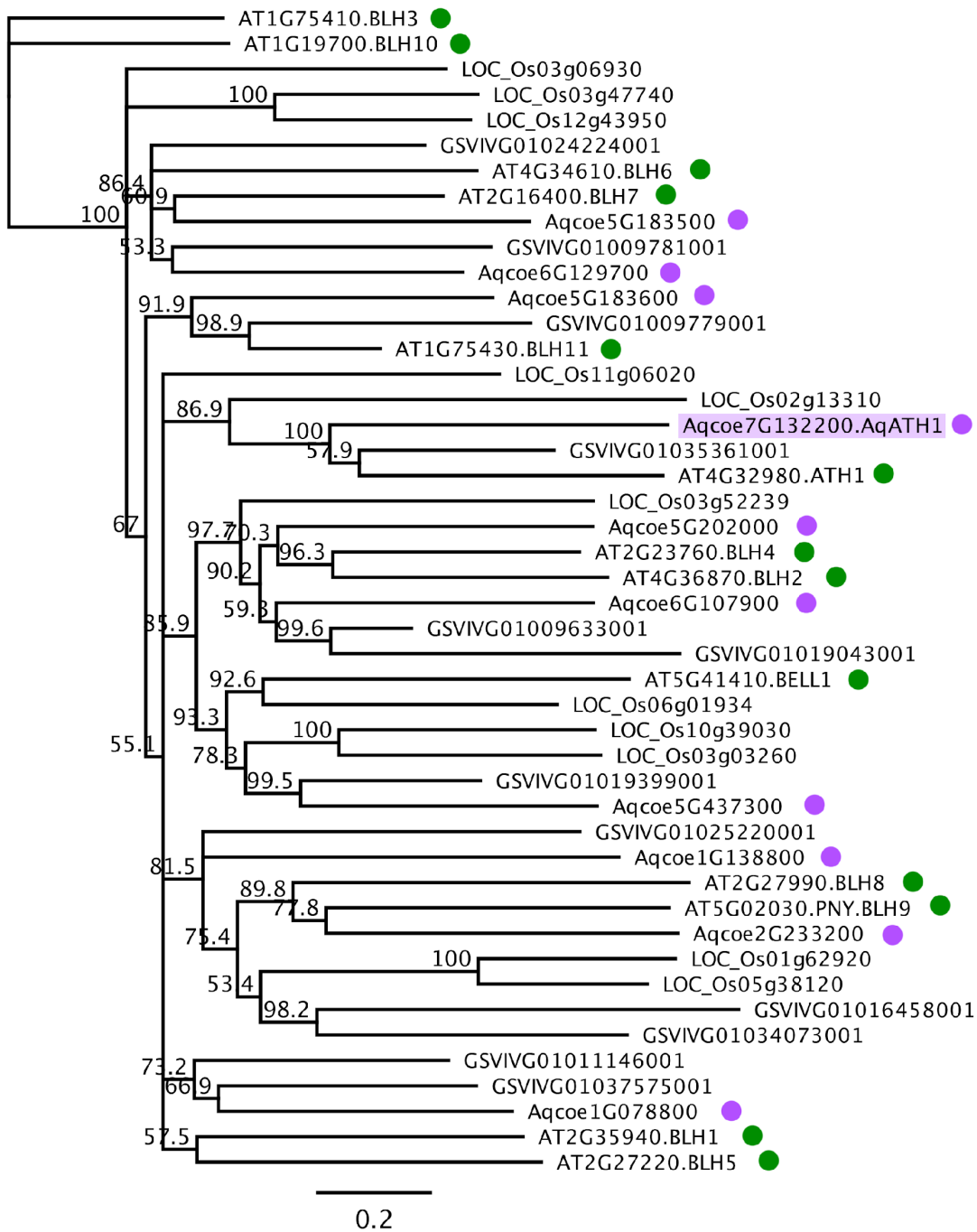


Figure C8: Gene phylogeny for AqATH1. Neighbor-joining phylogeny of BEL family members. Species included in this phylogeny and the prefix of their gene identifiers: *A. coerulea* (“Aqcoe”), *Vitis vinifera* (“GSVIVG”), *A. thaliana* (“AT”), and *Oryza sativa* (“LOC_Os”). All sequences were obtained from Phytozome (<https://phytozome-next.jgi.doe.gov/>). Homologs in *A. thaliana* and *A. coerulea* are indicated by green and purple dots, respectively. AqATH1 is highlighted in purple.

Table C1. Pairwise comparison of FM widths through early developmental stages. grp1=group1, grp2=group2 in the pairwise comparison. B: *A. brevistyla*, C: *A. canadensis*. Numbers in the parenthesis represented the number of stamen whorls initiated in the FM. Comparisons are conducted using the Wilcoxon tests and p-values are adjusted (p.adj) using the Bonferroni test. Pairs that are not significantly different from each other are shaded in light grey. n: number of the sections measured for each group. p.adj.sig: symbols indicating the adjusted p-values in the pairwise comparison; ns: not significant; *: p<0.05; **: p<0.01; ***: p<0.001; ****: p<0.0001.

	grp1	grp2	n (grp1)	n (grp2)	mean (μm, grp1)	mean (μm, grp2)	p	p.adj	p.adj.sig
By stages	B (0~2)	C (0~2)	37	39	147.06	156.13	0.004	0.019	*
	B (2~4)	C (2~4)	20	35	171.57	172.92	0.8	1	ns
	B (4~6)	C (4~6)	15	15	161.60	186.78	5.16E-08	2.58E-07	****
	B (6~7)	C (6~7)	16	17	179.06	197.29	4.12E-04	0.00206	**
	B (>=8)	C (>=8)	20	46	174.68	191.67	4.28E-06	2.14E-05	****
By species	B (0~2)	B (2~4)	37	20	147.06	171.57	1.42E-09	2.84E-08	****
	B (0~2)	B (4~6)	37	15	147.06	161.60	3.17E-05	6.34E-04	***
	B (0~2)	B (6~7)	37	16	147.06	179.06	2.54E-08	5.08E-07	****
	B (0~2)	B (>=8)	37	20	147.06	174.68	6.46E-10	1.29E-08	****
	B (2~4)	B (4~6)	20	15	171.57	161.60	0.005	0.1	ns
	B (2~4)	B (6~7)	20	16	171.57	179.06	0.157	1	ns
	B (2~4)	B (>=8)	20	20	171.57	174.68	0.425	1	ns
	B (4~6)	B (6~7)	15	16	161.60	179.06	8.96E-04	0.018	*
	B (4~6)	B (>=8)	15	20	161.60	174.68	0.002	0.04	*
	B (6~7)	B (>=8)	16	20	179.06	174.68	0.381	1	ns
	C (0~2)	C (2~4)	39	35	156.13	172.92	1.96E-06	3.92E-05	****
	C (0~2)	C (4~6)	39	15	156.13	186.78	6.93E-12	1.39E-10	****
	C (0~2)	C (6~7)	39	17	156.13	197.29	2.04E-14	4.08E-13	****
	C (0~2)	C (>=8)	39	46	156.13	191.67	4.31E-19	8.62E-18	****
	C (2~4)	C (4~6)	35	15	172.92	186.78	2.97E-04	5.94E-03	**
	C (2~4)	C (6~7)	35	17	172.92	197.29	3.12E-09	6.24E-08	****
	C (2~4)	C (>=8)	35	46	172.92	191.67	1.56E-08	3.12E-07	****
	C (4~6)	C (6~7)	15	17	186.78	197.29	0.005	0.1	ns
	C (4~6)	C (>=8)	15	46	186.78	191.67	0.169	1	ns
	C (6~7)	C (>=8)	17	46	197.29	191.67	0.057	1	ns

Table C2: No significant evidence supporting the presence of a second QTL on any chromosome. The two-dimensional genome scan method scans for all marker pairs of a given chromosome and calculate the LOD scores of the potential two-QTL models based on the marker pairs. The LOD values shown in the table for each chromosome are the highest LOD scores between all pairwise markers of a given chromosome.

LOD.fv1: the \log_{10} likelihood ratio comparing the two-QTL full model (including both additive effects and interactions) to the one-QTL model. Large *LOD.fv1* scores indicate evidence for a second QTL, allowing for the possibility of interaction.

LOD.av1: the \log_{10} likelihood ratio comparing the two-QTL model but only considering additive effects to the one-QTL model. Large *LOD.av1* scores indicate evidence for a second QTL, assuming no interaction.

LOD.int: the difference between *LOD.fv1* and *LOD.av1*, indicating evidence for interactions between potential QTL. "10% sig cut off" are the values of *LOD.fv1*, *LOD.av1*, and *LOD.int* above the 90% of their respective distributions generated from 1000 permutations. LOD values that are bigger than the 10% cut off are considered significant.

	<i>LOD.fv1</i>	<i>LOD.av1</i>	<i>LOD.int</i>
Chromosome 1	3.69	1.01	2.69
Chromosome 2	3.86	2.31	1.55
Chromosome 3	2.71	2.47	0.24
Chromosome 4	3.65	2.21	1.44
Chromosome 5	2.83	1.71	1.12
Chromosome 6	3.24	1.15	2.08
Chromosome 7	3.68	2.20	1.48
10% sig cut off	5.99	5.04	5.25

Table C3: Summary of number of genes under each potential QTL. Percentages shown in the parentheses are the percentage of the number of genes found in the RNA-seq data (Min & Kramer, 2020) to the total number of genes that are in the respective genomic interval. A gene was considered as expressed if its transcript had more than 1 million read counts in more than 1 samples in the RNA-seq experiment.

QTL	Chr	size (Mb)	Interval on the genome	No. of genes	Exp at any RNAseq stage
Q1	1	6	38,000,001..44,000,000	964	676 (70.12%)
Q2	2	36.5	3,500,001.. 40,000,000	3242	2315 (71.41%)
Q3	3	26.5	8,000,001..34,500,000	1844	1265 (68.60%)
Q4	4	3.8	2,000,001..5,800,000	383	176 (46.21%)
Q5	5	26.5	9,000,001..35,500,000	1919	1393 (72.59%)
Q6	6	1.5	6,000,001..7,500,000	226	170 (75.22%)
Q7	7	2.5	7,000,001..9,500,000	315	242 (76.83%)

Table C4: Expressed genes under Q4. A gene was considered as expressed if its transcript had more than 1 million read counts in more than 1 samples in the RNA-seq experiment (Min & Kramer, 2020). Best.hit.At: Top BLAST hit A. thaliana gene identifier. Genes under the 1 Mb region that contained the marker with the highest LOD are highlighted in blue.

Locus ID	Best.hit.At	Symbol	Annotation
Aqcoe4G024000	AT4G18960	AG1	K-box region and MADS-box transcription factor family protein
Aqcoe4G024300	AT3G58770	AG1	K-box region and MADS-box transcription factor family protein
Aqcoe4G024600	AT2G42790	CSY3	citrate synthase 3
Aqcoe4G024700	AT5G59840		Ras-related small GTP-binding family protein
Aqcoe4G024800	AT5G65750		2-oxoglutarate dehydrogenase, E1 component
Aqcoe4G025200	AT3G54950	PLA	patatin-like protein 6
Aqcoe4G025400	AT1G07650		Leucine-rich repeat transmembrane protein kinase
Aqcoe4G025600	AT1G29050	TBL38	TRICHOME BIREFRINGENCE-LIKE 38
Aqcoe4G026000	AT3G14840	LIK1	Leucine-rich repeat transmembrane protein kinase
Aqcoe4G026500	AT1G53440		Leucine-rich repeat transmembrane protein kinase
Aqcoe4G026600	AT1G53440		Leucine-rich repeat transmembrane protein kinase
Aqcoe4G027000	AT4G19840	PP2-A1	phloem protein 2-A1
Aqcoe4G027100	AT1G78700	BEH4	BES1/BZR1 homolog 4
Aqcoe4G027200	AT1G53460		
Aqcoe4G027300	AT4G18880	HSFA4A	heat shock transcription factor A4A
Aqcoe4G027400	AT1G78680	ATGGH2	gamma-glutamyl hydrolase 2
Aqcoe4G027500			
Aqcoe4G027900	AT1G78680	ATGGH2	gamma-glutamyl hydrolase 2
Aqcoe4G028000			
Aqcoe4G028600	AT1G06410	TPS7	trehalose-phosphatase/synthase 7
Aqcoe4G028700	AT1G53380		Plant protein of unknown function (DUF641)
Aqcoe4G028800	AT5G61970		signal recognition particle-related / SRP-related
Aqcoe4G028900	AT5G41020		myb family transcription factor
Aqcoe4G029100	AT2G30950	FTSH2	FtsH extracellular protease family
Aqcoe4G029200	AT4G18820		AAA-type ATPase family protein
Aqcoe4G029300	AT1G29340	ATPUB17	plant U-box 17
Aqcoe4G029700			
Aqcoe4G030000	AT2G42770		Peroxisomal membrane 22 kDa (Mpv17/PMP22) family protein
Aqcoe4G031000	AT3G19720	ARC5	P-loop containing nucleoside triphosphate hydrolases superfamily protein
Aqcoe4G031200			
Aqcoe4G031300	AT4G18800	RABA1D	RAB GTPase homolog A1D
Aqcoe4G031600	AT1G11330		S-locus lectin protein kinase family protein
Aqcoe4G031700	AT2G42760		
Aqcoe4G031800			
Aqcoe4G031900	AT2G42750		DNAJ heat shock N-terminal domain-containing protein
Aqcoe4G032000			
Aqcoe4G032200	AT5G45760		Transducin/WD40 repeat-like superfamily protein
Aqcoe4G032300	AT4G18780	CESA8	cellulose synthase family protein
Aqcoe4G032400	AT3G14067		Subtilase family protein
Aqcoe4G032600	AT5G01750		Protein of unknown function (DUF567)
Aqcoe4G032900	AT2G27260		Late embryogenesis abundant (LEA) hydroxyproline-rich glycoprotein family
Aqcoe4G033500	AT5G13690	NAGLU	alpha-N-acetylglucosaminidase family / NAGLU family

Aqcoe4G034000	AT5G22870		Late embryogenesis abundant (LEA) hydroxyproline-rich glycoprotein family
Aqcoe4G034100	AT4G35490	MRPL11	mitochondrial ribosomal protein L11
Aqcoe4G034500	AT4G18750	DOT4	Pentatricopeptide repeat (PPR) superfamily protein
Aqcoe4G034700			
Aqcoe4G034900	AT4G18750	DOT4	Pentatricopeptide repeat (PPR) superfamily protein
Aqcoe4G035000	AT5G35370		S-locus lectin protein kinase family protein
Aqcoe4G035500	AT5G43470	HRT	Disease resistance protein (CC-NBS-LRR class) family
Aqcoe4G035600	AT1G78770	APC6	anaphase promoting complex 6
Aqcoe4G035700	AT4G14440	ATECI3	3-hydroxyacyl-CoA dehydratase 1
Aqcoe4G035800	AT3G14570	ATGSL04	glucan synthase-like 4
Aqcoe4G035900	AT3G25780	AOC3	allene oxide cyclase 3
Aqcoe4G036000	AT2G30970	ASP1	aspartate aminotransferase 1
Aqcoe4G036100	AT5G16860		Tetratricopeptide repeat (TPR)-like superfamily protein
Aqcoe4G036200	AT3G59500		Integral membrane HRF1 family protein
Aqcoe4G036300	AT5G45780		Leucine-rich repeat protein kinase family protein
Aqcoe4G036400	AT2G30980	BIL1	SHAGGY-related protein kinase dZeta
Aqcoe4G036600	AT3G58690		Protein kinase superfamily protein
Aqcoe4G036700	AT5G26830		Threonyl-tRNA synthetase
Aqcoe4G036800	AT4G20020		
Aqcoe4G036900			
Aqcoe4G038100			
Aqcoe4G038200			
Aqcoe4G038400	AT1G06620		2-oxoglutarate (2OG) and Fe(II)-dependent oxygenase superfamily protein
Aqcoe4G038600	AT2G34960	CAT5	cationic amino acid transporter 5
Aqcoe4G039000	AT4G17760		damaged DNA binding;exodeoxyribonuclease IIIs
Aqcoe4G039600	AT5G48620		Disease resistance protein (CC-NBS-LRR class) family
Aqcoe4G040000	AT3G06240		F-box family protein
Aqcoe4G040200	AT5G48620		Disease resistance protein (CC-NBS-LRR class) family
Aqcoe4G040300	AT2G42690		alpha/beta-Hydrolases superfamily protein
Aqcoe4G040400	AT1G53530		Peptidase S24/S26A/S26B/S26C family protein
Aqcoe4G040500	AT5G45840		Leucine-rich repeat protein kinase family protein
Aqcoe4G040600	AT1G78810		
Aqcoe4G040700	AT2G42670		Protein of unknown function (DUF1637)
Aqcoe4G040800			
Aqcoe4G040900	AT3G14910		
Aqcoe4G041300	AT5G17540		HXXXD-type acyl-transferase family protein
Aqcoe4G042300	AT5G17540		HXXXD-type acyl-transferase family protein
Aqcoe4G042400	AT1G09850	XBCP3	xylem bark cysteine peptidase 3
Aqcoe4G042500			
Aqcoe4G042700	AT3G58640		Mitogen activated protein kinase kinase kinase-related
Aqcoe4G043000	AT1G14990		
Aqcoe4G043100	AT1G29195		
Aqcoe4G043200	AT5G54750		Transport protein particle (TRAPP) component
Aqcoe4G043300	AT3G04600		Nucleotidyl transferase superfamily protein
Aqcoe4G043400	AT3G04040		
Aqcoe4G043700	AT3G58630		sequence-specific DNA binding transcription factors
Aqcoe4G043800	AT2G42610	LSH10	Protein of unknown function (DUF640)
Aqcoe4G043900	AT1G17020	ATSRG1	senescence-related gene 1
Aqcoe4G044000			

Aqcoe4G044200	AT1G29170	SCAR3	Encodes a member of the SCAR family.
Aqcoe4G045300	AT5G32440		Ubiquitin system component Cue protein
Aqcoe4G045600	AT1G06630		F-box/RNI-like superfamily protein
Aqcoe4G045700	AT5G10770		Eukaryotic aspartyl protease family protein
Aqcoe4G046200	AT5G10870	ATCM2	chorismate mutase 2
Aqcoe4G046500	AT3G14940	ATPPC3	phosphoenolpyruvate carboxylase 3
Aqcoe4G047100	AT1G29930	AB140	chlorophyll A/B binding protein 1
Aqcoe4G047300			
Aqcoe4G047400	AT4G10780		LRR and NB-ARC domains-containing disease resistance protein
Aqcoe4G047500	AT1G29930	AB140	chlorophyll A/B binding protein 1
Aqcoe4G047600	AT1G29120		Hydrolase-like protein family
Aqcoe4G047700			
Aqcoe4G047800			
Aqcoe4G048000	AT1G16890	UBC13B	ubiquitin-conjugating enzyme 36
Aqcoe4G048200	AT2G42580	TTL3	tetratricopeptide-repeat thioredoxin-like 3
Aqcoe4G048400	AT1G22870		Protein kinase family protein with ARM repeat domain
Aqcoe4G048700	AT5G61190		putative endonuclease or glycosyl hydrolase with C2H2-type zinc finger domain
Aqcoe4G048800	AT4G16130	ARA1	arabinose kinase
Aqcoe4G049500	AT2G15480	UGT73B5	UDP-glucosyl transferase 73B5
Aqcoe4G049700	AT4G14850	LOI1	Pentatricopeptide repeat (PPR) superfamily protein
Aqcoe4G049800	AT4G17410		DWNN domain, a CCHC-type zinc finger
Aqcoe4G050000	AT4G33355		Bifunctional inhibitor/lipid-transfer protein/seed storage 2S albumin superfamily protein
Aqcoe4G050300	AT1G61180		LRR and NB-ARC domains-containing disease resistance protein
Aqcoe4G050700	AT3G09270	GSTU8	glutathione S-transferase TAU 8
Aqcoe4G050800	AT3G58610		ketol-acid reductoisomerase
Aqcoe4G050900	AT3G14980	ROS	Acyl-CoA N-acyltransferase with RING/FYVE/PHD-type zinc finger protein
Aqcoe4G051100	AT5G45900	APG7,	ThiF family protein
Aqcoe4G051300	AT1G53250		
Aqcoe4G051400			
Aqcoe4G051500			
Aqcoe4G051600			
Aqcoe4G051700	AT1G78750		F-box/RNI-like superfamily protein
Aqcoe4G051900	AT3G59200		F-box/RNI-like superfamily protein
Aqcoe4G052100	AT2G31130		
Aqcoe4G052600	AT4G19050		NB-ARC domain-containing disease resistance protein
Aqcoe4G052900	AT3G50120		Plant protein of unknown function (DUF247)
Aqcoe4G053000	AT2G34090	MEE18	maternal effect embryo arrest 18
Aqcoe4G053100	AT3G59010	PME61	pectin methylesterase 61
Aqcoe4G053200	AT1G56000		FAD/NAD(P)-binding oxidoreductase family protein
Aqcoe4G053300	AT1G56000		FAD/NAD(P)-binding oxidoreductase family protein
Aqcoe4G053600	AT5G44430	PDF1.2c	plant defensin 1.2C
Aqcoe4G053900	AT1G56000		FAD/NAD(P)-binding oxidoreductase family protein
Aqcoe4G054200	AT5G44430	PDF1.2c	plant defensin 1.2C
Aqcoe4G054300	AT2G47730	ATGSTF8	glutathione S-transferase phi 8
Aqcoe4G054400	AT1G55980		FAD/NAD(P)-binding oxidoreductase family protein
Aqcoe4G054700			
Aqcoe4G054800	AT1G17120	CAT8	cationic amino acid transporter 8
Aqcoe4G054900	AT5G48620		Disease resistance protein (CC-NBS-LRR class) family

Aqcoe4G055300	AT5G44430	PDF1.2c	plant defensin 1.2C
Aqcoe4G055400			
Aqcoe4G055600	AT5G44430	PDF1.2c	plant defensin 1.2C
Aqcoe4G055800	AT5G44430	PDF1.2c	plant defensin 1.2C
Aqcoe4G055900	AT5G44430	PDF1.2c	plant defensin 1.2C
Aqcoe4G056100	AT3G25750		F-box family protein with a domain of unknown function (DUF295)
Aqcoe4G056200	AT5G44430	PDF1.2c	plant defensin 1.2C
Aqcoe4G056300	AT5G44430	PDF1.2c	plant defensin 1.2C
Aqcoe4G056500	AT1G16670		Protein kinase superfamily protein
Aqcoe4G056800			
Aqcoe4G056900	AT1G29050	TBL38	TRICHOME BIREFRINGENCE-LIKE 38
Aqcoe4G057100	AT3G25690	CHUP1	Hydroxyproline-rich glycoprotein family protein
Aqcoe4G057300	AT1G78830		Curculin-like (mannose-binding) lectin family protein
Aqcoe4G057400	AT1G78850		D-mannose binding lectin protein with Apple-like carbohydrate-binding domain
Aqcoe4G057900	AT5G51040		
Aqcoe4G058000	AT3G23760		
Aqcoe4G058100			
Aqcoe4G058300	AT5G20040	ATIPT9	isopentenyltransferase 9
Aqcoe4G058400	AT5G45910		GDSL-like Lipase/Acylhydrolase superfamily protein
Aqcoe4G058500	AT1G53240	mMDH1	Lactate/malate dehydrogenase family protein
Aqcoe4G058600	AT1G06230	GTE4	global transcription factor group E4
Aqcoe4G058700	AT1G50410	FRG	SNF2 domain-containing protein / helicase domain-containing protein /zinc finger protein-related
Aqcoe4G058900	AT5G44430	PDF1.2c	plant defensin 1.2C
Aqcoe4G059300	AT1G73170		P-loop containing nucleoside triphosphate hydrolases superfamily protein
Aqcoe4G059500	AT1G73170		P-loop containing nucleoside triphosphate hydrolases superfamily protein
Aqcoe4G059800	AT4G18480	CH-42	P-loop containing nucleoside triphosphate hydrolases superfamily protein
Aqcoe4G059900	AT2G33980	NUDT22	nudix hydrolase homolog 22
Aqcoe4G060500	AT3G24800	PRT1	proteolysis 1
Aqcoe4G060600			
Aqcoe4G060700			
Aqcoe4G060900			
Aqcoe4G061000			
Aqcoe4G061200	AT1G53210		sodium/calcium exchanger family protein / calcium-binding EF hand family protein
Aqcoe4G061400	AT5G42820	U2AF35B	Zinc finger C-x8-C-x5-C-x3-H type family protein
Aqcoe4G061800	AT5G15380	DRM1	domains rearranged methylase 1
Aqcoe4G062100	AT1G11950		Transcription factor jumonji (jmjC) domain-containing protein

Table C5: Candidate genes under QTL.

Chr	Locus ID	Gene name	Genomic location (5')
1	Aqcoe1G411100	<i>AqLAS</i>	39,117,500
1	Aqcoe1G456700	<i>AqPTL</i>	42,021,250
2	Aqcoe2G139400	<i>AqZPR3a</i>	12,741,500
3	Aqcoe3G159700	<i>AqROXYa</i>	13,927,500
4	Aqcoe4G024000	<i>AqAG1</i>	2,002,500
5	Aqcoe5G235700	<i>AqSEU</i>	15,620,000
5	Aqcoe5G237200	<i>AqAGO5a</i>	15,842,500
6	Aqcoe6G121000	<i>AqHAN</i>	6,619,000
7	Aqcoe7G132200	<i>AqATH1</i>	8,222,500

Table C6: Primers used for constructing in situ hybridization probes.

Locus ID	Gene name	Forward primer (5'to 3')	Reverse primer (5' to 3')	Product size
Aqcoe2G057900	<i>AqWUS</i>	TGTCGAGCCATATCCATTTTTCAAC	TCATGCATGATGTTATCAGTCCTTTG	300 bp
Aqcoe2G139400	<i>AqZPR3a</i>	CAGAGCTTTACTTGAGGAATTTG	GAACTCTGGGATTTGGAGA	196 bp
Aqcoe3G159700	<i>AqROXYa</i>	AAATACCAAACACACCAACT	TTGACATGTATGACAACCTCC	220 bp
Aqcoe7G132200	<i>AqATH1</i>	GGCAGTTCTAGTTCTATTGC	TGAAGCTGTTGAAACATTTA	147 bp

REFERENCE

- Li S, Lauri A, Ziemann M, Busch A, Bhave M, Zachgo S. 2009. Nuclear Activity of ROXY1, a Glutaredoxin Interacting with TGA Factors, Is Required for Petal Development in *Arabidopsis thaliana*. *The Plant Cell* 21: 429–441.
- Min Y, Kramer EM. 2020. Transcriptome profiling and weighted gene co-expression network analysis of early floral development in *Aquilegia coerulea*. *Scientific Reports* 10: 19637.